Advances in Meteorology

Advances in Urban Biometeorology 2014

Guest Editors: Panagiotis Nastos, Andreas Matzarakis, Marialena Nikolopoulou, and Tzu-Ping Lin

Advances in Urban Biometeorology 2014

Advances in Meteorology

Advances in Urban Biometeorology 2014

Guest Editors: Panagiotis Nastos, Andreas Matzarakis, Marialena Nikolopoulou, and Tzu-Ping Lin

Editorial Board

Contents

Hindawi Publishing Corporation
Advances in Meteorology
Volume 2015, Article ID 273831, 3 pages
http://dx.doi.org/10.1155/2015/273831

Editorial

Advances in Urban Biometeorology 2014

Panagiotis Nastos,[1] Andreas Matzarakis,[2] Marialena Nikolopoulou,[3] and Tzu-Ping Lin[4]

[1]*Laboratory of Climatology and Atmospheric Environment, University of Athens, University Campus, 15784 Athens, Greece*
[2]*Albert-Ludwigs-University of Freiburg, 79085 Freiburg, Germany*
[3]*Kent School of Architecture, University of Kent, Canterbury, Kent CT2 7NR, UK*
[4]*Department of Architecture, National Cheng Kung University, 1 University Road, Tainan 701, Taiwan*

Correspondence should be addressed to Panagiotis Nastos; nastos@geol.uoa.gr

Received 15 April 2015; Accepted 15 April 2015

Biometeorological conditions in outdoor urban spaces and the energy consumption as well as thermal comfort in residential buildings are modified due to environmental factors and the complex structure and development of urban agglomerations. The quality of life in an urban or rural environment is influenced significantly by bioclimatic conditions, both short and long terms. The urban heat island, intensified by heat waves in the future projections [1, 2], not only affects quality of life, but in many cases also affects morbidity and mortality [3–6]. Thus, the quantification of thermal comfort conditions in urban residential areas and the required adaptation strategies [7–9], along with the implementation of green buildings, the decrease of energy consumption, and the urban planning and design [10–13] are considered of high concern by the scientific community and urban planners in order to mitigate the adverse consequences of urbanization.

This special issue, which has become the first issue in a series of special issues, which will be published each year, in order to have a long-term impact, focuses on the assessment/modeling of human thermal sensation within urban areas. The high quality papers concern different scales and climatic contexts, identifying the effect of urban configurations such as buildings, parks, streets, and residential areas on humans' health and well-being.

More specifically, the paper of H. L. Lokys et al. analyzes the impact of climate change on human thermal comfort over the next century using two common human-biometeorological indices, the Physiologically Equivalent Temperature (PET) and the Universal Thermal Climate Index (UTCI) in three regions of Luxembourg, Western-Central Europe. The climate change projections are based on a multimodel ensemble of 12 transient simulations (1971–2098) with a spatial resolution of 25 km. The findings of the analysis confirmed the general decrease in cold stress as well as the general increase in heat stress for the region of Luxembourg with respect to the human-biometeorological indices PET and UTCI in detail. Regarding the changes in the index classes, they can be distinguished between cold and heat stress. The changes in heat stress tend to already appear in the near future (2041–2050), whereas the heat stress levels changes become statistically significant in the far future (2091–2100).

Dynamic observations using a digital video camera, at a stepped plaza situated at the outdoor public recreational garden of National Museum of Natural Science (NMNS) in Taichung City, Taiwan, have been conducted by K.-T. Huang et al. in order to perform on-site measurements of the physical environment and observations of user behaviors, including their resting positions, movements, and stay durations. The primary findings of this study are as follows. (1) More people rested on the stepped plaza during the cool season compared with the hot season. The number of people present during the hot season decreased as temperatures increased. The temperature ranges at which most people were present were 34°C PET–36°C PET during the hot season and 20°C PET–22°C PET during the cool season. (2) More than 75% of users preferred shaded areas. Users also stayed longer in shaded areas than they did in sunny areas. (3) Besides, using thermal comfort theory and previous local on-site

investigations, the authors describe and verify the relation between behavior and the thermal environment. It is proved that the observed subjects demonstrated an extremely high tolerance to increased summer temperatures despite their psychological preferences for lower air temperatures. People substantially preferred to conduct activities in shaded areas even during the cool season.

R. Vitt et al. present a human-biometeorological information scheme developed for tourism purposes for the medium-sized Hungarian city of Szeged that could be used also for urban planning. It compares thermal and climatic differences between the city and its surroundings. Meteorological data comes from one urban and one rural station and covers the period 2000 to 2011. The thermal index Physiologically Equivalent Temperature (PET) at 14 CET was used in order to quantify thermal stress conditions by means of the frequencies of PET classes, and the precipitation conditions, for each ten-day interval of the month for all the year, were analyzed. The authors shed light on the Climate-Tourism/Transfer-Information-Scheme, which gives a clearly arranged overview of the most important meteorological and biometeorological factors, which influence tourism potential and recreation. The results indicate that there are differences of PET values during the day, as in summer heat stress occurs more frequently in urban areas at 14 CET, and thermal acceptance is more probable in the rural surroundings. On the contrary, cold stress is more frequent in rural areas during winter, due to the absence of heat storage of buildings and low wind speed. Based on the little horizontal distance between the urban and the rural stations, there are marginal differences of precipitation.

Microclimate characteristics, in relation to green-area development and the reflectivity of exterior coating materials, using field measurements of temperature in the urban area of Changwon City, South Korea, were performed by B. Song and K. Park. Furthermore, the effects from improving the thermal environment were identified for various land-use types, and their characteristics were determined by microclimate modeling of temperatures using ENVI-met model [14]. The analysis of the temperature change (according to the space design), taking into account increases in reflectivity and development of green areas for different types of land use, showed distinct temperature-reduction effects due to creation of green spaces in areas where buildings and artificial cover materials were densely distributed (i.e., commercial and single residential areas). Besides, the effects of thermal improvement due to green-area development and increasing reflectivity differ depending on land use.

B. Jänicke et al. studied the effects of façade greening on outdoor human bioclimate, using firstly observational data to answer the question: How large is the reduction of *Tmrt* in front of a greened façade compared to a bare one at a study site? Afterwards, they applied the models ENVI-met, RayMan, and SOLWEIG to the same site in order to evaluate the general performance of the models in simulating *Tmrt* and other variables relevant to assessment of human bioclimate, contributing to the intercomparison and evaluation of these models in a complex urban environment. Finally, the authors investigated if the models are able to simulate the observed alteration of *Tmrt* in front of the façade greening. In conclusion, the effect of façade greening on outdoor human bioclimate was limited in this case study because only a small reduction *Tmrt* in front of the façade greening was detected. Hence, façade greening has only a minor effect in reducing outdoor heat stress. With a façade greening attached to more than one façade in a street canyon or courtyard the effect on *Tmrt*, however, might be enlarged. The general ability of ENVI-met [14], RayMan [15], and SOLWEIG [16] models to simulate *Tmrt* was reasonable as expected for well-established models. Nevertheless, the deviations from observations vary largely between different studies. Additionally, the deviations from observations for other variables (specific humidity, long-wave downward, or short-wave upward radiation) were higher and might impede the models' ability to assess heat stress.

A long-term climate measurement in the third largest city of Taiwan was implemented by F.-C. Liao et al., for the check of accuracy of morphing approach on generating the hourly data of urban local climate. Based on observed and morphed meteorological data, building energy simulation software EnergyPlus was used to simulate the cooling energy consumption of an air-conditioned typical flat and the thermal comfort level of a naturally ventilated typical flat. The simulated results were used to quantitatively discuss the effect of urban microclimate on the energy consumption as well as thermal comfort of residential buildings. The result showed that the morphing approach has good accuracy in forecasting temperature and relative humidity. In terms of the error of cooling energy consumption, the percentage error of the observed and predicted meteorological data is slight with a range of 0.49%–1.06%. However, the meteorological data generated from the morphing approach made moderate errors in the assessment of thermal comfort in a naturally ventilated space. This suggests that the climatic data generated from morphing approach are suitable for the analysis of energy consumption of air-conditioned buildings, but not suitable for the diagnosis of indoor thermal comfort level of naturally ventilated buildings.

H. Liu et al. investigated whether urban development of Shenzhen City, China, has altered the heat balance of the ground surface, thereby influencing climatic variables as well as the reference crop evapotranspiration (ET_0) changes. The daily, monthly, and annual climatic variables and ET_0, from 1954 to 2012, were computed using the FAO Penman-Monteith equation (PM), and these parameters were analyzed to study the temporal trends of ET_0 and meteorological factors. The trends and the time points of abrupt changes of ET_0 and meteorological factors were tested using Mann-Kendall methods. The results of the analysis indicated that the development of Shenzhen City greatly affected the local climatic conditions. The mutation point for most climatic variables is observed at approximately 1978, the onset year for urban development. ET_0 first decreased from 1954 to 1978 and then increased quickly and reached a maximal value of 1373 mm during the period from 1992 to 2012. Besides, sensitivity analysis showed that ET_0 is most sensitive to relative humidity, followed by air temperature, sunshine hours, and wind speed.

Acknowledgments

As Guest Editors of this special issue, we would like to thank all the authors for their contributions to this volume and their adherence to the strict reviewing rules. We also wish to express our sincere appreciation to the international panel of reviewers for making available their expertise in the effort to achieve the highest scientific value of this volume.

Panagiotis Nastos
Andreas Matzarakis
Marialena Nikolopoulou
Tzu-Ping Lin

References

[1] D. Barriopedro, E. M. Fischer, J. Luterbacher, R. M. Trigo, and R. García-Herrera, "The hot summer of 2010: redrawing the temperature record map of Europe," *Science*, vol. 332, no. 6026, pp. 220–224, 2011.

[2] P. T. Nastos and J. Kapsomenakis, "Regional climate model simulations of extreme air temperature in Greece. Abnormal or common records in the future climate?" *Atmospheric Research*, vol. 152, pp. 43–60, 2015.

[3] B. G. Armstrong, Z. Chalabi, B. Fenn et al., "Association of mortality with high temperatures in a temperate climate: England and Wales," *Journal of Epidemiology and Community Health*, vol. 65, no. 4, pp. 340–345, 2011.

[4] F. C. Curriero, K. S. Heiner, J. M. Samet, S. L. Zeger, L. Strug, and J. A. Patz, "Temperature and mortality in 11 cities of the eastern United States," *American Journal of Epidemiology*, vol. 155, no. 1, pp. 80–87, 2002.

[5] WHO, "Improving public health responses to extreme weather/heat-waves—EuroHEAT," Technical Summary, WHO, 2009.

[6] P. T. Nastos and A. Matzarakis, "The effect of air temperature and human thermal indices on mortality in Athens, Greece," *Theoretical and Applied Climatology*, vol. 108, no. 3-4, pp. 591–599, 2012.

[7] R. de Dear and G. S. Brager, "The adaptive model of thermal comfort and energy conservation in the built environment," *International Journal of Biometeorology*, vol. 45, no. 2, pp. 100–108, 2001.

[8] T.-P. Lin, "Thermal perception, adaptation and attendance in a public square in hot and humid regions," *Building and Environment*, vol. 44, no. 10, pp. 2017–2026, 2009.

[9] F. Nicol, "Adaptive thermal comfort standards in the hot-humid tropics," *Energy and Buildings*, vol. 36, no. 7, pp. 628–637, 2004.

[10] K. Huang, W. Huang, T. Lin, and R. Hwang, "Implementation of green building specification credits for better thermal conditions in naturally ventilated school buildings," *Building and Environment*, vol. 86, pp. 141–150, 2015.

[11] F. Asdrubali, C. Buratti, F. Cotana et al., "Evaluation of green buildings' overall performance through in situ monitoring and simulations," *Energies*, vol. 6, no. 12, pp. 6525–6547, 2013.

[12] M. Fahmy, M. M. Mahdy, and M. Nikolopoulou, "Prediction of future energy consumption reduction using GRC envelope optimization for residential buildings in Egypt," *Energy and Buildings*, vol. 70, pp. 186–193, 2014.

[13] F. Yang, S. S. Y. Lau, and F. Qian, "Thermal comfort effects of urban design strategies in high-rise urban environments in a sub-tropical climate," *Architectural Science Review*, vol. 54, no. 4, pp. 285–304, 2011.

[14] M. Bruse and H. Fleer, "Simulating surface-plant-air interactions inside urban environments with a three dimensional numerical model," *Environmental Modelling & Software*, vol. 13, no. 3-4, pp. 373–384, 1998.

[15] A. Matzarakis, F. Rutz, and H. Mayer, "Modelling radiation fluxes in simple and complex environments—application of the RayMan model," *International Journal of Biometeorology*, vol. 51, no. 4, pp. 323–334, 2007.

[16] F. Lindberg, B. Holmer, and S. Thorsson, "SOLWEIG 1.0—modelling spatial variations of 3D radiant fluxes and mean radiant temperature in complex urban settings," *International Journal of Biometeorology*, vol. 52, no. 7, pp. 697–713, 2008.

Hindawi Publishing Corporation
Advances in Meteorology
Volume 2015, Article ID 323856, 10 pages
http://dx.doi.org/10.1155/2015/323856

Research Article

Future Changes in Human-Biometeorological Index Classes in Three Regions of Luxembourg, Western-Central Europe

Hanna Leona Lokys,[1,2] Jürgen Junk,[1] and Andreas Krein[1]

[1] *Luxembourg Institute of Science and Technology (LIST), Environmental Research and Innovation (ERIN) Department, 41 rue du Brill, 4422 Belvaux, Luxembourg*
[2] *University of Münster, Climatology Working Group, Heisenbergstraße 2, 48149 Münster, Germany*

Correspondence should be addressed to Hanna Leona Lokys; hanna.lokys@list.lu

Received 15 September 2014; Revised 9 January 2015; Accepted 18 January 2015

Academic Editor: Tzu-Ping Lin

Projected climate change will cause increasing air temperatures affecting human thermal comfort. In the highly populated areas of Western-Central Europe a large population will be exposed to these changes. In particular Luxembourg—with its dense population and the large cross-border commuter flows—is vulnerable to changing thermal stress. Based on climate change projections we assessed the impact of climate change on human thermal comfort over the next century using two common human-biometeorological indices, the Physiological Equivalent Temperature and the Universal Thermal Climate Index. To account for uncertainties, we used a multimodel ensemble of 12 transient simulations (1971–2098) with a spatial resolution of 25 km. In addition, the regional differences were analysed by a single regional climate model run with a spatial resolution of 1.3 km. For the future, trends in air temperature, vapour pressure, and both human-biometeorological indices could be determined. Cold stress levels will decrease significantly in the near future up to 2050, while the increase in heat stress turns statistically significant in the far future up to 2100. This results in a temporarily reduced overall thermal stress level but further increasing air temperatures will shift the thermal comfort towards heat stress.

1. Introduction

With very high confidence human health is influenced by climate change [1], as the thermoregulatory system of the human body interacts closely with the atmospheric system [2, 3]. The significant increase in air temperature is shown by different Global and Regional Climate Models (GCM and RCM) as presented, for example, in the framework of the ENSEMBLES [4] or EURO-CORDEX [5] projects. Most severe health effects could be associated with the projected increase of extreme events such as increasing frequency and intensity of heat waves [1, 6]. Nevertheless, adverse effects on human health could already be shown with moderate levels of heat stress, such as a characteristically temperature-mortality relationship even at air temperatures below 30°C [7].

Several studies on the impact of climate change on vegetation [8, 9], tourism [10], and human health effects [11] have been published for the region of Luxembourg. The latter focused on changes in extreme heat and cold periods. As Luxembourg is characterised by a temperate semioceanic climate with mild winters and moderate summers [8], the moderate heat and cold stress levels and their changes are dominant. A detailed analysis in space and time for human thermal stress in Luxembourg has not been conducted yet.

The thermal state of the environment is not sufficiently described by air temperature but comprises furthermore humidity, wind speed, thermal radiation (from the short and long wave domain), and facets of the physical environment [12]. To account for all parameters a large number of human thermal climate indices have been developed [12], whereof we chose two energy balance stress indices, the Physiological Equivalent Temperature (PET) [13] and the Universal Thermal Climate Index (UTCI) [14]. Both indices have been widely used and were shown to be suitable for human thermal stress assessments [3, 15–17].

Table 1: Regional climate change projection datasets. Given are the driving GCM, the RCM used for the dynamical downscaling, and the institutions responsible for the GCMs and RCMs.

Model ID	GCM	Institution running the GCM	RCM	Institution running the RCM
E01	HadCM3Q16	METO-HC	RCA3	C4I
E03	ARPEGE_RM5.1	CNRM	ALADIN	CNRM
E04	ECHAM5r3	MPI-MET	DMI-HIRHAM5	DMI
E05	ARPEGE	CNRM	HIRHAM5	DMI
E06	BCM	UIB	HIRHAM5	DMI
E07	HadCM3Q0	METO-HC	CLM	ETHZ
E09	HadCM3Q0	METO-HC	HadRM3Q0	METO-HC
E10	HadCM3Q3	METO-HC	HadRM3Q3	METO-HC
E12	ECHAM5r3	MPI-MET	RegCM	ICTP
E13	ECHAM5r3	MPI-MET	RACMO	KNMI
E16	ECHAM5r3	MPI-MET	REMO	MPI-M
E20	HadCM3Q3	METO-HC	RCA3	SMHI

The objective is to assess the impact of climate change on three different typical climatological regions of Luxembourg at a high spatial resolution. The assessment includes all classes of both human-biometeorological indices, evaluating the changes in time and space.

2. Materials and Methods

2.1. Climate Change Projections and Area of Investigation. For the climate projections we used a multimodel ensemble of 12 RCMs with a spatial resolution of 25 km per grid cell, in order to quantify the uncertainties related to these climate projections on a daily basis. Due to the calculation of a spatial mean from a 3 by 3 grid this results in only one time series for each ensemble member for Luxembourg [8]. In addition, we used a single RCM run with a spatial resolution of 1.3 km to perform a detailed analysis of different regions in Luxembourg on an hourly basis (Figure 1). Both approaches are based on the IPCC A1B emission scenario, which describes anthropogenic future emissions with rapid economic growth, a balanced use of energy resources, and an increasing global population until the middle of this century [18]. The measurements at Luxembourg Findel Airport from 2000 to 2010 lie within the spread of the multimodel ensemble [8] which accounts for the wide use of this GCM RCM combination in the area of investigation [10, 11, 19].

2.1.1. Global Climate Model (GCM). To quantify the uncertainties related to the climate change projection, a multimodel ensemble of 12 transient simulations from 1971 to 2098 provided by the EU FP6 ENSEMBLES project has been used [4]. The GCM RCM combinations and the institutions running the models can be found in Table 1. The results including daily mean air temperature (at 10 m), relative humidity, wind speed, and global radiation were retrieved from the Danish Meteorological Institute (http://ensemblesrt3.dmi.dk/, November 30, 2013). The projections are all based on the SERS emissions scenario A1B [18]. Due to the coarse resolution of the ENSEMBLES members, a single data point located in the centre of Luxembourg at N49°36′E006°07′ at a height of 259 m AMSL was selected (Figure 1).

2.1.2. Regional Climate Model (RCM). For the analysis of the regional differences in Luxembourg simulations with the spatial resolution of 1.3 km have been conducted with the regional climate model COSMO-CLM. Hourly values for air temperature, relative humidity wind speed at 2 m height, and global radiation at ground level were extracted from the model output. The nonhydrostatic limited area atmospheric prediction model of the consortium for small-scale modelling COSMO [22], version 4.8_clm11, is used as the underlying meteorological model. A three-step nesting approach (18, 4.5, 1.3 km) as described by Junk et al. [11] was used to generate the data for Luxembourg with a final resolution of 1.3 km. Three ten-year periods from 1991 to 2000 (reference period), 2041 to 2050 (near future), and 2090 to 2100 (far future) were calculated for three pseudo stations (Figure 1).

For the detailed spatial analysis of the CLM datasets, we implemented three pseudo stations in different characteristic landscapes of Luxembourg. The stations are (1) Reuler, at 492 m AMSL located in the north of Luxembourg in the "Oesling", (2) Esch-sur-Alzette, at 291 m AMSL located in the south of Luxembourg in the "Gutland", and (3) Wasserbillig at 190 m AMSL located in the Moselle valley (Figure 1).

RCM outputs suffer the problem of a bias compared to observational data [23]. Accordingly, bias-corrected data should be preferred over uncorrected ones. In the case of human-biometeorological indices the use of bias-corrected data is not possible, as there are no suitable bias correction schemes available for global radiation and especially for wind speed. Therefore, we used uncorrected data to calculate all human-biometeorological indices for this study, and we will focus our analyses on changes between the reference period and the future time spans.

2.2. Human-Biometeorological Indices. To evaluate the impact of the projected climate change on human health two common human-biometeorological indices were chosen for

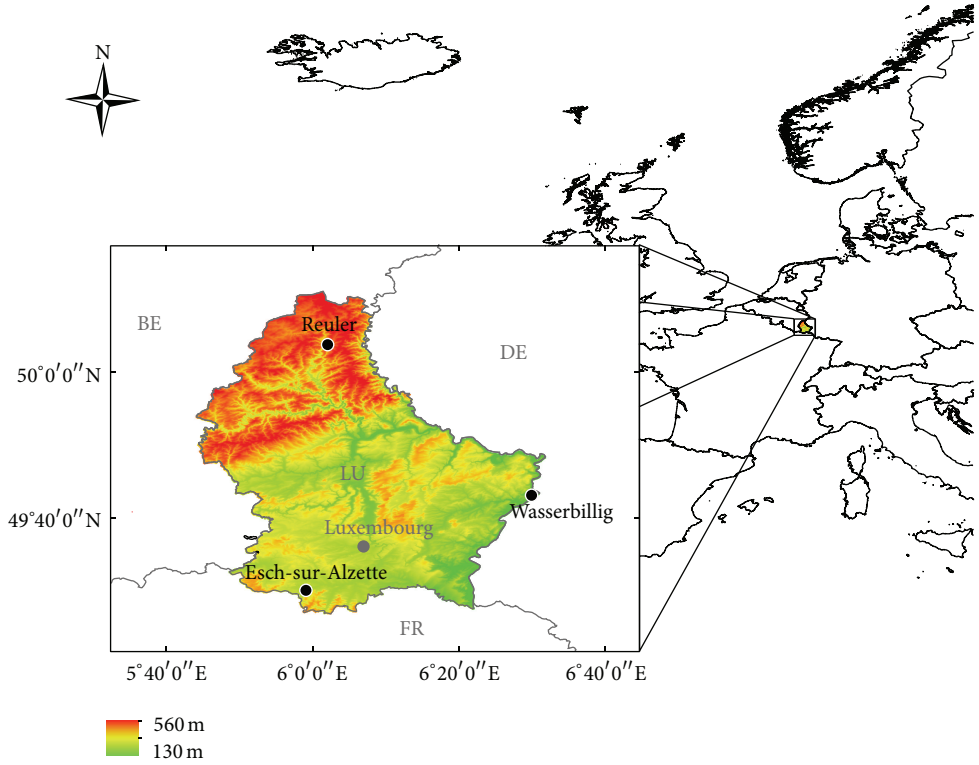

Figure 1: Application domain within Europe (WGS 84). High-resolution model domain in Luxembourg (1.3 km) including topography (m) above mean sea level. Black dots indicate the locations of the pseudo sites extracted from the COSMO-CLM data; the grey dot indicates the multimodel location.

our study. The analyses are based on the PET [13] and the UTCI [14]. Both indices are based on air temperature, wind speed, relative humidity, and mean radiant temperature. The mean radiant temperature was approached with the RayMan model using the geographical location and temporal data together with the meteorological input (especially global radiation). These variables were extracted from the ground based 3D output fields of the RCM simulation. Both human-biometeorological indices are not directly driven by relative humidity, but in combination with the provided temperature data, the water vapour pressure can be calculated to be used for the calculations of the indices. In addition to these parameters, physiological aspects of the human body, such as activity, clothing, sex, and age, are taken into account [24].

Notwithstanding PET and UTCI use the same input variables, they express differences in the number of classes they have. PET divides the thermal stress in 9 classes ranging from "extreme cold stress" to "extreme heat stress" [20] (Figure 2), whereas the UTCI has 10 classes "extreme cold stress" to "extreme heat stress" [21] (Figure 3). As the classes are developed in different ways, we do not intend to compare the indices directly but decided to use them independently for the analysis.

We used the freely available RayMan Pro model Ver. 2.1 [24] to calculate both indices on an hourly basis for the single model runs at the three pseudo stations. For the calculations we used the standard physiological configuration for the indices. For PET this is a 35-year-old male with a weight of 75 kg, a height of 1.75 m, a clothing value of 0.9, and an internal heat production of 80 W. For UTCI we used the UTCI specific standard subject.

PET (°C)	Grade of physiological stress
4	Extreme cold stress
8	Strong cold stress
13	Moderate cold stress
18	Slight cold stress
23	No thermal stress
29	Slight heat stress
35	Moderate heat stress
41	Strong heat stress
	Extreme heat stress

Figure 2: PET range with corresponding grade of physiological stress for humans [20]. Blue represents cold stress classes, white represents no thermal stress, and red represents heat stress classes.

As the calculated human-biometeorological indices are based on non-bias-corrected data, a reference period must be defined in order to evaluate the human-biometeorological changes in the future projections. Instead of the standard reference period of 30 years from 1961 to 1990, defined by

UTCI (°C)	Stress category
46	Extreme heat stress
38	Very strong heat stress
32	Strong heat stress
26	Moderate heat stress
9	No thermal stress
0	Slight cold stress
−13	Moderate cold stress
−27	Strong cold stress
−40	Very strong cold stress
	Extreme cold stress

Figure 3: UTCI range with corresponding stress category for humans [21]. Blue represents cold stress classes, white represents no thermal stress, and red represents heat stress classes.

the World Meteorological Organisation [25], we used a 10-year reference period from 1991 to 2000. We chose the shorter period due to the fact that the computational resources limited the simulations at the high spatial resolution of 1.3 km to three time spans of ten years. Various studies show that the use of a shorter reference period also leads to reliable results [11, 26, 27].

The decision not to focus on extreme events is based on the research of Hajat and Kosatky [28] and Kovats and Hajat [7], who demonstrated that adverse effects on human health are already detectable with only moderate levels of heat stress, such as a characteristically temperature-mortality relationship even at air temperatures below 30°C.

Due to the absence of a suitable bias correction for the input parameters, it is not recommended to work with the absolute results in the context of index changes. One possibility to deal with that fact is the use of relative changes compared to a reference period. As some of the more extreme index classes result in zero for the reference period, but not for the future periods, we decided not to use a relative approach as this would have caused the division by zero. To keep the information of which classes are more and which are less represented in the region, we refrain from using relative anomalies using the absolute values instead.

3. Results

3.1. Multimodel Ensemble Mean, Trends, and Spread. The analysis of the multimodel ensemble has been conducted to (1) account for the spread in future climate change projections and (2) get an overview of the change in the input parameters for human-biometeorological indices.

Figure 4 shows that there is a significant trend in daily mean air temperature (T) and vapour pressure (VP), whereas wind speed (WV) and global radiation (GR) do not show clear trends over the period from 1971 to 2098 for annual values. The slopes (calculated by Sen's method [29]) of the significant ($P < 0.05$) trends calculated from annual mean values by the Mann-Kendall test have a slope of 0.029 (0.29°C/10a) for daily mean air temperature (T) and 0.017 (0.17 hPa/10a) for vapour pressure (VP).

In addition to the trends, Figure 4 shows that, for all four model-driving parameters (air temperature (Figure 4(a)), vapour pressure (Figure 4(c)), wind speed (Figure 4(b)), and global radiation (Figure 4(d))), the results from the high-resolution CLM run (10-year average plotted) are within the spread of the multimodel ensemble. Wind speed results from the CLM model are, for all pseudo stations, below the multimodel mean. This results probably from the fact that the ENSEMBLE multimodel output includes wind speed at 10 m only, whereas the CLM model output contains wind speed at 2 meters. In Figure 4(c), the CLM results for Esch-sur-Alzette and Wasserbillig resemble each other so that the lines overlay each other. The increasing air temperatures and vapour pressure are causing the human-biometeorological indices to increase [30].

3.2. CLM Model Results. A detailed analysis of the human-biometeorological index PET in Luxembourg can be found in Figures 5 and 6. The corresponding results for the UTCI are presented in Figures 7 and 8.

3.2.1. PET. Figure 5 shows boxplots of the PET index classes at the three pseudo stations Esch-sur-Alzette (Figure 5(a)), Reuler (Figure 5(b)), and Wasserbillig (Figure 5(c)) for the reference period 1991–2000, near future 2041–2050, and far future 2091–2100. Each boxplot represents the number of hours with the corresponding PET class per year in the respective time period. Groups of boxplots per index class that are not significantly different ($P < 0.05$) are marked by the same letter underneath the plots. If a box shares the letters ab, it is not significantly different from a and b.

PET classes with the highest number of hours are the classes "strong cold stress", "moderate cold stress", and "slight cold stress" at all stations (Figure 5). The highest PET category "extreme heat stress" is not present at any station during the reference period and the near future. In the far future this category appears 10 and 9 times, respectively, in Esch-sur-Alzette and Wasserbillig (Figures 5(a) and 5(c)), but still not in Reuler (Figure 5(b)). Due to the low number of occurrences this change is not statistically significant at $P < 0.05$. The tendency of decreasing cold index classes and increasing hot index classes can be observed throughout all pseudo stations. Most significant changes occur in the transition between the near and far future. The only significant changes between the reference period and the near future can be found in the "extreme cold stress" index class at all pseudo stations. In Esch-sur-Alzette and Wasserbillig a significant change in the "slight cold stress" index class can only be observed in the transition from the reference period to the far future (Figures 5(a) and 5(c)); the amount of hours in this category in the near future is not different from the reference period and the far future. The most represented index class "moderate cold stress" does not show any significant changes at all.

While Figure 5 focuses on the changes in time, Figure 6 addresses the comparison between the three pseudo stations

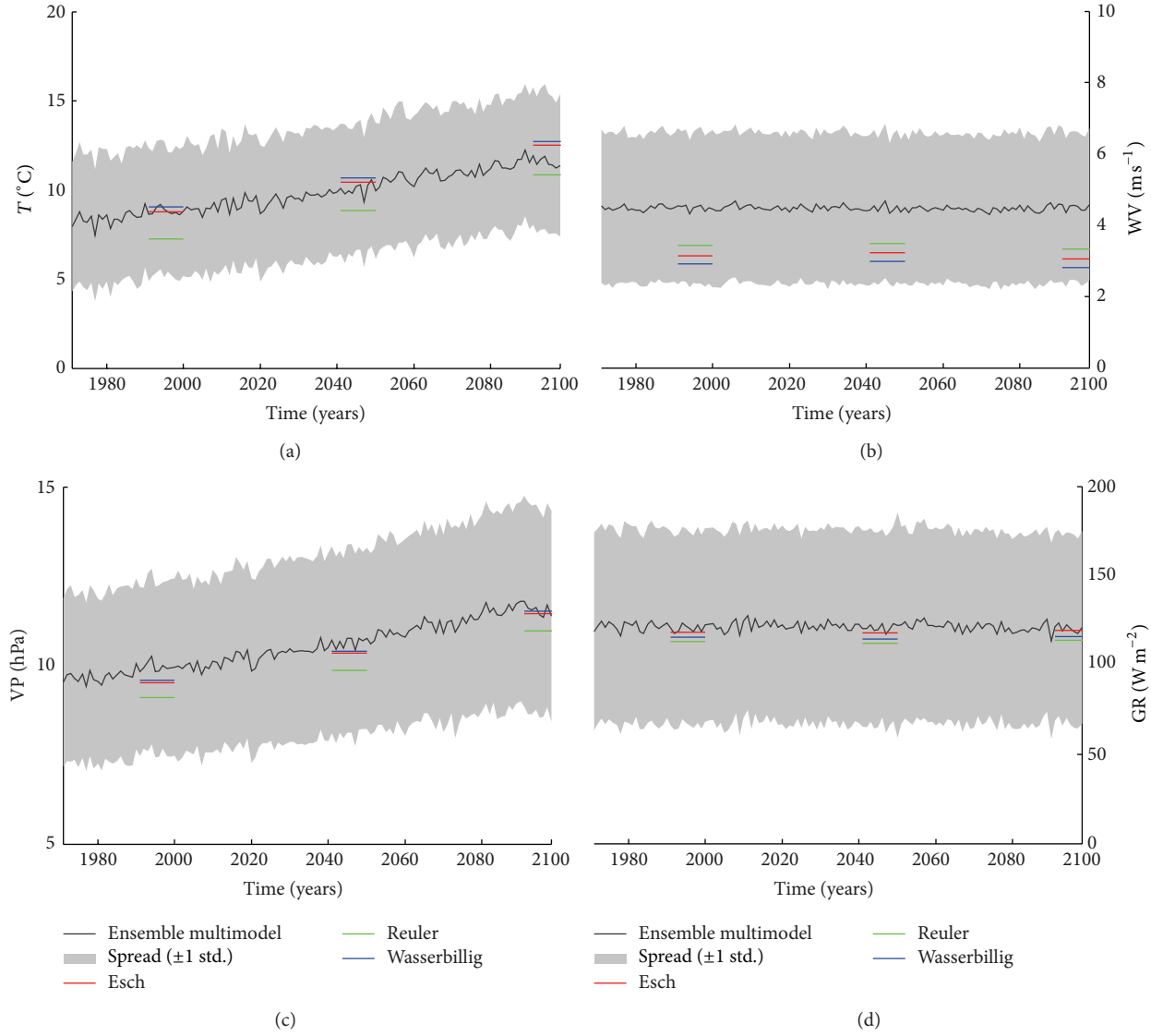

Figure 4: Projected meteorological parameters for the period from 1971 until 2098 using a multimodel ensemble of 12 transient simulations. Grey area shows the spread around the multi-model-mean (black line). Colored lines show the 10-year average results from high-resolution COSMO-CLM simulations for the three pseudo sites in Luxembourg.

during the three time slices, reference period 1991–2000 (Figure 6(a)), near future 2041–2050 (Figure 6(b)), and far future 2091–2100 (Figure 6(c)).

In addition to the information obtained from Figure 5, Figure 6 highlights that Reuler shows lower human-biometeorological indices compared to the other stations. This is only significant in the nonextreme index classes "strong cold stress", "slight cold stress", and "no thermal stress" in the reference period (Figure 6(a)). In the "slight heat stress" and "moderate heat stress" index classes only the difference from Reuler to Esch-sur-Alzette is significant ($P < 0.05$) in the reference period. In the near future, the differences between the stations decrease temporarily (Figure 6(b)). Here only in the index classes "strong cold stress", "slight cold stress", and "slight heat stress" differences between Reuler and other two stations appear. Most of the significant differences between Reuler and the other two regions of Luxembourg can be found in the far future ("strong cold stress", "no thermal stress", "slight heat stress", and "moderate heat stress") (Figure 6(c)). At least one significant difference can be found in that period for the "slight cold stress" and "strong heat stress" index classes. This is the first appearance of a significant regional difference in the "hot" index class. It becomes apparent that the number of hours in the higher index classes increases at all stations, but they are still the lowest at Reuler (Figure 6).

3.2.2. UTCI. The analyses for the UTCI show similarities to the PET results for the changes in time (Figure 7) and on a regional level (Figure 8). In most mid index classes (UTCI class "moderate cold stress" to "moderate heat stress"), the results for Reuler (Figure 8) differ significantly from the other

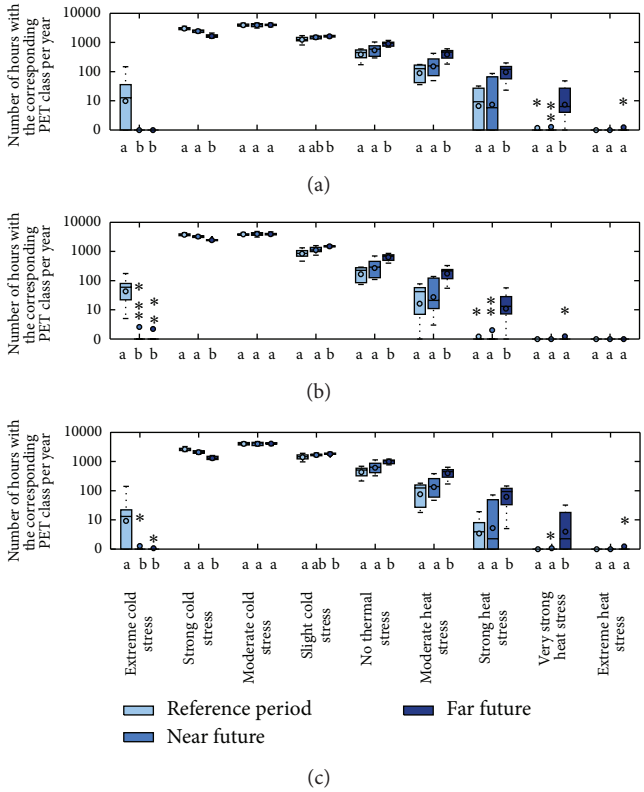

FIGURE 5: Boxplots of PET values for the three periods: reference period 1991–2000, near future 2041–2050, and far future 2091–2100 at the three pseudo stations Esch-sur-Alzette (a), Reuler (b), and Wasserbillig (c). Boxplots show the number of hours within the corresponding PET class per year. The whisker length is determined by 1.5 ∗ interquartile range (IQR). All values larger than 1.5 ∗ IQR are treated as outliers. Median values are indicated by the line inside the box, mean values by the dot. Groups that are sharing the same letters are not significantly different ($P < 0.05$).

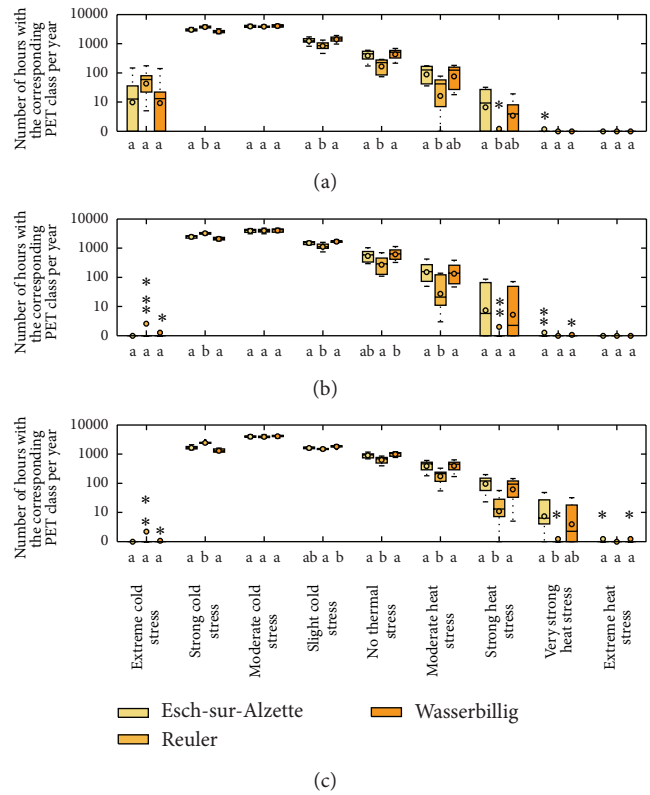

FIGURE 6: Boxplots of PET values for the three pseudo stations Esch-sur-Alzette, Reuler, and Wasserbillig separated by the three periods: reference period 1991–2000 (a), near future 2041–2050 (b), and far future 2091–2100 (c). Boxplots show the number of hours within the corresponding PET class per year. The whisker length is determined by 1.5 ∗ interquartile range (IQR). All values larger than 1.5 ∗ IQR are treated as outliers. Median values are indicated by the line inside the box; mean values are highlighted by the dot. Groups that are sharing the same letters are not significantly different ($P < 0.05$).

regions. The cold stress decreases through the three time slices at all stations, while the heat stress increases in all regions. A significant increase in the "strong heat stress" class can be found at all stations in the far future (Figure 7). The significant change in the amount of hours in the "strong cold stress" class already takes place in the transition from the reference period to the near future.

3.2.3. Stress Periods. Merging the index classes into three categories "cold stress", "no thermal stress", and "heat stress", it can be seen for PET that the number of hours causing any form of cold stress decreases through all stations (−5.6 to −8.0% for the far future compared to the reference period). In contrast, the number of hours in the comfortable and heat stress class increases. The increase in heat stress for the far future ranges from 264.6% (Reuler) to 447.6% (Esch-sur-Alzette). In total these changes result in fewer hours with thermal stress in the future. For the far future this reduction ranges from 3205 h to 3394 h over ten years. Similar results can be obtained when analysing the UTCI. The decrease in cold stress ranges from −17.4 to −23.4% for the far future, while the increase in heat stress for Reuler is 358.7% and for Esch-sur-Alzette 596.9%. The total reduction of heat stress ranges from 5745 h (Reuler) to 7407 h (Esch-sur-Alzette) over ten years regarding the UTCI.

To account for the increasing stress level at prolonged periods of thermal stress exposure, we calculated the duration of "cold stress", "no thermal stress", and "heat stress" (Figures 2 and 3) for both indices at all pseudo stations during all three time slices. To attribute one of the three categories to each day, we identified the most frequent category per day and assigned it as the day's heat stress level. The generated daily data was used to calculate the duration of days in the same category. From the reference period to the near future, the duration of cold stress is reduced by 27.7 to 53.9% (PET), respectively, 0.5 to 15.4% (UTCI). The lowest reduction can always be observed at Reuler, which had the longest periods of consecutive "cold stress" days in the reference period. For the far future, the reduction of consecutive "cold stress" days continues, resulting in a reduction up to 78.3% for PET, respectively, 35.0% for the UTCI. Regarding heat stress, the results for near and far future differ. In the near future,

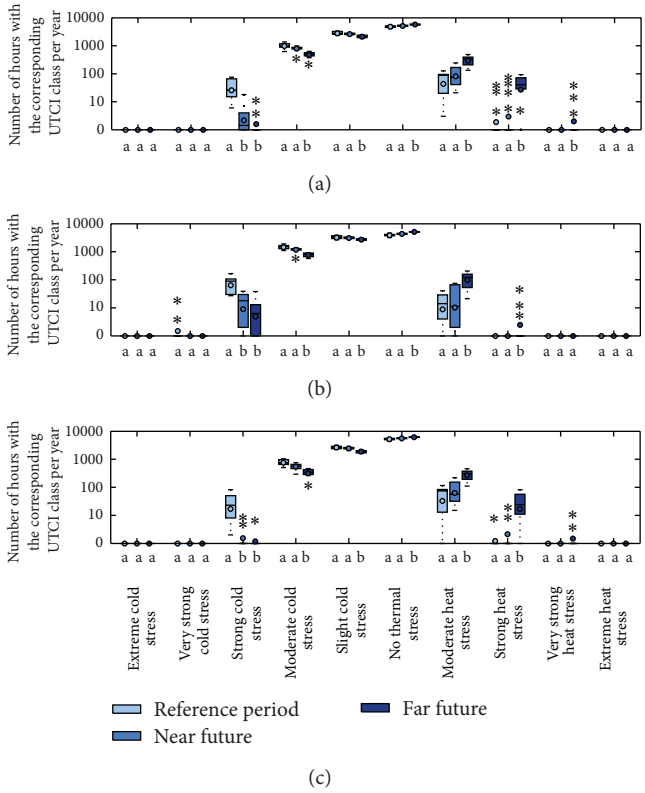

Figure 7: Boxplots of UTCI values for the three periods: reference period 1991–2000, near future 2041–2050, and far future 2091–2100 at the three pseudo stations Esch-sur-Alzette (a), Reuler (b), and Wasserbillig (c). Boxplots show the number of hours within the corresponding UTCI class per year. The whisker length is determined by 1.5 ∗ interquartile range (IQR). All values larger than 1.5 ∗ IQR are treated as outliers. Median values are indicated by the line inside the box, mean values by the dot. Groups that are sharing the same letters are not significantly different ($P < 0.05$).

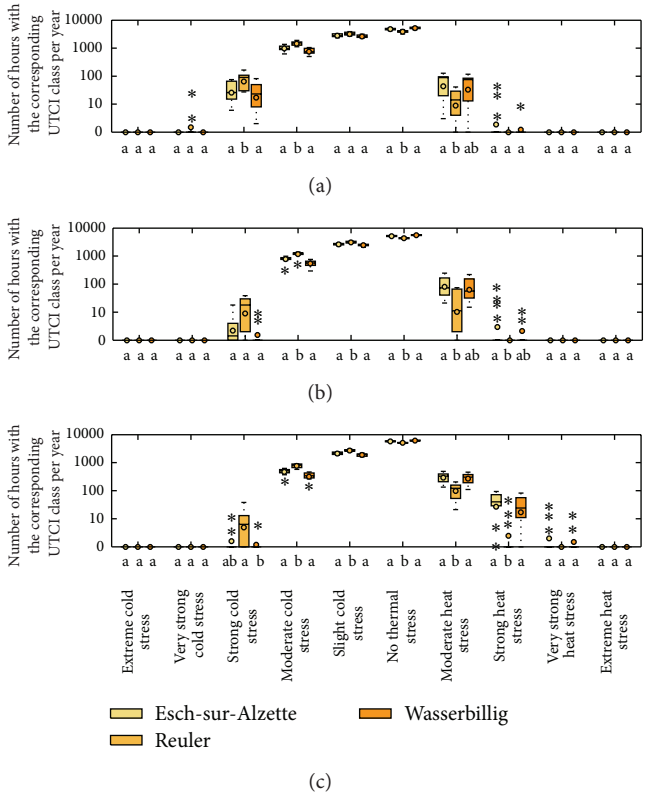

Figure 8: Boxplots of UTCI values for the three pseudo stations Esch-sur-Alzette, Reuler, and Wasserbillig separated by the three periods: reference period 1991–2000 (a), near future 2041–2050 (b), and far future 2091–2100 (c). Boxplots show the number of hours within the corresponding UTCI class per year. The whisker length is determined by 1.5 ∗ interquartile range (IQR). All values larger than 1.5 ∗ IQR are treated as outliers. Median values are indicated by the line inside the box; mean values are highlighted by the dot. Groups that are sharing the same letters are not significantly different ($P < 0.05$).

the length of "heat stress" periods is reduced by 4.0 to 26.7% (PET), respectively, 5.0 to 10.0% (UTCI). In the far future, the length of these periods, however, increases by 29.4 to 34.8% (PET), respectively, 20.0 to 57.1% (UTCI). Only Reuler represents an exception for the PET as the length of "heat stress" periods is reduced by 8.3%.

4. Discussion

Both human-biometeorological indices are capable of reflecting the climate change towards higher air temperatures as a positive trend in air temperature (Figure 4) goes along with a trend towards higher human-biometeorological indices (Figures 5 to 8). These findings correspond well with the results of Molitor et al. [31] who showed that the frost risk in the region of Luxembourg will almost disappear until the end of the century and the finding of Matzarakis et al. [10] who found a strong increase in heat stress based on the REMO (Regional Model of the Max Planck Institute for Meteorology, Hamburg) data sets. In addition, Junk et al. [11] concluded that there is not only an increase in the average air temperature or human-biometeorological index, but also an increased duration of hot periods in the future. This indicates a possible underestimation of heat stress by only analysing the index classes, as prolonged heat waves cause more severe health outcomes due to the higher thermal stress [32]. Our analysis of the duration of thermal stress showed that the overall stress level in the near future is reduced, while in the far future the duration of heat stress increases. The more frequent occurrence of heat stress, as well as its longer duration, shows the potential health risk of the far future heat stress. In our study we analysed all hours of the day including night time hours as heat stress during night times has been identified as significantly dangerous to human health [33, 34]. This results in less pronounced heat stress, as temperatures over night are usually lower than at daytime. The fact that the projected CLM wind speed results are given at 2-meter height adds to the underestimation of heat stress.

The analysis of the CLM data set in terms of regional differences within Luxembourg showed that the lowest human-biometeorological indices are found in the north of Luxembourg at the pseudo station Reuler throughout all time

periods, whilst the highest occurrence of hot index classes in both human-biometeorological indices can be found in Esch-sur-Alzette. These findings are in line with the results from the REMO model analysed by Matzarakis et al. [10]. Regional differences that are already present in the reference period remain throughout the following time slices in most cases. There are two exceptions. The first one is the "slight cold stress" PET class, where the difference between Reuler and Esch-sur-Alzette becomes no longer significant in the far future. The second one is the "strong cold stress" UTCI class where the difference between Reuler and the two other stations disappears in the near future and becomes a significant difference between Reuler and Wasserbillig in the far future.

In general, the index classes above "no thermal stress" show regional differences in the future periods. The only exception here is the "warm" PET class where an existing regional difference temporarily disappears in the near future, to come back in the far future.

In terms of the periods, where changes in the classes occur, we can distinguish again between the index classes below and above "no thermal stress." The changes in the classes below "no thermal stress" mostly occur in the transition from the reference period to the near future or the far future, while changes in the classes above "no thermal stress" become significant only for the far future.

Our analysis shows that the stress level in total decreases in the future. This is caused by the fact that the absolute number of hours in the cold stress range decreases, while the number of days in the heat stress range does not increase by the same quantity. The global climate change also leads, for the area of Luxembourg, to a higher amount of hours in the "no thermal stress" range for the projected future. As this process continues, hours that are now present in the comfort range might then shift towards heat stress levels. These findings might lead to the conclusion that the climate change including temporarily reduced stress levels, especially reduced cold stress, leads to reduced morbidity and mortality during winter time. According to Donaldson and Keatinge [35, 36], low temperature increases the risk of mortality. In contrast, a recent study by Staddon et al. [37] shows that decreasing cold stress no longer leads to decreasing mortality rates in temperate countries. This is due to the better housing and the fact that people prevent themselves well from being exposed to the winter climate. Staddon et al. [37] identified influenza as the only significant parameter influencing the number of excess winter deaths from 1971 on.

On the other hand, the increasing heat stress is likely to cause an increase in heat related mortality and morbidity [32, 38, 39]. Together with the findings of the increasing duration of heat waves in Luxemburg by Junk et al. [11] it can be assumed that the influences of heat stress tend to be even more severe than assumed by just the number of hours in the heat stress classes.

5. Conclusion

Our study confirms the general decrease in cold stress and the general increase in heat stress for the region of Luxembourg by analysing the human-biometeorological indices PET and UTCI in detail. The analysis revealed that the change in stress levels is caused by significant trends in air temperature and vapour pressure.

It could be shown that there are significant differences in stress levels amongst the different regions of Luxembourg. The coldest climate conditions are found in the "Oesling", a region in the north of the country, resulting in the highest levels of cold stress and the lowest levels of heat stress. The lowest level of cold stress can be found in Esch-sur-Alzette in the "Gutland" region in south Luxembourg, which also exhibits the highest levels of heat stress. The Moselle valley exhibits slightly lower levels of heat stress than found in the "Gutland" region.

Regarding the changes in the index classes, we can distinguish between cold and heat stress. The changes in heat stress tend to already appear in the near future (2041–2050), whereas the heat stress levels changes become statistically significant in the far future (2091–2100).

In total the number of hours in index classes that are considered to be stressful for the human body decreases in the future. This is caused by the fact that the number of hours with cold stress decreases, but the number of hours causing heat stress does not increase by the same amount. To evaluate if this also causes a decrease in thermal stress related mortality and morbidity, further studies for the region are foreseen.

Conflict of Interests

The authors declare that there is no conflict of interests regarding the publication of this paper.

Acknowledgments

The authors gratefully acknowledge the financial support of the National Research Fund in Luxembourg (4965163-FRESHAIR). Parts of the work have been done in the framework of the "Small Particles-environmental behaviour and toxicity of nanomaterials and particulate matter" (SMALL) project. Dr. Lucien Hoffmann and Vanessa Peardon are thanked for final proofreading. COSMO-CLM data were taken from the CLIMPACT Project funded by the National Research Fund of Luxembourg through Grant FNR C09/SR/16.

References

[1] K. R. Smith, A. Woodward, D. Campbell-Lendrum et al., "Human health: impacts, adaptation, and co-benefits," in *Climate Change 2014: Impacts, Adaptation, and Vulnerability*, U. Confalonieri and A. Haines, Eds., chapter 11, IPCC, New York, NY, USA, 2013.

[2] A. Matzarakis and B. Amelung, "Physiological equivalent temperature as indicator for impacts of climate change on thermal comfort of humans," in *Seasonal Forecasts, Climatic Change and Human Health*, M. Thomson, R. Garcia-Herrera, and M. Beniston, Eds., pp. 161–172, Springer, Dordrecht, Netherlands, 2008.

[3] P. T. Nastos and A. Matzarakis, "The effect of air temperature and human thermal indices on mortality in Athens, Greece,"

Theoretical and Applied Climatology, vol. 108, no. 3-4, pp. 591–599, 2012.

[4] P. van der Linden and J. Mitchell, *ENSEMBLES: Climate Change and Its Impacts: Summary of Research and Results from The ENSEMBLES Project*, Met Office Hadlec Centre, Exeter, UK, 2009.

[5] D. Jacob, J. Petersen, B. Eggert et al., "EURO-CORDEX: new high-resolution climate change projections for European impact research," *Regional Environmental Change*, vol. 14, no. 2, pp. 563–578, 2014.

[6] M. Beniston, D. B. Stephenson, O. B. Christensen et al., "Future extreme events in European climate: an exploration of regional climate model projections," *Climatic Change*, vol. 81, no. 1, supplement, pp. 71–95, 2007.

[7] R. S. Kovats and S. Hajat, "Heat stress and public health: a critical review," *Annual Review of Public Health*, vol. 29, pp. 41–55, 2008.

[8] K. Goergen, J. Beersma, L. Hoffmann, and J. Junk, "ENSEMBLES-based assessment of regional climate effects in Luxembourg and their impact on vegetation," *Climatic Change*, vol. 119, no. 3-4, pp. 761–773, 2013.

[9] J. Junk, M. Eickermann, K. Görgen, M. Beyer, and L. Hoffmann, "Ensemble-based analysis of regional climate change effects on the cabbage stem weevil (*Ceutorhynchus pallidactylus* (Mrsh.)) in winter oilseed rape (*Brassica napus* L.)," *Journal of Agricultural Science*, vol. 150, no. 2, pp. 191–202, 2012.

[10] A. Matzarakis, J. Rammelberg, and J. Junk, "Assessment of thermal bioclimate and tourism climate potential for central Europe—the example of Luxembourg," *Theoretical and Applied Climatology*, vol. 114, no. 1-2, pp. 193–202, 2013.

[11] J. Junk, A. Matzarakis, A. Ferrone, and A. Krein, "Evidence of past and future changes in health-related meteorological variables across Luxembourg," *Air Quality, Atmosphere & Health*, vol. 7, no. 1, pp. 71–81, 2014.

[12] C. R. de Freitas and E. A. Grigorieva, "A comprehensive catalogue and classification of human thermal climate indices," *International Journal of Biometeorology*, vol. 59, no. 1, pp. 109–120, 2015.

[13] H. Mayer and P. Höppe, "Thermal comfort of man in different urban environments," *Theoretical and Applied Climatology*, vol. 38, no. 1, pp. 43–49, 1987.

[14] G. Jendritzky, R. de Dear, and G. Havenith, "UTCI—why another thermal index?" *International Journal of Biometeorology*, vol. 56, no. 3, pp. 421–428, 2012.

[15] O. Lesne, P. Sicard, and C. Talbot, *PASODOBLE Validation Report—Observation and Alert Platform for Public Health at East-PACA Regional Level*, 2013, Edited by: A. De Rudder.

[16] S. Muthers, A. Matzarakis, and E. Koch, "Climate change and mortality in Vienna—a human biometeorological analysis based on regional climate modeling," *International Journal of Environmental Research and Public Health*, vol. 7, no. 7, pp. 2965–2977, 2010.

[17] A. Urban and J. Kyselý, "Comparison of UTCI with other thermal indices in the assessment of heat and cold effects on cardiovascular mortality in the Czech Republic," *International Journal of Environmental Research and Public Health*, vol. 11, no. 1, pp. 952–967, 2014.

[18] N. Nakicenovic and R. Swart, *Special Report on Emissions Scenarios: A Special Report of the Working Group III of the Intergovernmental Panel on Climate Change*, Cambridge University Press, Cambridge, UK, 2000.

[19] I. Ott, D. Duethmann, J. Liebert et al., "High-resolution climate change impact analysis on medium-sized river catchments in germany: an ensemble assessment," *Journal of Hydrometeorology*, vol. 14, no. 4, pp. 1175–1193, 2013.

[20] A. Matzarakis and H. Mayer, "Another kind of environmental stress: thermal stress," *WHO Colloborating Centre for Air Quality Management and Air Pollution Control, Newsletters*, vol. 18, pp. 7–10, 1996.

[21] K. Błazejczyk, G. Jendritzky, P. Bröde et al., "An introduction to the Universal Thermal Climate Index (UTCI)," *Geographia Polonica*, vol. 86, no. 1, pp. 5–10, 2013.

[22] M. Baldauf, A. Seifert, J. Förstner, D. Majewski, M. Raschendorfer, and T. Reinhardt, "Operational convective-scale numerical weather prediction with the COSMO model: Description and sensitivities," *Monthly Weather Review*, vol. 139, no. 12, pp. 3887–3905, 2011.

[23] C. Piani, J. O. Haerter, and E. Coppola, "Statistical bias correction for daily precipitation in regional climate models over Europe," *Theoretical and Applied Climatology*, vol. 99, no. 1-2, pp. 187–192, 2010.

[24] A. Matzarakis, F. Rutz, and H. Mayer, "Modelling radiation fluxes in simple and complex environments—application of the RayMan model," *International Journal of Biometeorology*, vol. 51, no. 4, pp. 323–334, 2007.

[25] WMO, *WMO Statement on The Status of The Global Climate in 2013*, WMO, Geneva, Switzerland, 2013.

[26] C. Chotamonsak, E. P. Salathé, J. Kreasuwan, S. Chantara, and K. Siriwitayakorn, "Projected climate change over Southeast Asia simulated using a WRF regional climate model," *Atmospheric Science Letters*, vol. 12, no. 2, pp. 213–219, 2011.

[27] M. N. Nũez, S. A. Solman, and M. F. Cabré, "Regional climate change experiments over southern South America. II: climate change scenarios in the late twenty-first century," *Climate Dynamics*, vol. 32, no. 7-8, pp. 1081–1095, 2009.

[28] S. Hajat and T. Kosatky, "Heat-related mortality: a review and exploration of heterogeneity," *Journal of Epidemiology and Community Health*, vol. 64, no. 9, pp. 753–760, 2010.

[29] P. K. Sen, "Estimates of the regression coefficient based on Kendall's tau," *Journal of the American Statistical Association*, vol. 63, no. 324, pp. 1379–1389, 1968.

[30] P. Bröde, K. Błażejczyk, D. Fiala et al., "The universal thermal climate index UTCI compared to ergonomics standards for assessing the thermal environment," *Industrial Health*, vol. 51, no. 1, pp. 16–24, 2013.

[31] D. Molitor, A. Caffarra, P. Sinigoj, I. Pertot, L. Hoffmann, and J. Junk, "Late frost damage risk for viticulture under future climate conditions: a case study for the Luxembourgish winegrowing region," *Australian Journal of Grape and Wine Research*, vol. 20, no. 1, pp. 160–168, 2014.

[32] E. M. Kilbourne, K. Choi, T. S. Jones, and S. B. Thacker, "Risk factors for heatstroke. A case-control study," *Journal of the American Medical Association*, vol. 247, no. 24, pp. 3332–3336, 1982.

[33] A. Matzarakis, M. de Rocco, and G. Najjar, "Thermal bioclimate in Strasbourg—the 2003 heat wave," *Theoretical and Applied Climatology*, vol. 98, no. 3-4, pp. 209–220, 2009.

[34] D. O. Astrom, B. Forsberg, and J. Rocklov, "Heat wave impact on morbidity and mortality in the elderly population: a review of recent studies," *Maturitas*, vol. 69, no. 2, pp. 99–105, 2011.

[35] G. C. Donaldson and W. R. Keatinge, "Excess winter mortality: influenza or cold stress? Observational study," *British Medical Journal*, vol. 324, no. 7329, pp. 89–90, 2002.

[36] G. C. Donaldson and W. R. Keatinge, "Early increases in ischaemic heart disease mortality dissociated from and later changes associated with respiratory mortality after cold weather in south east England," *Journal of Epidemiology and Community Health*, vol. 51, no. 6, pp. 643–648, 1997.

[37] P. L. Staddon, H. E. Montgomery, and M. H. Depledge, "Climate warming will not decrease winter mortality," *Nature Climate Change*, vol. 4, no. 3, pp. 190–194, 2014.

[38] K. M. A. Gabriel and W. R. Endlicher, "Urban and rural mortality rates during heat waves in Berlin and Brandenburg, Germany," *Environmental Pollution*, vol. 159, no. 8-9, pp. 2044–2050, 2011.

[39] M. E. Loughnan, N. Nicholls, and N. J. Tapper, "When the heat is on: threshold temperatures for AMI admissions to hospital in Melbourne Australia," *Applied Geography*, vol. 30, no. 1, pp. 63–69, 2010.

Hindawi Publishing Corporation
Advances in Meteorology
Volume 2015, Article ID 324502, 11 pages
http://dx.doi.org/10.1155/2015/324502

Research Article

Changing Trends in Meteorological Elements and Reference Evapotranspiration in a Mega City: A Case Study in Shenzhen City, China

Haijun Liu, Xian Zhang, Liwei Zhang, and Xuming Wang

College of Water Sciences, Beijing Normal University, Beijing 100875, China

Correspondence should be addressed to Haijun Liu; shanxilhj@bnu.edu.cn

Received 26 September 2014; Revised 3 January 2015; Accepted 5 January 2015

Academic Editor: Andreas Matzarakis

Shenzhen city was a farmland region before 1978, and it then developed to a mega city in China. This type of change in city can greatly affect the climatic conditions. In this study, the daily, monthly, and annual climatic variables and the reference crop evapotranspiration (ET_0) for Shenzhen from 1954 to 2012 were computed using the FAO Penman-Monteith equation (PM), and these parameters were analyzed to study the temporal trends of ET_0 and meteorological factors. The trends and the time points of abrupt changes of ET_0 and meteorological factors were tested using Mann-Kendall methods. Results show that, in the past 59 years, the annual ET_0 first decreased from 1954 to 1978, then increased from 1979 to 1990, and now varied slightly after 1990. The mean air temperature rose gradually, and the relative humidity decreased as a whole. These trends finally resulted in an increasing trend in vapor pressure deficit (VPD). The wind speed showed a slightly decreasing trend. Both the annual total sunshine duration and net radiation showed trends of rapid decline. ET_0 change is sensitive to the hours of sunshine and VPD. The significant increase in ET_0 after 1979 was mainly due to the increased air temperature and decreased relative humidity.

1. Introduction

It has been confirmed that there has been a change in the global climate that is closely related to increases in the concentrations of atmospheric greenhouse gases (CO_2, NO_x) [1]. These changes in climate are expected to cause major changes in various climatic variables, such as precipitation, air temperature, relative humidity, and solar radiation [2]. According to the IPCC report [1], the air temperature at the earth's surface level increased by 0.74°C from 1906 to 2005, and this rising trend of the air temperature is likely to continue in the 21st century, which will cause changes in the hydrological cycle by affecting precipitation and evaporation [3, 4]. Bates et al. (2008) pointed out that, over the last century, precipitation has primarily increased over land in high northern latitudes but decreased from 10°S to 30°N since the 1970s and globally the area of land classified as very dry has more than doubled since the 1970s due to climate change [4].

The trends for changes in the city climate may differ from those for farmland and forest regions because of changes in the energy balance caused by the surface albedo and components of air. In cities, the ground surface is primarily covered by concrete and asphalt, and the green ground surface and water surface only account for a small portion of the total area. For example, it has been reported that the percentage of green ground surface and water surface of the total city area is approximately 20.7% for Beijing City (2012), 38.3% for Shanghai City (2012), and 42.6% for Tianjin City (2012). Due to the high albedo rate and low heat capacity of concrete and asphalt compared to those of green surfaces and water bodies, the air temperature is recorded as much higher in a city than in farmland [1, 4–7]. The climate is also dryer in cities than in farmland due to the lower amount of water vapor caused by smaller evaporative surface prevailing in cities [1, 4, 5].

The composition of the air may also change the energy balance in cities. With city development, a larger number of

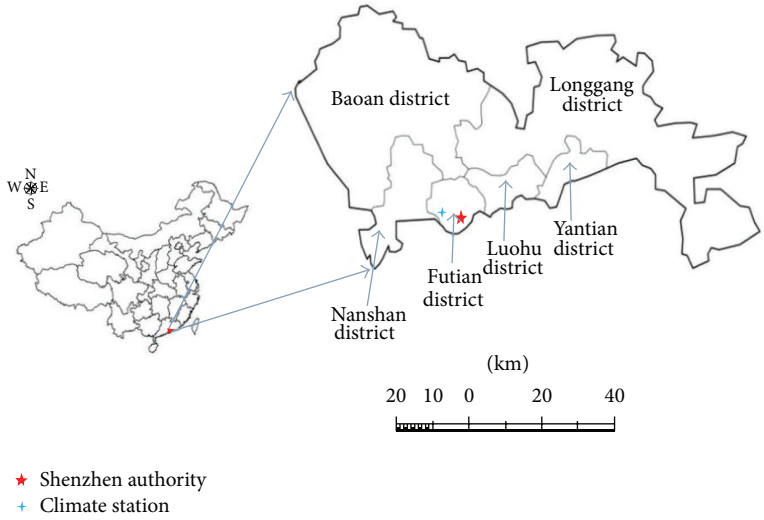

Figure 1: Schematic diagram of the research region (Shenzhen) and the meteorological station.

particles and particles with more complicated compositions are emitted into the air. In Beijing City, it has been reported that vehicular emissions of HC, CO, and NO_x were estimated to reach 13.33×10^4, 100.02×10^4, and 7.55×10^4 tons, respectively, in 2005 [8], and vehicle emissions in the urban area made up 75% of the total emissions in Beijing in 2002 for vehicle-related pollutants [9]. In recent years, the "gray sky" phenomenon caused by fine particles (particles less than 2.5 μm in aerodynamic diameter, or $PM_{2.5}$) is an increasing public concern, caused by fossil fuels that play a decisive role in the development of economic and urban growth in the current period in China. In Shanghai, for example, the annual average $PM_{2.5}$ concentrations in 2005 reached 56 $\mu g/m^3$, which was much higher than the value proposed by the World Health Organization Air Quality Guidelines (WHO AQG) [10]. This phenomenon was also found in certain other areas abroad. Aziz and Bajwa (2008) showed that the major source of urban air pollution is the growing motor vehicular emission [11]. They pointed out that motor vehicular emission is a mixture of five key pollutants, namely, carbon monoxide (CO), hydrocarbons (HC), particulate matter (PM_{10}), nitrogen oxides (NO_x), and ozone (O_3).

Shenzhen city constitutes a special place in Chinese history. Before 1978, it was a small town, occupied by farmland and fishing areas, with a population of approximately 314,000 permanent residents. After that year, it was chosen as the first Special Economic Zone in China, after which the city developed quickly; nowadays it is one of the four largest cities in China. By the end of 2012, the city had a population of 10.55 million permanent residents, approximately 35 times the number compared with 1978 and it had a gross domestic product (GDP) of 20937 million dollars, approximately 6600 times higher than that in 1978. From 1979 to 2012, the farmland area decreased from 63553 to 8520 ha, whereas the construction area increased from 29 to 5260 ha.

We suppose that the urban development of Shenzhen may have altered the heat balance of the ground surface, thereby influencing climatic variables as well as the reference evapotranspiration changes.

2. Data and Methods

2.1. Site. Shenzhen city (22°27′–22°52′N, 113°46′–114°47′E) lies in the southern region of Guangdong province in southeastern China (Figure 1). The area administered by the Shenzhen municipal government is 2,020 km^2. Shenzhen has a typical subtropical maritime climate with plenty of rain, a mild climate, and numerous sunshine hours. The yearly mean precipitation is 1914 mm and the rainy season can range between April and September. The minimum precipitation is 912 mm (1962) and the maximum is 2747 mm (2001). The annual mean air temperature is 22.3°C, with a minimum daily air temperature of 0.2°C (February 11, 1957) and a maximum of 38.7°C (July 10, 1980). The mean yearly total sunshine hours are 2120 hours.

2.2. Meteorological Data. All meteorological data were collected from a national climatic station (22°33′N, 114°06′E, 182 m above surface level) (Figure 1). The meteorological data include the atmospheric pressure, daily values of the precipitation, the mean, maximum, and minimum air temperatures, mean relative humidity, mean wind speed, and sunshine hours from 1954 to 2012.

2.3. Methods

2.3.1. Reference Crop Evapotranspiration. The reference crop evapotranspiration (ET_0) was calculated using the FAO Penman-Monteith method (hereafter denoted as PM). The PM method is [12]

$$ET_0 = \frac{0.408\Delta\left(R_n - G\right) + \gamma\left(900/\left(T + 273\right)\right)U_2\left(e_s - e_a\right)}{\Delta + \gamma\left(1 + 0.34U_2\right)}, \quad (1)$$

where ET_0 is the reference crop evapotranspiration, mm·day^{-1}; R_n is the net radiation, MJ·m^{-2}·day^{-1}; G is the soil heat flux that can be neglected at daily intervals [12], MJ·m^{-2}·day^{-1}; γ is the psychrometric constant, kPa·°C^{-1}; U_2 is the wind speed measured at 2 m above ground surface, m·s^{-1}; e_s and e_a are the saturation and the actual vapor pressure, kPa; and Δ is the slope of the saturation vapor pressure curve at the air temperature, kPa·°C^{-1}. The monthly or yearly total ET_{0s} is the sum of daily ET_0 in an entire month or year.

The net radiation was not directly measured at Shenzhen station. Therefore, the net radiation was calculated using data for the daily sunshine hours and the maximum and minimum air temperatures, following the method suggested by Allen et al. (1998) [12].

The actual daily vapor pressure (e_a) and vapor pressure deficit (VPD) were based on the daily mean air temperature and relative humidity and were calculated in the following way:

$$\begin{aligned} e_a &= \mathrm{RH} \times e^o\left(T_{\mathrm{mean}}\right), \\ \mathrm{VPD} &= (1 - \mathrm{RH}) \times e^o\left(T_{\mathrm{mean}}\right), \end{aligned} \tag{2}$$

where RH is daily mean relative humidity, %; T_{mean} is the daily mean temperature, °C; and $e^o(T_{\mathrm{mean}})$ is saturated vapor pressure at T_{mean}, kPa. $e^o(T_{\mathrm{mean}})$ is calculated as follows:

$$e^o\left(T_{\mathrm{mean}}\right) = 0.6108 \exp\left(\frac{17.27 T_{\mathrm{mean}}}{T_{\mathrm{mean}} + 237.3}\right). \tag{3}$$

2.3.2. Mann-Kendall Test. The Mann-Kendall test is one of the most widely used nonparametric tests to detect significant trends in climatic variables and potential evapotranspiration in time series [13–15].

Mann-Kendall Test for Temporal-Trend Analysis. The Mann-Kendall test is based on the statistic S [16]:

$$S = \sum_{i=1}^{N-1} \sum_{j=i+1}^{N} \mathrm{sign}\left(x_j - x_i\right), \tag{4}$$

where x_i and x_j are two generic sequential data values of the variable, N is the length of the data set, and the sign (X) takes the following values:

$$\mathrm{sign}\,(X) = \begin{cases} +1 & \text{if } X > 0 \\ 0, & \text{if } X = 0 \\ -1 & \text{if } X < 0. \end{cases} \tag{5}$$

A positive S in (4) represents a positive trend in the observed data series, and vice versa. Under the null hypothesis of no trend in the data, H_0, the statistic S is approximately normally distributed with the mean $E(S) = 0$. For data sets with more than ten values, the variance associated with the Mann-Kendall statistic S (VAR(S)) can be calculated after considering the distribution as very close to normal:

$$\begin{aligned} \mathrm{VAR}\,(S) = \frac{1}{18} \Bigg[& N(N-1)(2N+5) \\ & - \sum_{p=1}^{q} t_p \left(t_p - 1\right)\left(2t_p + 5\right) \Bigg], \end{aligned} \tag{6}$$

where q is the number of tied groups and t_p is the number of data values in the pth group.

The values of S and VAR(S) are used to compute the test statistic Z as follows:

$$Z = \begin{cases} \dfrac{S-1}{\sqrt{\mathrm{VAR}\,(S)}} & \text{if } S > 0 \\ 0, & \text{if } S = 0 \\ \dfrac{S+1}{\sqrt{\mathrm{VAR}\,(S)}} & \text{if } S < 0. \end{cases} \tag{7}$$

The presence of a statistically significant trend is evaluated using the Z value. A positive (negative) value of Z indicates an upward (downward) trend. The statistic Z has a normal distribution. To test for either an upward or downward monotonic trend (a two-tailed test) at the α level of significance, H_0 is rejected if the absolute value of Z is greater than $Z_{1-\alpha/2}$, where $Z_{1-\alpha/2}$ is obtained from the standard normal cumulative distribution tables. The tested significance level, α, was set to 0.01 in this study.

Mann-Kendall Test for Mutation Point Analysis. We suppose that a time series $(x_1, x_2, \ldots, x_n)$ exists. One order series, m_i, is constructed to represent the sample accumulative number of $x_i > x_j$ $(1 \le j \le i)$. d_k is defined in the following way:

$$d_k = \sum_{1}^{k} m_i \quad (2 \le k \le n). \tag{8}$$

The mean value and variance of d_k can be approximately expressed as follows:

$$E\left(d_k\right) = \frac{k(k-1)}{4}, \tag{9}$$

$$\mathrm{var}\left(d_k\right) = \frac{n(n-1)(2n+5)}{72}, \quad (2 \le k \le n). \tag{10}$$

Under the hypothesis that the time series is random and independent, the statistic is defined in the following way:

$$\mathrm{UF}_k = \frac{d_k - E\left(d_k\right)}{\mathrm{var}\left(d_k\right)} \quad (k = 1, 2, \ldots, n). \tag{11}$$

Given the significance level of α, $|\mathrm{UF}_k| > \mathrm{UF}_{\alpha/2}$ means that the series has an obvious change trend. Time series x_i is arranged in reverse order and is calculated with (9), while ensuring that

$$\begin{aligned} \mathrm{UB}_k &= -\mathrm{UF}_k \\ k &= n + 1 - k. \end{aligned} \tag{12}$$

By analyzing the statistical series UF_k and UB_k, the change trend of series x_i can be further analyzed, and the mutation time and region can be determined. $UF_k > 0$ indicates that the series tends to increase, and $UF_k < 0$ indicates that the series tends to decrease. When the series exceed the credibility line, they exhibit an obvious increasing or decreasing trend. If an intersection point exists between the curves of UF_k and UB_k and falls between the credibility lines, the corresponding time of the intersection point is the starting moment of mutation.

In this study, the statistical analysis software DPS (version DPS 14.5, developed by Zhejiang University, China) was used to analyze the mutation point of the temporal trends of ET_0 and the meteorological variables [17]. The credibility line is drawn at the significance level of $\alpha = 0.01$.

2.3.3. Sensitivity-Analysis Method. Sensitivity analysis was employed to identify the climatic variables that most strongly influence ET_0 following the method proposed by Möller et al. (2004) and Liu et al. (2014) [15, 18]. In this study, the temporal trends of most climatic variables showed abrupt change in 1978, and the climatic variables during 1954–1978 were significantly ($P < 0.01$) higher or lower than those during 1992–2012; see Sections 3.1.1 to 3.1.6 in the following text. Hence, data during these two periods were used to assess the climate change impact on ET_0. The detailed processes of the sensitivity analysis are described as follows: (1) the mean values of the air temperature, relative humidity, wind speed, and sunshine hours in each day of a year were calculated using climatic data from 1954 to 1978, and the corresponding daily and annual ET_0 were calculated using these mean daily values and the Penman-Monteith method. The mean daily value for each climatic variable was set as the reference climatic variable, and the calculated ET_0 was set as the reference ET_0. (2) The sensitivity of each climatic variable to ET_0 was analyzed by comparing the reference ET_0 and the ET_0 calculated by changing one variable with a rate of −15, −10, −5, 5, 10, and 15% and keeping the other variables identical to the reference climatic variables. Then, a figure was drawn based on these data (Figure 10). (3) The mean values of the air temperature, relative humidity, wind speed, and sunshine hours in each day of a year were calculated using climatic data from 1992 to 2012. The corresponding ET_0 was calculated by setting one climatic variable as those during 1992 and 2012 and the others as the reference climatic variable (in step (1)) and then calculating ET_0 and comparing it with the reference ET_0. The relative change in ET_0 caused by each climatic change during 1992 to 2012 is marked in Figure 10. The most sensitive variable to a change in ET_0 is determined by comparing the relative ET_0 changes caused by each variable.

3. Results

3.1. Annual Distributions and Trends in the Changes of Climatic Variables

3.1.1. Sunshine Hours and Solar Radiation. The annual sunshine duration and annual total radiation during the period from 1954 to 2012 are given in Figures 2 and 3. It can be seen in Figure 2 that the annual sunshine duration showed

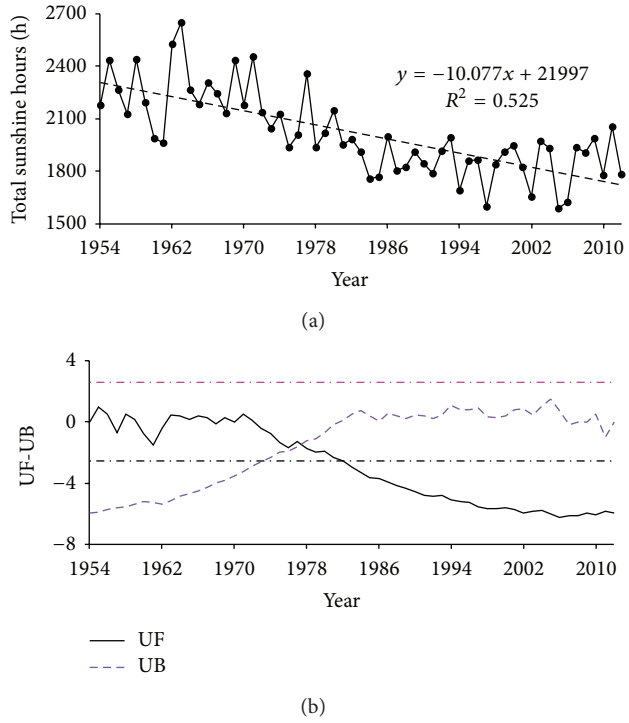

Figure 2: Temporal change in the yearly sunshine duration (a) and the trend results from the Mann-Kendall method (b).

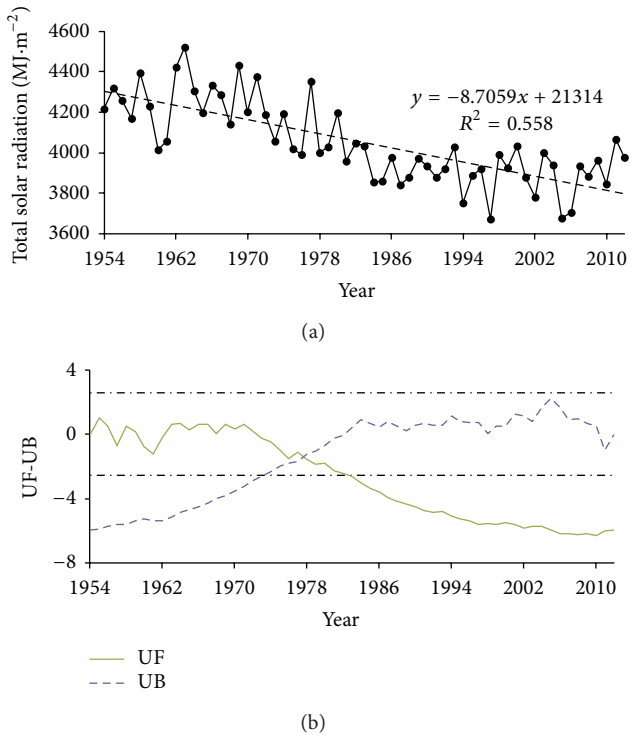

Figure 3: Temporal trend in the yearly total solar radiation (a) and the trend results from the Mann-Kendall method (b).

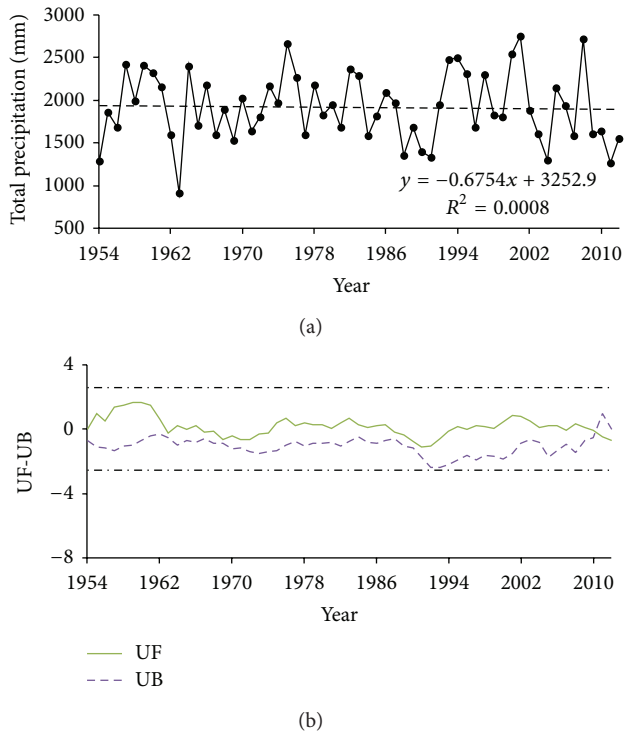

Figure 4: Temporal trend of the yearly total precipitation (a) and the trend results from the Mann-Kendall method (b).

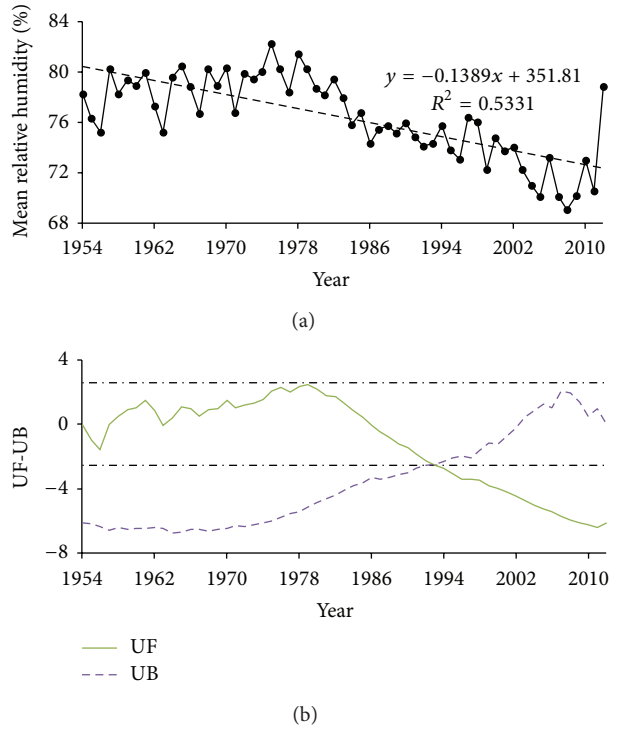

Figure 5: Temporal trend of the mean relative humidity (a) and the trend results from the Mann-Kendall method (b).

an obvious decline, which decreased from 2651 to 1590 hours with an average of 2014 hours (Figure 2(a)). Through the two-tailed test (UF and UB lines), we found that the decreasing trend of the sunshine hours is obvious for the period from 1982 to 2012, and the increasing trend is obvious for the period of 1954 to 1973. Similar to the trend for the sunshine duration, the solar radiation also showed an obvious declining trend, which ranges from 3672 to 4520 MJ·m^{-2}, with an average of 4050 MJ·m^{-2} (Figure 3(a)). The two-tailed test showed that the solar radiation values from 1982 to 2012 were significantly lower than those from 1954 to 1973. The shifting mutation points of the sunshine duration and the solar radiation are all found in 1978 using the Mann-Kendall mutational test ($P < 0.01$) (Figures 2 and 3(b)).

3.1.2. Precipitation. The annual total precipitation values during the period from 1954 to 2012 are given in Figure 4. It can be seen in Figure 4 that the highest precipitation value was 2747 mm in 2001 and the lowest was 912 mm in 1963 (Figure 4(a)). The annual mean was 1914 mm during the period from 1954 to 2012. The precipitation varied greatly over the years, whereas the trend test showed that the temporal trend of the annual precipitation is not significant, and a mutation point has not been tested (Figure 4(b)).

3.1.3. Relative Humidity. The daily mean relative humidity during the period from 1954 to 2012 is given in Figure 5. It can be seen that the daily mean relative humidity increased slightly in the first 20 years followed by an obvious decline after 1978; the range is from 69.1% to 82.2%, and the average is 76.4% (Figure 5(a)). From the Mann-Kendall test ($P < 0.01$), we found that the averaged relative humidity value during the period from 1992 to 2012 is significantly ($P < 0.01$) lower than the period from 1954 to 1992.

3.1.4. Air Temperature. The mean air temperature during the period from 1954 to 2012 is shown in Figure 6. According to Figure 6 the mean air temperature showed an obviously increasing trend, and the values range from 21.5 to 23.9°C with an average value of 22.6°C (Figure 6(a)). The statistical result showed that the mean air temperature over the period from 1990 to 2012 is significantly ($P < 0.01$) higher than those over the period from 1954 to 1983 (Figure 6(b)).

3.1.5. Vapor Pressure Deficit. Figure 7(a) shows the temporal trend of the vapor pressure deficit (VPD) during the period from 1954 to 2012. VPD ranges from 0.449 to 0.867 kPa, and the average is 0.648 kPa. There is no significant temporal trend for VPD from 1954 to 1977, and after 1978, VPD increased greatly. It was found that the average VPD during the period from 1992 to 2012 is significantly ($P < 0.01$) higher than the values from 1954 to 1991, according to the Mann-Kendall mutational test.

3.1.6. Wind Speed. The annual mean wind speed varied greatly during the period from 1954 to 2012 (Figure 8(a)). Clearly, decreasing trends were found from 1954 to 1977 and from 1987 to 2012, whereas increasing trend was found from

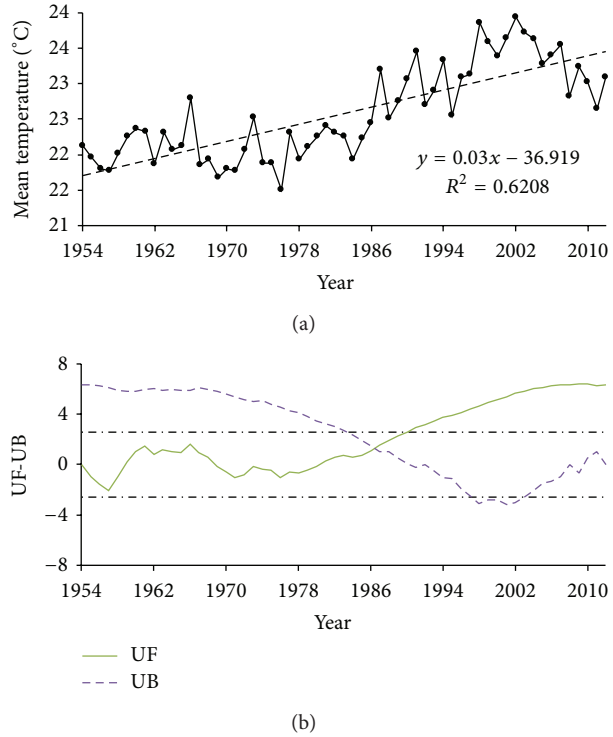

Figure 6: Temporal trend of the mean temperature (a) and the trend results from the Mann-Kendall method (b).

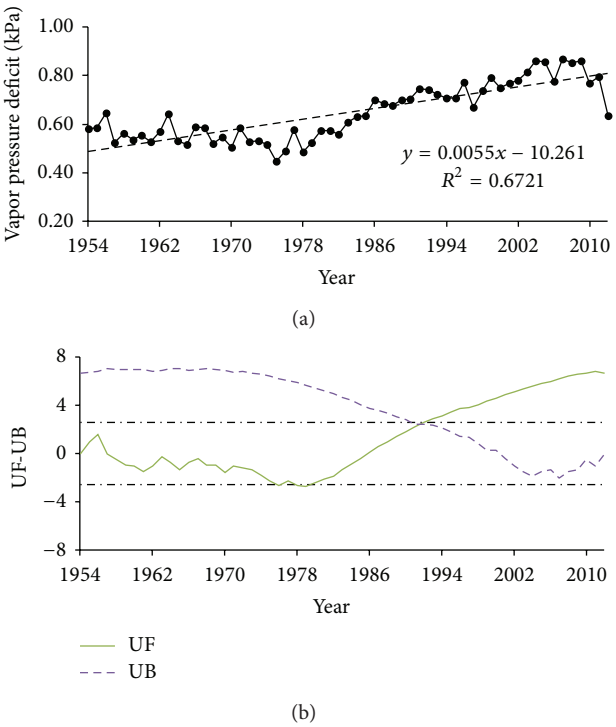

Figure 7: Temporal trend of the mean vapor pressure deficit (a) and the trend results from the Mann-Kendall method (b).

1978 to 1986. It can be seen in Figure 8(a) that the maximum wind speed was 3.72 m/s in 1954, the minimum was 1.78 m/s

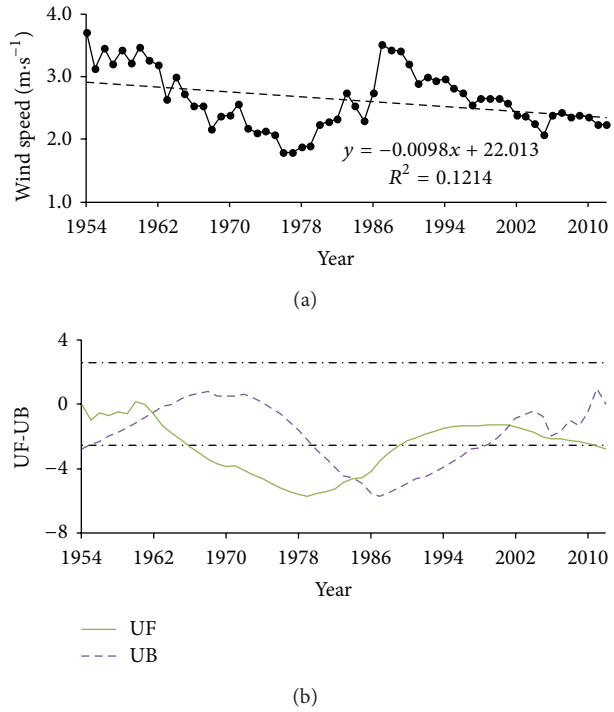

Figure 8: Temporal trend of the mean wind speed (a) and the trend results from the Mann-Kendall method (b).

in 1977, and the annual mean was 2.60 m/s. The statistical results show that there were no significant temporal trends from 1954 to 2012.

3.2. Reference Evapotranspiration (ET_0). The annual total ET_0 varied from 946 to 1373 mm with a total mean of 1187 mm. Figure 9(a) shows the change in the annual ET_0 over the past 59 years. According to Figure 9(a) ET_0 firstly decreased gradually from 1954 to 1978, then increased from 1978 to 1992, and lastly varied slightly after 1992. From 1954 to 1978 the annual total ET_0 decreased from 1285 to 946 mm with a mean value of 1110 mm; afterwards, the annual total ET_0 increased from 1118 to 1373 mm with a mean value of 1284 mm during the period from 1992 to 2012. The mean ET_0 in the period of 1992–2012 increased by 15.6% over those in the period of 1954–1978, indicating a great increase in evaporation potential. The statistical results based on the Mann-Kendall test ($P < 0.01$) (Figure 9(b)) showed that ET_0 during the period from 1972 to 1987 was significantly lower than that from 2001 to 2012, which was significantly higher than those in other periods. The shifting mutation point for ET_0 is found at 1992 by the Mann-Kendall test (Figure 9(b)).

For analyzing the yearly ET_0 distribution, the total ET_0 for each month was calculated and the averaged month total ET_{0s} in period of 1954–1978 and 1992–2012 were calculated, respectively. The monthly ET_0 distributions in these two periods and in all study period (1954–2012) are showed in Figure 10. The highest monthly ET_0 generally appears in July and August, and the lowest in January and February. Monthly ET_0 from May to November are generally higher than 100 mm,

Table 1: Mean values of each climatic variable in the periods of 1954–1978 and 1992–2012 and changes of each climatic variable to ET_0 variation.

	Air temperature ˚C	Relative humidity %	Sunshine hours Hours/day	Wind speed m/s
Mean values				
1954–1978	22.0	78.9	6.08	2.68
1992–2012	23.3	73.2	5.04	2.52
Climate change amount	−5.7	1.3	−0.16	−1.04
Climate change percentage (%)	−7.2	5.9	−6.0	−17.1
ET_0 change percentage caused by each climatic variable (%)	14.6	5.3	−1.3	−3.2

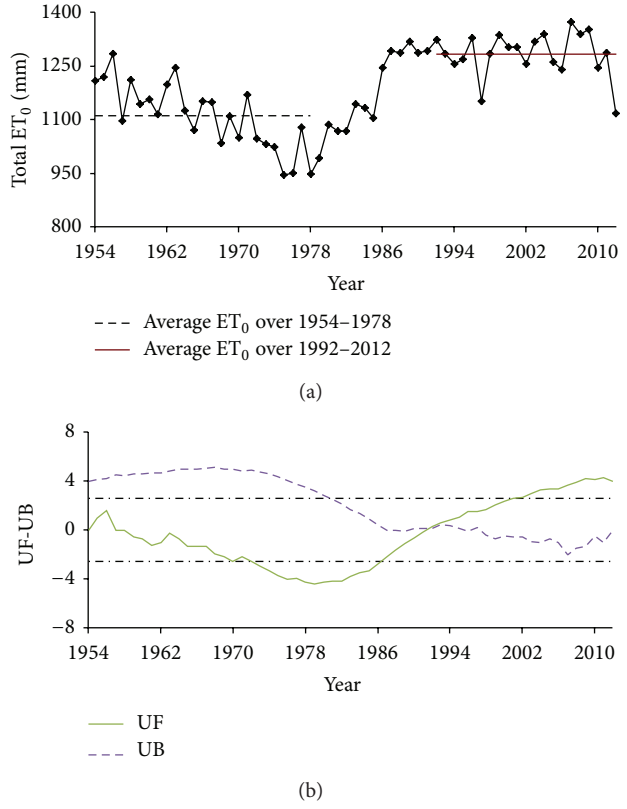

Figure 9: Temporal trend of the yearly total ET_0 (a) and the trend results from the Mann-Kendall method (b).

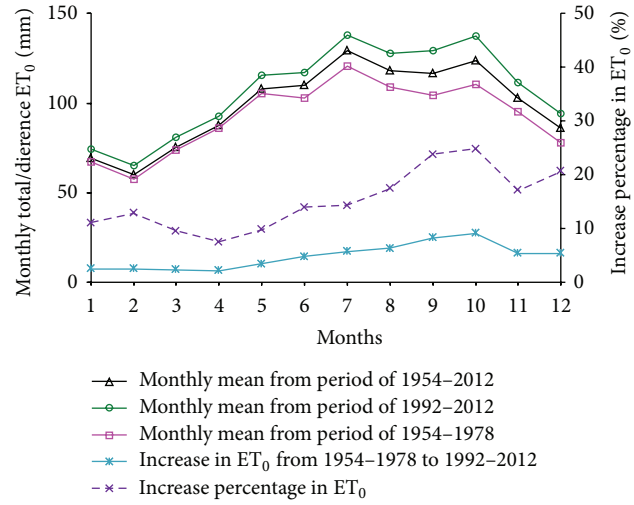

Figure 10: Yearly distribution of ET_0 averaged in the periods of 1954–1978, 1992–2012, and 1954–2012. ET_0 increase amount and the corresponding increase percentage in each month from periods of 1954–1978 to 1992–2012 were showed.

and the total ET_0 in this period accounts for approximately 1/3 the yearly total. Monthly ET_{0s} in the period of 1992–2012 are all higher by 5–30 mm or 7–25% than those in the 1954–1978 period. The most increases in monthly ET_0 are found in period from July to September, and the lowest from January to April with an increase of less than 7 mm. Therefore, the great increase in ET_0 in summer (generally from June to October) makes main contribution to yearly ET_0.

3.3. Sensitivity Analysis of ET_0 to the Change of Climatic Variables. Figures 2 to 8 show that most mutation points for most of the climatic variables were found during the period from 1978 to 1992, and the mean values of the climatic variables over the period from 1954 to 1978 were significantly ($P < 0.01$) higher/lower than those during the period from 1992 to 2012. Hence, the mean values of each variable during the two periods from 1954 to 1978 and from 1992 to 2012 were calculated and used to analyze their change effects on the ET_0 changes, following the method described in Section 2.3.3. The summary of the mean values of each climate and their effects on ET_0 were listed in Table 1 and Figure 11.

It can be seen in Table 1 that the daily mean relative humidity, daily mean air temperature, wind speed, and sunshine hours from the period of 1954–1978 to 1992–2012 were −7.2, 5.9, −6.0, and −17.1%, respectively, which resulted in ET_0 changes by 14.6, 5.3, −1.3, and −3.2%, respectively. The contribution of each climate variable's variation from 1954–1978 to 1992–2012 to ET_0 change is shown in Figure 11. It can be found that decrease in relative humidity accounted for approximately 60% variation in ET_0, followed by temperature increase with a contribution of 22%, and sunshine hours reduction of 13%. Wind speed accounted for 6% variation in ET_0. Similarly in another mega city, Beijing in China, the order of climate change to ET_0 variation from main to weak is air temperature, relative humidity, sunshine hours, and wind speed [14].

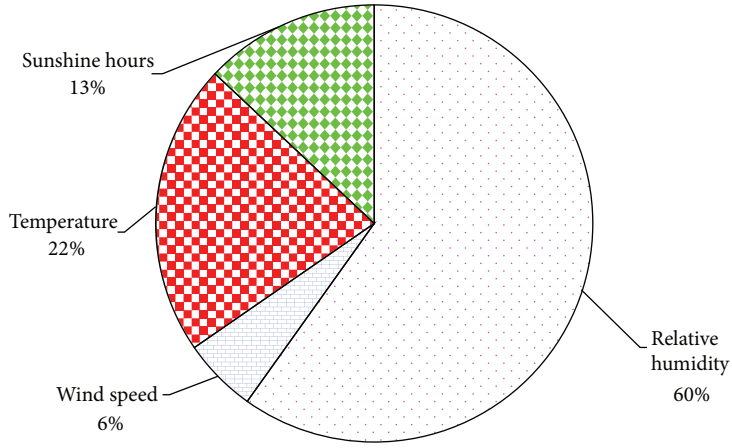

Figure 11: The contribution of each climatic variable change to ET_0 variation.

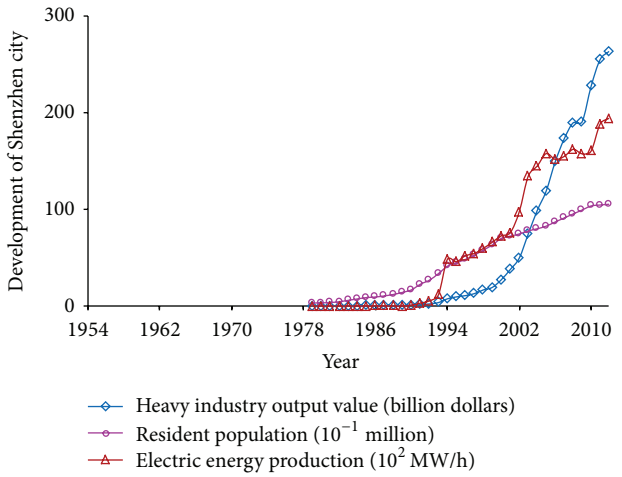

Figure 12: Temporal trend of the development of Shenzhen city.

4. Discussion

4.1. Change in the Sunshine Hours and Urban Development. Sunshine hours generally depend on the cloud cover, manmade aerosols, and certain air pollutants (including SO_2, NO_x, and PM) [19, 20]. Recent studies indicated that the most probable cause for the depression of sunshine hours or solar radiation is in the increased concentrations of manmade aerosols and other air pollutants [1, 19–22]. In this study, the sunshine hours and amount of radiation showed clear decreasing trends after 1970, and they were significantly lower after 1980 during rapid urban development.

Figure 12 shows the increasing trends of the resident population, heavy industry output value, and electric energy production. It is confirmed that the increasing trend in the energy consumption corresponds to increased emission of polluted particles, including CO, CO_2, NO_x, SO_x, $PM_{2.5}$, O_3, and HC. These particles may result in an increase in the atmospheric aerosol concentration [23–27], which can directly attenuate the surface solar radiation (SSR) by scattering and absorbing solar radiation (direct effect) or can indirectly attenuate SSR by their ability to act as cloud condensation nuclei, thereby increasing the cloud reflectivity and lifetime (first and second indirect effects) [24, 28]. A remarkable decline in SSR between the 1950s and the 1980s was found in several studies that were performed at selected observation stations based on sites in Europe, the Baltics, the South Pole, Germany, and the former Soviet Union [21]. Today, a comprehensive literature exists that confirms the declines of SSR during this period in many places around the world [29]. In Beijing and several other Chinese cities, the decline of sunshine hours and SSR has also been reported [15, 30].

4.2. Air Temperature Change and Urban Development. It has been confirmed that there is a large air temperature difference in urban and rural areas [4–7]. These air temperature differences result from the influence of the thermal emissivity properties of urban surfaces and the three-dimensional configuration and heat capacity of erected structures onto the air temperature patterns in an urban region [7, 15, 31]. Most of the world's cities thus show higher air temperatures in the urban core than in the surrounding rural areas [4, 5, 7]. For example in Beijing City, China, Kuang et al. [32] measured that the mean land surface temperature of urban impervious surfaces was about 6–12°C higher than that of the urban green space and that in built-up areas was on average 3–6°C higher than in rural areas. They showed the main reason is the higher ratio of sensible heat to net radiation (0.63) and lower ratio of the latent heat to net radiation (0.19) on the urban impervious surface as compared to the corresponding rates of 0.30 and 0.63 in green space and cropland. In this study, there is no obvious temporal trend in the air temperature before 1978, whereas, after that time, the temperature increased greatly, although it showed a slight declining trend in recent years. The large air temperature increase from 1978 to 2002 may be due to the increasing area of construction and the decrease in farmland [32]. Figure 13 shows the changes in the farmland and construction areas. It can be found that there was a rapid increase in construction areas and an abrupt decrease in farmland areas after 1978, which led to a change in the thermal balance and then resulted in the increase in the air temperature in Shenzhen city.

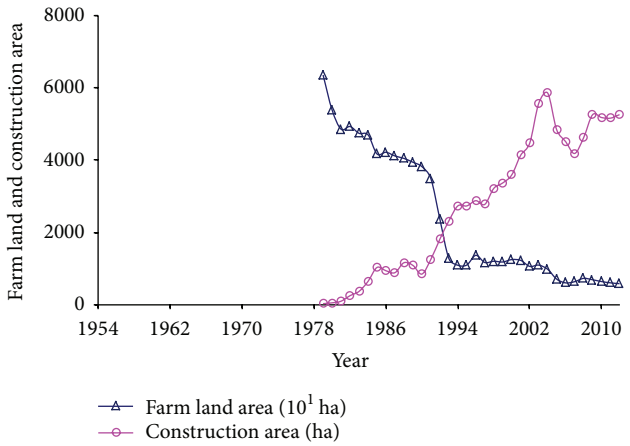

FIGURE 13: Temporal trend of the farmland area and the floor space of the buildings under construction.

4.3. Changes in the Relative Humidity and the Vapor Pressure Deficit due to Urban Development. The vapor pressure deficit was calculated by the air temperature and the relative humidity following the method of Allen et al. (1998) [12]. It is clearly shown in the calculation method that the vapor pressure deficit (VPD) increases with air temperature and decreases with relative humidity. In this study, both relative humidity and mean air temperature varied slightly during the period from 1954 to 1980 (Figures 5 and 6), which consequently resulted in a slight change in the vapor pressure deficit. After that period, the mean air temperature increased significantly, and the relative humidity was decreased remarkably. These trends resulted in an increase in the vapor pressure deficit (Figure 7).

The relative humidity is defined as the ratio of the water vapor density (mass per unit volume) to the saturation water vapor density, and it is also approximately the ratio of the actual to the saturation vapor pressure. A greater evaporative area may produce more water vapor for the atmosphere and then increase the water vapor density as well as the relative humidity at a given temperature. In the city study area, the farmland area decreased, whereas the construction area increased (Figure 13). These data indicate a decreasing trend in the evaporative area, which may result in a decrease in the water vapor density as well as the relative humidity [33]. Similarly, a decreasing trend of relative humidity and an increase in the vapor pressure deficit were observed in Beijing, Datong in Shanxi province, Zhang Jiakou in Hebei Province, and Bet Dagan in Israel [15, 34, 35]. In Beijing, it was shown that the VPD increased with air temperature and decreased with relative humidity from 1951 to 2010 [15]. Cohen et al. (2002) showed that the main factor responsible for the increased pan evaporation was the growth in the aerodynamic component of evaporation, which was due to increases in both the air VPD and the wind speed at Bet Dagan from 1964 to 1997 [35].

The vapor pressure deficit represents a gradient across which water vapor is removed from the evapotranspiring surface into the surrounding air [12]. A greater vapor pressure deficit generally causes a higher evaporative rate. Hence, the increasing vapor pressure deficit in the Shenzhen area will result in increasing plant evapotranspiration.

4.4. ET_0 Change and City Development. In the current study area, ET_0 first decreased from 1950s to 1970s and then increased greatly in the 1980s. During the 1990s and 2000s it varied slightly, with a mean value of 1287 mm. It was observed that, after the onset of urban development in 1978, the ET_0 value increased and became higher than this for the period prior to the urban development. Figures 2, 5, 6, and 8 show that the mutation points for most climatic variables were observed near the onset year of urban development and sensitivity analysis shows that the higher ET_0 during the period of 1992–2012 is mainly attributed to the relative humidity decrease and air temperature increase. Hence, it could be concluded that the quick development of Shenzhen city altered the climatic conditions and hence increased the local ET_0. In other large cities, an increasing ET_0 trend was also found in recent decades. For example, in Beijing City, the annual ET_0 increased significantly from 1951 to 2010 and from the 1950s to 2000s, it increased from 1039 to 1148 mm [15]. The annual potential evapotranspiration (PET) displays a significant, upward trend from 1970 to 2006, and the trend varied from 1 to 4 mm per year in the Pyrénées-Orientales and Aude administrative departments, respectively, and the western part of the French Mediterranean area with an average increase in PET of between 34 mm and 150 mm in the last 36 years [36].

The increasing trend in ET_0 that was observed in large cities is different than this that was found in the farmland. For example, in the Haihe River basin in northern China, decreasing trends were observed in 26 stations while 16 stations showed significant decreasing trends from 1950 to 2007 with rates from −2.0 to −3.7 mm $year^{-1}$ [34]. Similarly, a significant decreasing trend of ET_0 with a rate of −3 mm per year was found in the arid region of northwest China [37]. The difference trend in ET_0 between the large cities and the farmland may be due to the variations in the energy balance and the evaporative potential. In the farmland areas, more than 60–80% of the net radiation is used for plant evapotranspiration [33, 38, 39]. This effect not only reduces the available heat for heating the air environment but also increases the water vapor in the near atmosphere. The latter effect may increase the relative humidity and reduce the vapor pressure deficit and lastly it may reduce the reference evapotranspiration. For urban conditions, the decrease in green land will decrease the energy consumption caused by crop evapotranspiration, increasing the available heat and decreasing the water vapor, which ultimately results in an increase in the evaporative potential.

It should be noted in Figure 9 that the ET_0 values in 1997 and 2012 were much lower than those in the neighboring years. It is estimated that ET_0 in 1997 and 2012 decreased by −10.4% and −13.0% compared to the mean value for the period from 1990 to 2012. The sensitive analysis method described in Section 3.3 was used to determine the effects of each variable on the ET_0 changes in 1997 and 2012 compared to the mean value during the period of 1990–2012. The

results showed that the changes in the relative humidity, air temperature, sunshine hours, and wind speed in 1997 resulted in changes in ET_0 by −7.2, −0.8, −2.0, and −0.5%, respectively, and by −12.6, −0.8, −0.6, and −4.2% in 2012, respectively. It could be concluded that the increase in the relative humidity is the main factor for ET_0 reduction, followed by the wind speed, air temperature, and sunshine hours in the two years.

Based on the mean values of the climatic variables averaged over the periods of 1954–1978 and 1992–2012, ET_0 increased by 14.5% in the latter period. For the sensitivity analysis, changes in the relative humidity, air temperature, wind speed, and sunshine hours during 1992–2012 caused the variation of ET_0 by 14.6, 5.0, −1.3, and −3.8%, respectively, compared to those for the period 1954–1978. The total amount of change in ET_0 was 15.6%, based on the sensitivity analysis. This value is similar to the rate of increase of 14.5% by comparison of the ET_0 values between the two time periods. Liu et al. (2014) [15] calculated the ET_0 change rates by directly comparing the mean values and summing each ET_0 change rate caused by climatic variables using the same sensitive analysis method: the ET_0 change rates were 10.7% and 10.5%, respectively. Liu et al. (2009) [40] found that ET_0 inside the screenhouse was reduced by 39% compared to that in the open field. By considering the effect of each climatic variable change to ET_0 using the sensitivity analysis, the total ET_0 change rate sums to 44%, which is similar to the value of 39%. Therefore, it could be concluded that the sensitivity-analysis method used in this study is reliable and easy to use, and hence it is recommended for the analysis of the effect of climate change on ET_0.

5. Conclusions

(1) The development of Shenzhen city greatly affected the local climatic conditions. Before the onset of urban development, each climatic variable varied slightly, whereas, afterward, the air temperature increased significantly, and the sunshine hours and relative humidity decreased significantly. The mutation point for most climatic variables is observed at approximately 1978, the onset year for urban development.

(2) ET_0 first decreased from 1954 to 1978 and then increased quickly and reached a maximal value of 1373 mm during the period from 1992 to 2012. The mean ET_0 value for the period from 1954 to 1978 was 1110 mm and increased to 1284 mm during the period from 1992 to 2012, indicating an increasing trend of the evaporative demand.

(3) Sensitivity analysis showed that ET_0 is most sensitive to relative humidity, followed by air temperature, sunshine hours, and wind speed.

Conflict of Interests

The authors declare that there is no conflict of interests regarding the publication of this paper.

Acknowledgments

This paper is partially supported by the National Science Foundation of China (Grant nos. 51179005, 51479004). The authors greatly acknowledge the comments from the editor and the two anonymous reviewers.

References

[1] IPCC, *Climate Change 2014: Synthesis Report. An Assessment of Intergovernmental Panel on Climate Change*, IPCC, Geneva, Switzerland, 2014, http://ipcc.ch/index.html.

[2] J. D. Haskett, Y. A. Pachepsky, and B. Acock, "Effect of climate and atmospheric change on soybean water stress: a study of Iowa," *Ecological Modelling*, vol. 135, no. 2-3, pp. 265–277, 2000.

[3] T. G. Huntington, "Evidence for intensification of the global water cycle: review and synthesis," *Journal of Hydrology*, vol. 319, no. 1–4, pp. 83–95, 2006.

[4] B. C. Bates, Z. W. Kundzewicz, S. Wu, and J. Palutikof, "Climate change and water," Technical Paper of the Intergovernmental Panel on Climate Change, IPCC Secretariat, Geneva, Switzerland, 2008.

[5] C. M. Philandras, D. A. Metaxas, and P. T. Nastos, "Climate variability and urbanization in Athens," *Theoretical and Applied Climatology*, vol. 63, no. 1-2, pp. 65–72, 1999.

[6] R. L. Wilby, "Past and projected trends in London's urban heat island," *Weather*, vol. 58, no. 7, pp. 251–260, 2003.

[7] N. Schwarz, U. Schlink, U. Franck, and K. Großmann, "Relationship of land surface and air temperatures and its implications for quantifying urban heat island indicators—an application for the city of Leipzig (Germany)," *Ecological Indicators*, vol. 18, pp. 693–704, 2012.

[8] H. Wang, L. Fu, X. Lin, Y. Zhou, and J. C. Chen, "A bottom-up methodology to estimate vehicle emissions for the Beijing urban area," *Science of the Total Environment*, vol. 407, no. 6, pp. 1947–1953, 2009.

[9] DESE (Department of Environmental Science and Engineering/Tsinghua University), *Mobile Source Database, Emission Inventory and Treatment Proposal for Beijing*, Tsinghua University, Beijing, China, 2005.

[10] H. Kan, S. J. London, G. Chen et al., "Differentiating the effects of fine and coarse particles on daily mortality in Shanghai, China," *Environment International*, vol. 33, no. 3, pp. 376–384, 2007.

[11] A. Aziz and I. U. Bajwa, "Erroneous mass transit system and its tended relationship with motor vehicular air pollution (An integrated approach for reduction of urban air pollution in Lahore)," *Environmental Monitoring and Assessment*, vol. 137, no. 1–3, pp. 25–33, 2008.

[12] R. G. Allen, L. S. Perreira, D. Raes, and M. Smith, *Crop Evapotranspiration: Guidelines for Computing Crop Water Requirements*, FAO Irrigation and Drainage Paper no. 56, FAO, Rome, Italy, 1998.

[13] K. H. Hamed, "Trend detection in hydrologic data: the Mann-Kendall trend test under the scaling hypothesis," *Journal of Hydrology*, vol. 349, no. 3-4, pp. 350–363, 2008.

[14] L. Q. Liang, L. J. Li, and Q. Liu, "Temporal variation of reference evapotranspiration during 1961–2005 in the Taoer River basin of Northeast China," *Agricultural and Forest Meteorology*, vol. 150, no. 2, pp. 298–306, 2010.

[15] H. Liu, Y. Li, T. Josef, R. H. Zhang, and G. H. Huang, "Quantitative estimation of climate change effects on potential evapotranspiration in Beijing during 1951–2010," *Journal of Geographical Sciences*, vol. 24, no. 1, pp. 93–112, 2014.

[16] M. G. Kendall and A. Stuart, *The Advanced Theory of Statistics*, Griffin, London, UK, 1973.

[17] Q.-Y. Tang and C.-X. Zhang, "Data Processing System (DPS) software with experimental design, statistical analysis and data mining developed for use in entomological research," *Insect Science*, vol. 20, no. 2, pp. 254–260, 2013.

[18] M. Möller, J. Tanny, Y. Li, and S. Cohen, "Measuring and predicting evapotranspiration in an insect-proof screenhouse," *Agricultural and Forest Meteorology*, vol. 127, no. 1-2, pp. 35–51, 2004.

[19] G. Kitsara, G. Papaioannou, A. Papathanasiou, and A. Retalis, "Dimming/brightening in athens: trends in sunshine duration, cloud cover and reference evapotranspiration," *Water Resources Management*, vol. 27, no. 6, pp. 1623–1633, 2013.

[20] Y. Wang, Y. Yang, S. Han, Q. X. Wang, and G. H. Zhang, "Sunshine dimming and brightening in Chinese cities (1955–2011) was driven by air pollution rather than clouds," *Climate Research*, vol. 56, no. 1, pp. 11–20, 2013.

[21] G. Stanhill and S. Cohen, "Global dimming: a review of the evidence for a widespread and significant reduction in global radiation with discussion of its probable causes and possible agricultural consequences," *Agricultural and Forest Meteorology*, vol. 107, no. 4, pp. 255–278, 2001.

[22] Q. Liu and Z. Yang, "Quantitative estimation of the impact of climate change on actual evapotranspiration in the Yellow River Basin, China," *Journal of Hydrology*, vol. 395, no. 3-4, pp. 226–234, 2010.

[23] D. I. Stern, "Reversal of the trend in global anthropogenic sulfur emissions," *Global Environmental Change*, vol. 16, no. 2, pp. 207–220, 2006.

[24] I. Koren, J. V. Martins, L. A. Remer, and H. Afargan, "Smoke invigoration versus inhibition of clouds over the Amazon," *Science*, vol. 321, no. 5891, pp. 946–949, 2008.

[25] D. Rosenfeld, Y. J. Kaufman, and I. Koren, "Switching cloud cover and dynamical regimes from open to closed Benard cells in response to the suppression of precipitation by aerosols," *Atmospheric Chemistry and Physics*, vol. 6, no. 9, pp. 2503–2511, 2006.

[26] C. Ruckstuhl, R. Philipona, K. Behrens et al., "Aerosol and cloud effects on solar brightening and the recent rapid warming," *Geophysical Research Letters*, vol. 35, no. 12, Article ID L12708, 2008.

[27] D. G. Streets, Y. Fang, C. Mian et al., "Anthropogenic and natural contributions to regional trends in aerosol optical depth, 1980–2006," *Journal of Geophysical Research: Atmospheres*, vol. 114, no. 10, Article ID D00D18, 2009.

[28] V. Ramanathan, P. J. Crutzen, J. T. Kiehl, and D. Rosenfeld, "Atmosphere—aerosols, climate, and the hydrological cycle," *Science*, vol. 294, no. 5549, pp. 2119–2124, 2001.

[29] M. Wild, "Enlightening global dimming and brightening," *Bulletin of the American Meteorological Society*, vol. 93, no. 1, pp. 27–37, 2012.

[30] G. D. Liu, Y. Li, H. J. Liu, and J. Xiao, "Changing trend of reference crop evapotranspiration and its dominated meteorological variables in Shanxi province in the past 55 years," *Journal of Irrigation and Drainage*, vol. 31, no. 4, pp. 26–30, 2012.

[31] C.-S. Rim, "The effects of urbanization, geographical and topographical conditions on reference evapotranspiration," *Climatic Change*, vol. 97, no. 3, pp. 483–514, 2009.

[32] W. Kuang, Y. Liu, Y. Dou et al., "What are hot and what are not in an urban landscape: quantifying and explaining the land surface temperature pattern in Beijing, China," *Landscape Ecology*, 2014.

[33] Z. Qin, Q. Yu, S. Xu et al., "Water, heat fluxes and water use efficiency measurement and modeling above a farmland in the North China Plain," *Science in China D: Earth Sciences*, vol. 48, no. 1, pp. 207–217, 2005.

[34] B. Tang, L. Tong, S. Z. Kang, and L. Zhang, "Impacts of climate variability on reference evapotranspiration over 58 years in the Haihe river basin of north China," *Agricultural Water Management*, vol. 98, no. 10, pp. 1660–1670, 2011.

[35] S. Cohen, A. Ianetz, and G. Stanhill, "Evaporative climate changes at Bet Dagan, Israel, 1964–1998," *Agricultural and Forest Meteorology*, vol. 111, no. 2, pp. 83–91, 2002.

[36] K. Chaouche, L. Neppel, C. Dieulin et al., "Analyses of precipitation, temperature and evapotranspiration in a French Mediterranean region in the context of climate change," *Comptes Rendus Geoscience*, vol. 342, no. 3, pp. 234–243, 2010.

[37] Z. Huo, X. Dai, S. Feng, S. Kang, and G. Huang, "Effect of climate change on reference evapotranspiration and aridity index in arid region of China," *Journal of Hydrology*, vol. 492, pp. 24–34, 2013.

[38] G. Peng, X. Cai, H. Zhang, A. Li, F. Hu, and M. Y. Leclerc, "Heat flux apportionment to heterogeneous surfaces using flux footprint analysis," *Advances in Atmospheric Sciences*, vol. 25, no. 1, pp. 107–116, 2008.

[39] Y. Q. Zhang, Y. J. Shen, C. M. Liu et al., "Measurement and analysis of water, heat and CO_2 flux from a farmland in the North China plain," *Acta Geographica Sinica*, vol. 57, no. 3, pp. 333–342, 2002 (Chinese).

[40] H.-J. Liu, G.-H. Huang, S. Cohen, and J. Tanny, "Change in crop evapotranspiration and associated influencing factors under screenhouse conditions," *Chinese Journal of Eco-Agriculture*, vol. 17, no. 3, pp. 484–488, 2009 (Chinese).

Hindawi Publishing Corporation
Advances in Meteorology
Volume 2015, Article ID 585623, 9 pages
http://dx.doi.org/10.1155/2015/585623

Research Article

Influence of Urban Microclimate on Air-Conditioning Energy Needs and Indoor Thermal Comfort in Houses

Feng-Chi Liao,[1] Ming-Jen Cheng,[2] and Ruey-Lung Hwang[3]

[1]*Ph.D. Program in Civil and Hydraulic Engineering, Feng Chia University, 100 Wenhwa Road, Taichung 407, Taiwan*
[2]*Department of Architecture, Feng Chia University, 100 Wenhwa Road, Taichung 407, Taiwan*
[3]*Department of Architecture, National United University, 1 Lienda, Miaoli 360, Taiwan*

Correspondence should be addressed to Ruey-Lung Hwang; rueylung@nuu.edu.tw

Received 24 September 2014; Revised 19 March 2015; Accepted 24 March 2015

Academic Editor: Panagiotis Nastos

A long-term climate measurement was implemented in the third largest city of Taiwan, for the check of accuracy of morphing approach on generating the hourly data of urban local climate. Based on observed and morphed meteorological data, building energy simulation software EnergyPlus was used to simulate the cooling energy consumption of an air-conditioned typical flat and the thermal comfort level of a naturally ventilated typical flat. The simulated results were used to quantitatively discuss the effect of urban microclimate on the energy consumption as well as thermal comfort of residential buildings. The findings of this study can serve as a reference for city planning and energy management divisions to study urban sustainability strategies in the future.

1. Introduction

Approximately 70% of Taiwan's population lives in cities. With the expansion of the urban scale, the urban heat island (UHI) effect has become increasingly significant. Lin et al. [1] indicated that UHI is common to cities of Taiwan, especially metropolises. The population/area of the three major cities of Taiwan, namely, Taipei, Kaohsiung, and Taichung, is, respectively, 2.6 million/272 km^2, 1.5 million/154 km^2, and 1.2 million/163 km^2. They are also the top three cities in the UHI intensity, which is 4.5°C, 3.2°C, and 2.7°C, respectively. Increasingly UHI effect and global warming accelerate the deterioration of urban microclimate, thereby influencing the urban livability significantly. Architects are thus confronted with more austere challenges in architectural design.

Urban microclimate change directly influences building energy consumption and indoor thermal comfort; this has become a topical subject in many countries. Kolokotroni et al. [2] found that the UHI effect is an important factor in the underestimation of urban building energy consumption. Taking Britain as an example, the rural office building energy consumption for cooling is only 84% of urban consumption. Jusuf et al. [3] simulated the differences in the energy consumption of office buildings in various large cities of the USA under the UHI effect. The results showed that the urban ambient temperature, due to the UHI effect, was higher than the suburban temperature by 2°C on average. The energy consumption for cooling buildings was increased by 17.25%, and energy consumption for heating was reduced by 17.04%. Sun and Augenbroe [4] found that the cooling degree hours of 15 big cities of the USA were greater than that of rural districts by 25.3% on average due to the UHI effect. In Australia, Ren et al. [5] conducted thermal performance simulation for the buildings in urban, rural, and urban-green regions. The results showed that a green area could reduce the downtown maximum ambient temperature by 0.8°C, which changed the heat stress risk level of buildings from "severe" to "moderate." Oxizidis et al. [6] reported that in Lisbon, due to the UHI effect, the energy consumption for heating of buildings in the city center was lower than that in the suburbs. Wong et al. [7] found that different block designs in Singapore influence the urban ambient temperature by 0.9–1.2°C. Therefore, if urban blocks are planned properly, the energy consumption for cooling of buildings can be reduced by 5–10%. Wong et al. [8] indicated that microclimate change in a campus could change the building energy consumption by 2.3–14.3%. Chan

[9] indicated that the energy consumption for cooling urban buildings in Hong Kong was higher than that of suburban buildings by about 10%.

The goal of building designers is to create an energy-saving and comfortable residential environment. Therefore, it is necessary and urgent to explore the influence of urban microclimate on building energy consumption and indoor thermal environments and collect a set of highly reliable urban local climate data. To our best knowledge, there is no related research in Taiwan. In view of this, this study collects the microclimate data of different locations in the city by long-term field measurement and the morphing approach and used EnergyPlus [10] to simulate energy consumption for cooling and indoor thermal comfort of residential construction. The quantified data on the effect of the variance of Taiwan's urban microclimate on building energy consumption and indoor environment quality can serve as reference data for city planning and energy management divisions to study urban sustainability strategies in the future.

2. Methodology

2.1. Morphing Approach. Current building thermal performance is evaluated based on the hourly meteorological data of weather stations by simulation software, such as EnergyPlus, in order to simulate the energy consumption of buildings. However, as the weather stations are located in the suburbs and each city usually has only one weather station, it is difficult to obtain the hourly microclimate data of any site in the city. Therefore, studies [5, 7–9], which analyzed the effect of urban microclimate change on energy consumption, used field measurements and the morphing approach [11] to create the hourly data of urban microclimate. This approach uses the weather station data as the baseline climate and uses the measured data of urban climates to correct the climatic contrasts by shift and linear stretch. Finally, the hourly meteorological data of various places of a city are created. The equations of morphing approach are as follows:

$$\begin{aligned} T &= T_0 + \Delta T_m + \alpha T_m \left(T_0 - T_m\right), \\ \alpha T_m &= \frac{\Delta T_{\max,m} - \Delta T_{\min,m}}{T_{\max,m} - T_{\min,m}}, \\ s &= s_0 \times \alpha s_m, \\ \alpha s_m &= 1 + \frac{\mathrm{SPHU}_m}{100}, \end{aligned} \tag{1}$$

where T_0 is the hourly ambient temperature from the weather station; T_m, $T_{\max,m}$, and $T_{\min,m}$ are the monthly mean values of ambient temperature, daily maximum temperature, and daily minimum temperature, respectively, for month m; ΔT_m, $\Delta T_{\max,m}$, and $\Delta T_{\min,m}$ are the variations between weather station and urban areas in the monthly mean of ambient temperature, daily maximum temperature, and daily minimum temperature, respectively, for month m; s and s_0 are the hourly specific humidity in urban areas and from weather station; SPHU_m is the change in monthly mean specific humidity given as a percentage for month m; αT_m and αs_m are the fractional change in monthly mean temperature change and monthly mean differences of specific humidity, respectively, for month m.

2.2. Field Measurement. Taichung, the third largest city of Taiwan, was chosen for investigation in this study, because the increase of its annual mean ambient temperature is higher than the other cities of Taiwan, which is +0.40°C/10 years in the past 30 years [12]. Taichung is located in central Taiwan (24°15′N; 120°40′E), and its population is about 1.2 million. The development in the city is centered on the area around the main train station and expands to the new districts. The older buildings are mostly 5 stories or below; the buildings in new districts are mostly 6 to 15 stories. The buildings of 16 stories or above are concentrated along the main road going through the new district.

In terms of climate, Taichung is located in hot-humid climate zone, where the mean annual temperature is 23.3°C in the recent three decades. The maximum monthly mean temperature occurs in July, and the monthly mean temperature in July in the most recent 30 years is 28.6°C. The UHI effect intensity is about 2.7°C in summer.

According to (1), in order to use the morphing approach to create the hourly data of urban microclimate, the monthly mean of hourly temperature, daily maximum temperature, daily minimum temperature, and monthly average specific humidity of the local climate should be known beforehand. Figure 1 shows the positions of the 10 selected sites in the city, as well as a brief description of peripheral environments, including building density and the underlying surface of bared ground, roads, and green area. Two principals applied to select the sites for field measurement are as follows.

(i) All of the selected sites uniformly are distributed from the downtown to suburban areas of the city approximately.

(ii) The selected sites are expected to have different levels of UHI intensity.

The field measurements were collected from July to September 2013. The calibrated ESCORT iLog [13] temperature/humidity data logger was used to measure the air temperature and relative humidity (RH) at each selected site. The data loggers were attached to the electricity posts or lampposts in selected sites, as shown in Figure 2, and configured at 5-minute interval throughout the measurement periods. The air temperature/RH data were obtained by sampling at a height of 3.0 m for each of the selected sites. As a reference, meteorological data were gathered from nearby weather stations, which had been located in a metropolitan park with a large area of water bodies and vegetation. The weather station is maintained by the Central Weather Bureau of Taiwan.

2.3. Building Model. In order to analyze the impact of the UHI effect on building energy consumption and indoor thermal comfort level, this study chose a typical flat as the building model. This was done purposely as there are a wide variety of apartment styles in the country. However, the

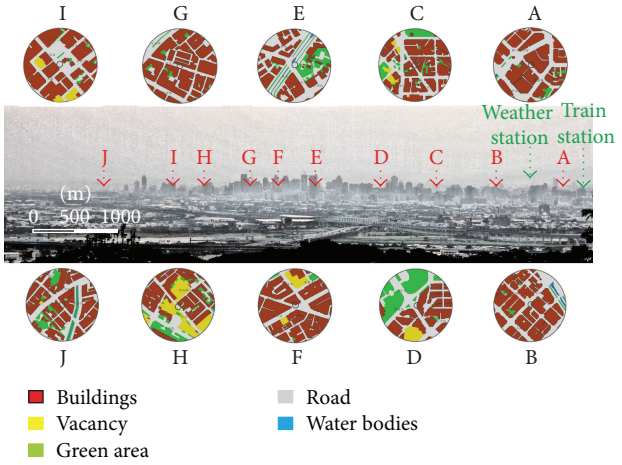

Figure 1: Position and underlying surface type of selected sites for field measurement.

Figure 2: Installation of temperature/humidity data logger at a selected site.

energy simulation of typical buildings under representative operation conditions may contribute to a better understanding on the average energy performance of buildings in Taiwan. The analysis can serve as a preliminary comparison of the impact of UHI.

The residential apartment is a 3-bedroom residential flat of area 90 m^2 with a rectangular living/dining room. The prevailing summer wind in Taiwan is south wind; thus the windows of flat are arranged on the south and north façade for natural ventilation. The south wall has an overhang, and the south windows are shaded by the attached overhang. Other pieces of information for the construction of walls/windows, internal gains, and air conditioner used in this typical flat are listed in Table 1.

2.4. Calculation of Energy Consumption for Cooling and Thermal Comfort. The typical flat was simulated in air-conditioned and naturally ventilated scenarios (Figure 3).

Table 1: Specifications of construction and air-conditioning system in a typical residential flat.

Item	Description
External wall construction	5 mm mosaic tile (outer layer) 10 mm cement 150 mm heavy concrete 10 mm cement (inner layer)
Glass type	6 mm single clear glass
Gross floor area	90 m^2/flat
Equipment power intensity	140 W/room
Lighting power intensity	8 W/m^2
Indoor design temperature	28°C
Occupancy intensity	4 persons/flat
Operating hours of air conditioner	7:00 pm to 11:00 pm (living room) 8:00 pm to 8:00 am (bedroom)
C.O.P.	3.0

Building simulation software EnergyPlus was used to calculate the cooling energy consumption of air-conditioned typical flat as well as the indoor thermal conditions of naturally ventilated typical flat.

The inclusion of adaptive thermal comfort model in the ASHRAE Standard 55 [14] and EN 15251 [15] exemplifies the increasing effort of improving indoor environmental quality in naturally ventilated or hybrid ventilated buildings. Based on the report by Hwang et al. [16], when the upper limit of the comfort zones projected by these models was compared, the predictability of the ASHRAE model appeared to be less than that of the EN model in the warm condition like Taiwan. The EN comfort zones of Categories I and II were more consistent with field observations than the ASHRAE comfort zones 90 and 80%. Hence, the EN adaptive comfort model was to evaluate the indoor thermal comfort of the typical flat in this study.

As the comfort temperature is influenced by people's clothing, behavior, and level of adaptation, thus the EN adaptive approach considers the comfort temperature to be related to a person's thermal history with more recent experiences being more influential. This makes the exponential weighting attractive as a weight for past temperatures [17]. The exponential weighting system results in decay in the importance of any past temperature. Based on a weekly running average outside air temperature (T_{rm}), the EN adaptive comfort model recommended the upper boundaries of thermal comfort zones for Category II, which is suitable for residential spaces, as given in

$$T_c = 0.33 \times T_{rm} + 21.8 \quad \text{for } 25 \le T_c \le 32^\circ\text{C},$$
$$T_{rm} = \left(T_{-1} + 0.8 \times T_{-2} + 0.6 \times T_{-3} + 0.5 \times T_{-4} + 0.4 \times T_{-5} + 0.3 \times T_{-6} + 0.2 \times T_{-7}\right) \cdot (3.8)^{-1}, \tag{2}$$

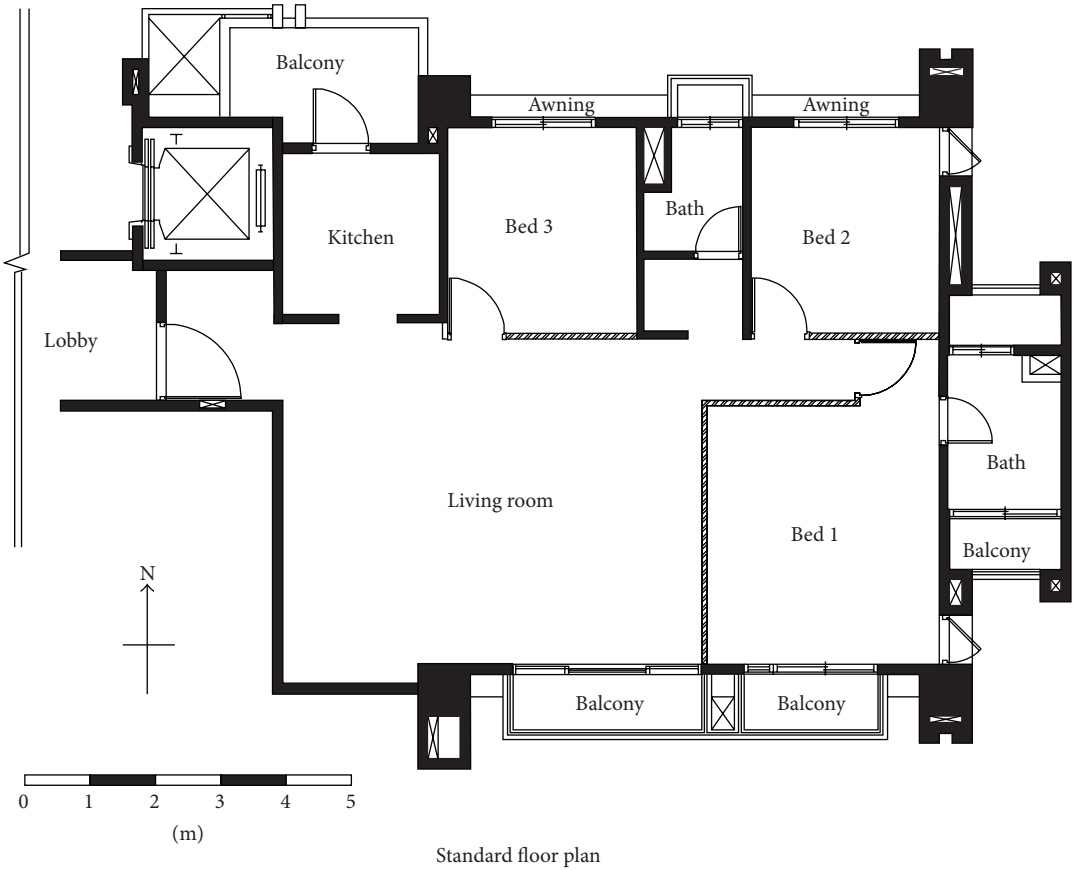

Figure 3: Plan view of the typical flat used in the study.

where T_{-1} is the mean outside air temperature of the previous day, T_{-2} is the mean outside air temperature two days ago, and so forth.

For long-term indoor thermal environment comfort evaluation, ISO 7730 [18] recommends the following two methods:

(i) hours of exceedance (H_e): calculate the number of hours that the building is occupied, and the operative temperature (t_{op}) is outside a specified range ($t_{o,limit}$);

(ii) weighted exceedance (W_e): the time during which the actual operative temperature exceeds the specified range during the occupied hours is weighted with a factor which is a function of how many degrees the range has been exceeded. The weighting factor (wf) must equal 1 for $t_{op} = t_{o,limit}$. The weighting factor is calculated as follows:

$$wf = 1 + \frac{\left|t_{op} - t_{op,limit}\right|}{\left|t_{op,optimal} - t_{op,limit}\right|}. \quad (3)$$

For a characteristic warm period during a year, the product of the weighting factor, wf, and time t is summed and the result expressed in hours:

$$\sum wf \cdot t \quad \text{for } t_{op} > t_{op,limit}. \quad (4)$$

3. Result of Field Measurement

Figure 4 shows the variation of daily mean temperatures, as measured at the 10 selected sites and from the weather stations during the experimental period. In the four months of the experiment, the daily mean temperature from the weather station was in the range of 25°C–31.6°C. Site D that contained a large area of vegetation had the minimum mean temperature among the 10 selected sites. Site F, surrounded by intensive high-rise buildings and extensive heat discharge from vehicles, had the maximum mean temperature. The mean temperatures measured at various measuring sites were higher than the mean temperature measured at the weather station, and the temperature difference was 1.3°C–2.1°C. In addition, the mean temperature, the maximum daily mean temperature, and minimum daily mean temperature at the 10 selected sites were higher than those from the weather station. Figure 5 shows the daily mean RH from the weather station and selected sites during the experimental period. In the experimental period, the maximum difference of mean RH between selected site and weather station occurred at site G, and the difference was 6%. The values of T_m, $T_{max,m}$, $T_{min,m}$, ΔT_m, $\Delta T_{max,m}$, $\Delta T_{min,m}$, and RH_m of the selected sites and weather station from July to October are as listed in Table 2.

Table 2: Summary of T_m, $T_{\max,m}$, $T_{\min,m}$, ΔT_m, $\Delta T_{\max,m}$, $\Delta T_{\min,m}$ (°C), and RH_m (%) for selected sites.

Month	Climatic variables	Selected sites									
		A	B	C	D	E	F	G	H	I	J
Jul.	T_m	29.7	30.2	29.7	29.4	29.9	30.2	29.9	29.3	29.7	29.7
	$T_{\max,m}$	34.9	35.5	34.8	34.2	35.5	35.6	35.1	34.5	35.3	34.8
	$T_{\min,m}$	26.3	26.7	26.2	26.1	26.0	26.5	26.4	25.8	26.1	26.2
	RH_m	72	71	72	72	72	74	71	74	78	73
	ΔT_m	1.6	2.0	1.6	1.3	1.7	2.1	1.8	1.2	1.5	1.6
	$\Delta T_{\max,m}$	3.0	3.6	2.9	2.3	3.6	3.7	3.2	2.6	3.4	2.9
	$\Delta T_{\min,m}$	1.1	1.5	1.0	0.9	0.7	1.3	1.2	0.6	0.9	1.0
Aug.	T_m	29.7	30.2	29.7	29.4	29.9	30.2	29.9	29.3	29.7	29.7
	$T_{\max,m}$	35.4	35.9	35.3	34.8	36.0	36.1	35.6	35.3	35.7	35.3
	$T_{\min,m}$	27.4	27.7	27.3	27.1	26.9	27.5	27.5	26.9	27.2	27.3
	RH_m	68	67	68	69	69	71	67	70	75	69
	ΔT_m	1.6	2.1	1.6	1.3	1.8	2.2	1.9	1.3	1.6	1.8
	$\Delta T_{\max,m}$	2.9	3.4	2.8	2.4	3.5	3.6	3.1	2.8	3.2	2.8
	$\Delta T_{\min,m}$	1.4	1.8	1.4	1.2	1.0	1.6	1.6	1.0	1.3	1.4
Sep.	T_m	29.2	29.7	29.3	29.0	29.3	29.8	29.5	29.1	29.2	29.3
	$T_{\max,m}$	34.0	34.6	34.0	33.4	34.4	34.7	34.1	34.1	34.1	33.8
	$T_{\min,m}$	26.3	26.7	26.3	26.1	25.9	26.5	26.5	26.0	26.2	26.3
	RH_m	75	73	74	75	76	77	73	76	82	75
	ΔT_m	1.5	2.1	1.6	1.3	1.7	2.2	1.9	1.4	1.5	1.7
	$\Delta T_{\max,m}$	2.8	3.4	2.8	2.2	3.2	3.5	3.0	2.9	3.0	2.6
	$\Delta T_{\min,m}$	1.4	1.8	1.4	1.2	1.0	1.6	1.6	1.0	1.2	1.4
Oct.	T_m	28.3	28.8	28.4	28.0	28.5	28.9	28.6	28.1	28.3	28.4
	$T_{\max,m}$	33.9	34.5	33.8	33.3	34.0	34.4	33.9	33.8	34.1	33.7
	$T_{\min,m}$	25.0	25.4	25.0	24.8	24.7	25.2	25.2	24.6	24.9	25.0
	RH_m	69	68	69	70	70	72	68	71	76	70
	ΔT_m	1.5	2.0	1.5	1.2	1.7	2.1	1.8	1.3	1.5	1.6
	$\Delta T_{\max,m}$	3.0	3.6	3.0	2.4	3.2	3.6	3.1	2.9	3.2	2.8
	$\Delta T_{\min,m}$	1.2	1.5	1.1	1.0	0.9	1.3	1.3	0.8	1.1	1.1

Table 3: Values of αT_m and αs_m, for the morphing approach.

Item	Month	Selected sites									
		A	B	C	D	E	F	G	H	I	J
αT_m	Jul.	0.28	0.31	0.28	0.22	0.43	0.37	0.30	0.30	0.38	0.29
	Aug.	0.22	0.25	0.22	0.18	0.39	0.31	0.23	0.28	0.30	0.22
	Sep.	0.23	0.26	0.23	0.17	0.36	0.31	0.22	0.30	0.28	0.20
	Oct.	0.26	0.29	0.26	0.20	0.32	0.32	0.24	0.31	0.31	0.24
αs_m	Jul.	1.00	1.01	0.99	0.99	1.01	1.07	0.99	1.00	1.07	1.01
	Aug.	0.98	1.00	0.99	0.98	1.01	1.06	0.99	1.00	1.09	1.01
	Sep.	1.01	1.02	1.01	1.01	1.04	1.09	1.01	1.02	1.11	1.02
	Oct.	0.99	1.00	0.98	0.98	1.01	1.06	0.98	1.00	1.09	1.00

4. Accuracy of Morphing Approach

4.1. Comparison of Climatic Data. Table 3 lists the calculated αT_m and αs_m for each selected site. By using the morphing approach, the calculated αT_m, αs_m, T_m, $T_{\max,m}$, $T_{\min,m}$, ΔT_m, $\Delta T_{\max,m}$, $\Delta T_{\min,m}$, and RH_m were used to generate the hourly meteorological data for each selected site. Taking site A as an example, Figure 6 compares the observed temperature and forecasted temperature obtained from the morphing approach in the experiment period. Figure 7 shows the comparison of relative humidity. In addition, the mean absolute bias error (MABE), the index of agreement (IA), and the coefficient of determination R^2 for each selected site were calculated and listed in Table 4. As shown in Table 4, R^2 is >0.88, MABE is <0.98°C, and IA is >0.97 for temperature prediction, and R^2 is >0.85, MABE is <2.38%, and IA is >0.96

Table 4: The R^2, MABE, and IA of $y = ax + b$ for selected sites.

Item	Selected sites									
	A	B	C	D	E	F	G	H	I	J
Temp.										
a	1.02	1.03	1.01	1.01	0.97	0.99	1.00	1.00	1.01	1.03
b	0.60	0.80	0.24	0.26	0.86	0.34	0.13	0.08	0.29	0.92
R^2	0.95	0.95	0.95	0.95	0.88	0.93	0.94	0.93	0.92	0.94
MABE	0.56	0.56	0.54	0.51	0.98	0.75	0.63	0.67	0.76	0.60
IA	0.99	0.99	0.99	0.99	0.97	0.98	0.98	0.98	0.98	0.98
RH										
a	0.85	0.88	0.84	0.84	0.87	0.85	0.82	0.84	0.84	0.85
b	11.5	9.3	11.6	11.9	9.9	11.8	13.5	12.5	12.5	11.5
R^2	0.94	0.93	0.93	0.93	0.87	0.89	0.90	0.90	0.85	0.91
MABE	2.88	2.87	2.98	2.83	3.99	3.85	3.54	3.55	4.39	3.02
IA	0.98	0.98	0.98	0.98	0.96	0.97	0.97	0.97	0.96	0.97

Table 5: Energy consumption for cooling based on observed and morphed weather data.

Energy consumption	Selected sites									
	A	B	C	D	E	F	G	H	I	J
Observed	19.5	20.9	19.6	18.8	20.2	21.8	20.2	19.1	20.6	19.9
Morphed	19.7	21.1	19.8	19.0	20.4	22.0	20.4	19.2	20.7	20.0
Error	1.03	0.96	1.02	1.06	0.99	0.92	0.99	0.52	0.49	0.50

Unit: energy consumption in kWh/m^2; error in %.

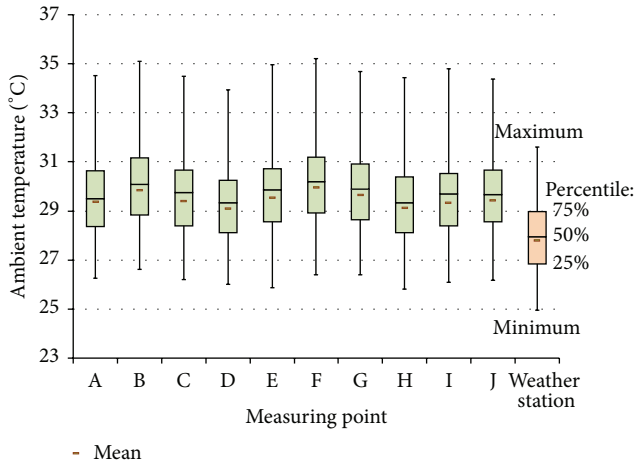

Figure 4: Variation of daily mean ambient temperature of all selected sites as well as the weather station during July to October 2013.

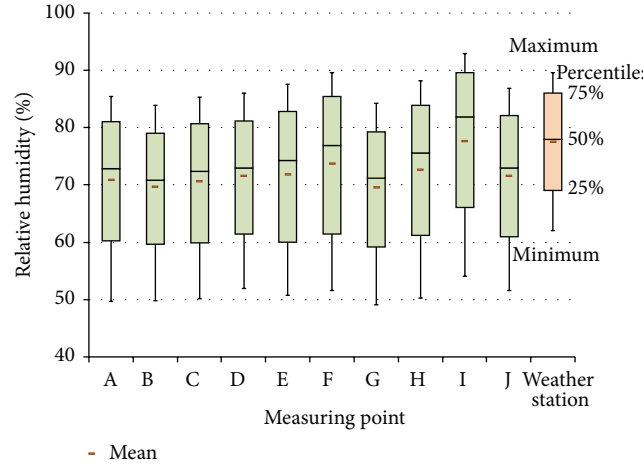

Figure 5: Variation of daily mean RH of all selected sites as well as the weather station during July to October 2013.

for RH prediction. Therefore, it seems reasonable to make a conclusion that the morph approach could be used to forecast urban microclimate.

4.2. Comparison of Energy Consumption for Cooling. In order to determine the effect of the error of the morphing approach in temperature forecasting on the air-conditioning energy consumption and indoor thermal comfort of buildings, the observed meteorological data and morphed meteorological data from the morphing approach were simultaneously used as the input meteorological data for EnergyPlus simulation.

Table 5 summarizes the EnergyPlus simulation results of cooling energy consumption of typical flat in selected sites. As shown in Table 5, the cooling energy consumption for the selected sites, based on observed meteorological data, falls in the range of 21.8–18.8 kWh/m^2, with an average of 20.1 kWh/m^2. Meanwhile, the cooling energy consumption for the selected sites, based on morphed meteorological data, is in the range of 22.0–19.0 kWh/m^2, and the average is

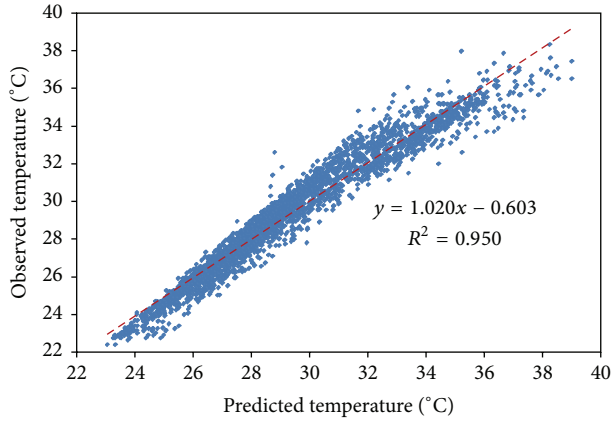

Figure 6: Comparison between measured and morphed hourly temperature at site A.

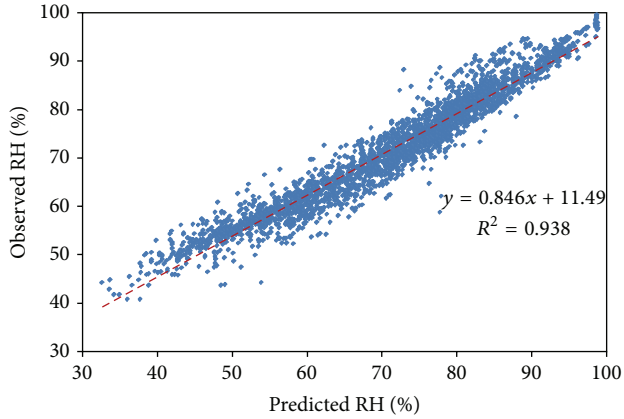

Figure 7: Comparison between observed and morphed hourly RH at site A.

20.2 kWh/m^2. Table 5 also lists the errors, resulting from the usage of different meteorological data source, of the cooling energy consumption at each selected site. As shown in Table 5, the percentage error is only 0.58%–0.83%, which is very low.

4.3. Comparison of Thermal Comfort. Table 6 shows the simulated results of indoor thermal conditions in the naturally ventilated typical flat, based on observed and morphed meteorological data, respectively. Table 6 shows that the H_e and W_e based on morphed meteorological data are higher than the values based on observed meteorological data, with percentage errors for H_e and W_e of 0.7%–17.0% and 5.3%–24.5%, respectively, with an average of 8.8% and 14.2%, respectively, for living room, and for the master bedroom the percentage error of H_e is 8.8%–63.3% with average of 32.8% and the percentage error of W_e is 13.1%–73.0% with an average of 38.5%.

According to the error analysis mentioned above, the urban microclimate data generated from the morphing approach resulted in a slight error on the cooling energy consumption of an air-conditioned typical flat; however, there

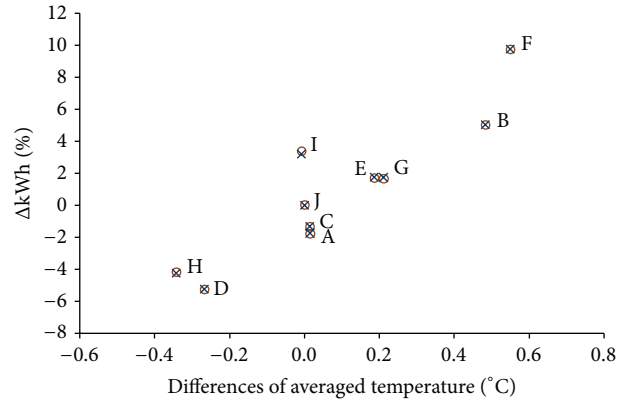

Figure 8: The percentage of ΔkWh versus difference of averaged temperature during July to October 2013.

was a moderate large error in the indoor thermal comfort level of a naturally ventilated typical flat. In other words, the hourly urban microclimate data generated by morphing methodology were probably only applicable to forecasting the energy consumption of air-conditioned houses. If morphing methodological data were used for analyzing the indoor thermal comfort level of naturally ventilated spaces, additional attention should be paid because of the moderate errors they did.

5. Impact of Urban Microclimate

Figure 8 shows the scatter plot of the percentage, compared to the baseline site, of cooling energy consumption change (ΔkWh) against the differences, between baseline site and remainder sites, of mean ambient temperature in the experiment period. Since Lin et al. [1] used the temperature in urban fringe as baseline temperature to determine the UHI intensity of Taichung, site J, which locates in the urban fringe, rather than the weather station, was selected as baseline site. This is helpful for the linkage of the findings between previous study and this study.

The data showed that the cooling energy consumption at the site F, which has the hottest urban microclimate during the experiment period, is higher by 10% than that at baseline site J. For site D with a large green area to relieve its microclimate, the energy consumption for cooling is lower than that at baseline site J by 5%. According to the simulated results, a 1°C of increase in averaged ambient temperature in urban areas during the experiment period would lead to an increase of cooling energy consumption by 14.2%, when compared to that in the suburbs.

The H_e and W_e of site J are used as the baseline values, and the differences between H_e and W_e of the living room and master bedroom at baseline site and remainder sites (i.e., ΔH_e and ΔW_e) are calculated, in order to learn the effect of the variance in urban microclimate on the indoor thermal comfort of a naturally ventilated house.

Figure 9 shows the percentage of H_e change (ΔH_e), and the percentage of W_e change (ΔW_e) is shown in Figure 10. At

Table 6: H_e and W_e for naturally ventilated living room and bedroom at each site.

Item	Weather data	Selected sites									
		A	B	C	D	E	F	G	H	I	J
Living room											
H_e	Obser.	391	516	408	326	381	526	464	311	360	432
	Morph.	420	536	428	365	439	546	497	364	416	435
	Error	7.4	3.9	4.9	12.0	15.2	3.8	7.1	17.0	15.6	0.7
W_e	Obser.	485	684	512	400	474	698	595	374	447	546
	Morph.	548	738	562	460	591	765	667	462	545	575
	Error	12.9	7.8	9.7	15.0	24.5	9.6	12.2	23.3	21.8	5.3
Master bedroom											
H_e	Obser.	357	625	374	257	311	596	491	205	305	445
	Morph.	460	680	480	341	508	720	588	334	451	508
	Error	28.9	8.8	28.3	32.7	63.3	20.8	19.8	62.9	47.9	14.2
W_e	Obser.	417	764	437	296	365	727	582	234	355	524
	Morph.	556	864	582	403	631	927	733	400	548	617
	Error	33.4	13.1	33.2	36.3	73.0	27.4	26.0	70.5	54.4	17.6

Unit: H_e in hour; W_e in ˚C-hour; error in %.

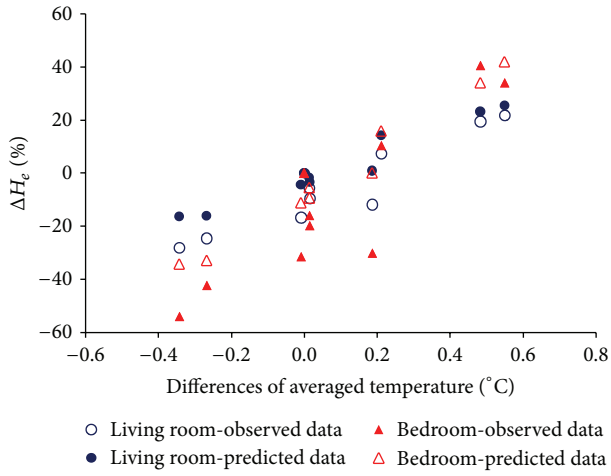

Figure 9: The percentage of ΔH_e versus difference of averaged temperature during investigated period.

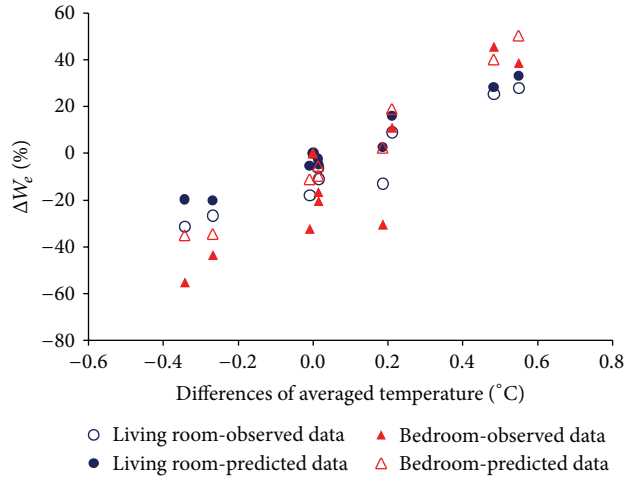

Figure 10: The percentage of ΔW_e versus difference of averaged temperature during the research period.

the hottest site F, the overheating hours of the living room and master bedroom are longer, by 22% and 34%, respectively, than baseline site J. At the coolest site D, the overheating hours are shorter by 25% and 42% for living room and master bedroom, respectively. As compared to the simulated data in suburban, if the mean outside air temperature in the urban was increased by 1˚C, the hours of exceedance for the naturally ventilated living room and bedroom would be increased by 56% and 100%, respectively.

Regarding the effect of UHI on W_e, as compared with the result of baseline site J, when the difference of averaged temperature increases from the minimum −0.34˚C to the maximum 0.55˚C, the percentage of W_e of the living room increases from −27% to 28%, while that of the master bedroom increases from −44% to 39%. If the mean outside air temperature in urban increases by 1˚C, the weighted exceedance of naturally ventilated living room and bedroom would be increased by 66% and 108%, respectively. Figures 9 and 10 also show the results based on predicted weather data for comparison.

6. Conclusion

This study quantitatively discussed the effect of UHI on building energy consumption for cooling and indoor thermal comfort by long-term field measurements and EnergyPlus simulation. Moreover, it verified the accuracy of the morphing approach in generating urban microclimate data. The important findings are as follows.

Three statistical indices, including R^2, MABE, and IA, were used to observe the accuracy of morphing approach in forecasting the urban microclimate data. The result showed

that the morphing approach has good accuracy in forecasting temperature and RH. In terms of the error of cooling energy consumption, the percentage error of the observed and predicted meteorological data is slight with a range of 0.49%–1.06%. However, the meteorological data generated from the morphing approach made moderate errors in the assessment of thermal comfort in a naturally ventilated space. This suggests that the climatic data generated from morphing approach are suitable for the analysis of energy consumption of air-conditioned buildings but not suitable for the diagnosis of indoor thermal comfort level of naturally ventilated buildings.

Moreover, the cooling energy consumption, hours of exceedance, and weighted exceedance are positively correlated with the mean outside air temperature. With the suburban selected site as the baseline, an increase of mean ambient temperature by 1°C during the experiment period (July to October) will make an increment of 14.2% in cooling energy consumption in an air-conditioned typical flat. The hours of exceedance of the living room and master bedroom of a naturally ventilated typical flat are increased by 56% and 100%, respectively. The weighted exceedance is increased by 66% and 108%, respectively. The findings of this study can serve as a reference for city planning and energy management divisions to study urban sustainability strategies in the future.

Disclaimer

The funding source was not involved in the study design, the collection, analysis, and interpretation of data, the writing of report, or the decision to submit the paper for publication.

Conflict of Interests

The authors declare that there is no conflict of interests regarding the publication of this paper.

Acknowledgment

The authors offer their sincere appreciation for assistance in grant to the Ministry of Science and Technology, Taiwan, under Project no. NSC-103-2221-E-239-020.

References

[1] H. T. Lin, K. P. Lee, K. T. Chen, L. J. Lin, H. C. Kuo, and T. C. Chen, "Experimental analyses of urban heat island effects of the four metropolitan cities in Taiwan (I)—the comparison of the heat island intensities between Taiwan and the world cities," *The Journal of Architecture*, vol. 31, pp. 51–73, 1999.

[2] M. Kolokotroni, I. Giannitsaris, and R. Watkins, "The effect of the London urban heat island on building summer cooling demand and night ventilation strategies," *Solar Energy*, vol. 80, no. 4, pp. 383–392, 2006.

[3] S. K. Jusuf, N. H. Wong, E. Hagen, R. Anggoro, and Y. Hong, "The influence of land use on the urban heat island in Singapore," *Habitat International*, vol. 31, no. 2, pp. 232–242, 2007.

[4] Y. Sun and G. Augenbroe, "Urban heat island effect on energy application studies of office buildings," *Energy and Buildings*, vol. 77, pp. 171–179, 2014.

[5] Z. Ren, X. Wang, D. Chen, C. Wang, and M. Thatcher, "Constructing weather data for building simulation considering urban heat island," *Building Services Engineering Research & Technology*, vol. 35, no. 1, pp. 69–82, 2014.

[6] S. Oxizidis, A. V. Dudek, and A. M. Papadopoulos, "A computational method to assess the impact of urban climate on buildings using modeled climatic data," *Energy and Buildings*, vol. 40, no. 3, pp. 215–223, 2008.

[7] N. H. Wong, S. K. Jusuf, N. I. Syafii et al., "Evaluation of the impact of the surrounding urban morphology on building energy consumption," *Solar Energy*, vol. 85, no. 1, pp. 57–71, 2011.

[8] N. H. Wong, S. K. Jusuf, A. A. la Win, H. K. Thu, T. S. Negara, and W. Xuchao, "Environmental study of the impact of greenery in an institutional campus in the tropics," *Building and Environment*, vol. 42, no. 8, pp. 2949–2970, 2007.

[9] A. L. S. Chan, "Developing a modified typical meteorological year weather file for Hong Kong taking into account the urban heat island effect," *Building and Environment*, vol. 46, no. 12, pp. 2434–2441, 2011.

[10] D. B. Crawley, L. K. Lawrie, F. C. Winkelmann et al., "EnergyPlus: creating a new-generation building energy simulation program," *Energy and Buildings*, vol. 33, no. 4, pp. 319–331, 2001.

[11] S. E. Belcher, J. N. Hacker, and D. S. Powell, "Constructing design weather data for future climates," *Building Services Engineering Research and Technology*, vol. 26, no. 1, pp. 49–61, 2005.

[12] Central Weather Bureau, *Analysis on the Trend of Global and Taiwan's Climate*, Central Weather Bureau, Taipei, Taiwan, 2010, http://www.cwb.gov.tw/V7/climate/climate_info/monitoring/monitoring_7.html.

[13] Cryopak, *ESCORT iLog User Guide*, Cryopak, New York, NY, USA, 2013, http://www.cryopak.com/en/verification-products/data-loggers/ilog/.

[14] "Thermal environmental conditions for human occupancy," ASHRAE Standard 55, American Society of Heating, Refrigerating and Air Conditioning Engineering, Atlanta, Ga, USA, 2004.

[15] CEN, "Indoor environmental input parameters for design and assessment of energy performance of buildings addressing indoor air quality, thermal environment, lighting and acoustics," CEN Standard EN 15251:2007, CEN, Brussels, Belgium, 2007.

[16] R. L. Hwang, C. P. Chen, F. Y. Lin, W. M. Shih, and K. T. Huang, "Applicability of ASHRAE standard 55 and EN 15251 adaptive thermal comfort models in hot-and-humid climate," in *Proceedings of the Conference of the ISEE, the ISES, and the ISIAQ on Environment and Health*, vol. 55, Basel, Switzerland, August 2013.

[17] F. Nicol and M. Humphreys, "Derivation of the adaptive equations for thermal comfort in free-running buildings in European standard EN15251," *Building and Environment*, vol. 45, no. 1, pp. 11–17, 2010.

[18] International Standards Organization, "Moderate thermal environments—determination of the PMV and PPD indices and specification of the conditions for thermal comfort," ISO 7730:2005, International Standards Organization, Geneva, Switzerland, 2005.

Hindawi Publishing Corporation
Advances in Meteorology
Volume 2015, Article ID 747259, 15 pages
http://dx.doi.org/10.1155/2015/747259

Research Article

Evaluating the Effects of Façade Greening on Human Bioclimate in a Complex Urban Environment

Britta Jänicke,[1] Fred Meier,[1] Marie-Therese Hoelscher,[2] and Dieter Scherer[1]

[1]*Chair of Climatology, Department of Ecology, Berlin Institute of Technology, Rothenburgstraße 12, 12165 Berlin, Germany*
[2]*Chair of Soil Conservation, Department of Ecology, Berlin Institute of Technology, Ernst-Reuter-Platz 1, 10587 Berlin, Germany*

Correspondence should be addressed to Britta Jänicke; britta.jaenicke@tu-berlin.de

Received 26 September 2014; Revised 19 December 2014; Accepted 19 December 2014

Academic Editor: Tzu-Ping Lin

The evaluation of the effectiveness of countermeasures for a reduction of urban heat stress, such as façade greening, is challenging due to lacking transferability of results from one location to another. Furthermore, complex variables such as the mean radiant temperature (T_{mrt}) are necessary to assess outdoor human bioclimate. We observed T_{mrt} in front of a building façade in Berlin, Germany, which is half-greened while the other part is bare. T_{mrt} was reduced (mean 2 K) in front of the greened compared to the bare façade. To overcome observational shortcomings, we applied the microscale models ENVI-met, RayMan, and SOLWEIG. We evaluated these models based on observations. Our results show that T_{mrt} (MD = −1.93 K) and downward short-wave radiation (MD = 14.39 W/m^2) were sufficiently simulated in contrast to upward short-wave and long-wave radiation. Finally, we compare the simulated reduction of T_{mrt} with the observed one in front of the façade greening, showing that the models were not able to simulate the effects of façade greening with the applied settings. Our results reveal that façade greening contributes only slightly to a reduction of heat stress in front of building façades.

1. Introduction

Heat stress risk in cities threatens human health [1] and effective countermeasures are not clearly identified. Even though many measures to reduce outdoor urban heat stress are proposed from various disciplines and at different spatial scales [2], their effectiveness is still disputed. Assessing the effectiveness of countermeasures is challenging for many reasons. For example, the transferability of results from one location to another is limited due to the complexity of the urban system and various climates [3]. Moreover, the impact of a countermeasure on outdoor human bioclimate cannot be described sufficiently by simple climate elements, such as surface or air temperature. The mean radiant temperature (T_{mrt}) is an important variable for the assessment of human bioclimate in urban environments because it includes long-wave and short-wave radiation that reaches the human body [4, 5].

Façade greening is a promising countermeasure to reduce urban heat. It can be attached to a large area in cities [6] and features several cobenefits, such as insulating buildings [7–9] or serving as habitat for wildlife [6]. The knowledge about the effectiveness of façade greening to reduce outdoor heat stress risks, however, is still incomplete due to limits in transferring of results to other sites [10]. The cooling effects of façade greening regarding surface and air temperature depend on solar irradiance, vegetation properties, and the particular greening system [11–13]. Also, the mechanisms of cooling (e.g., through shadowing or transpiration) vary between different plant species [13]. The effects of façade greening on air temperature were found to be small to negligible [7, 11, 14]. Wall temperatures decreased more strongly [14, 15] as well as the emitted long-wave radiation [16]. T_{mrt} was reduced by 2 K to 13 K in the tropics [15], but the effects for other locations are unknown. Studies that quantify the influence of façade greening on T_{mrt} are rare [15] because so far architecture and engineering disciplines are dominant with a focus on air and surface temperature and its influence on the building [10].

Microclimate models can be applied to expand the knowledge of the effects of façade greening on human bioclimate. Microclimate models, such as ENVI-met, RayMan, or

SOLWEIG, are often used in different disciplines. Particularly over the last few years, the number of studies applying ENVI-met and RayMan has grown rapidly. This is an encouraging trend as it may present an increasing awareness of the topic of human bioclimate in cities and may accelerate the implementation of countermeasures. Nevertheless, the reliability and the uncertainty of the results from studies solely based on simulations may vary appreciably. The deviations between observations and simulations have sparsely been evaluated in a comprehensive way. Thus, the inaccuracies in simulating countermeasures or real case situations are insufficiently known even apart from the special case of façade greening. A comparison of T_{mrt} simulated by ENVI-met, RayMan, and SOLWEIG under the same conditions was so far performed by Chen et al. [17]. Other variables, such as short-wave and long-wave radiation, did not undergo an intercomparison [36].

So far the models have not been applied to simulate façade greening and we are not aware of other models that are able to simulate façade greening with regard to outdoor human bioclimate. ENVI-met, RayMan, and SOLWEIG include plants, but specific vegetation types, such as façade greening, are not explicitly declared to be supported. Nevertheless, all of the models should be able to consider some aspects of façade greening. RayMan supports different trees with a specific emissivity and albedo as well as changes due to vegetation in the sky view factor (SVF). Thus, albedo and emissivity are modified due to façade greening. SOLWEIG considers vegetation in SVF and reduction of short-wave radiation through transmissivity and sets sunlit leaf temperatures to air temperature. Hence, especially long-wave radiation is expected to alternate in front of a building with façade greening. ENVI-met moreover simulates evapotranspiration. Thus, several effects of façade greening are expected to be reproduced, such as changes in SVF, increased water-vapor fluxes, decreased long-wave radiation, or modified short-wave radiation.

In order to study the effects of façade greening on outdoor human bioclimate, we will firstly use observational data to answer the following question: (1) How large is the reduction of T_{mrt} in front of a greened façade compared to a bare one at a study site? Afterwards, we will apply the models ENVI-met, RayMan, and SOLWEIG to the same site in order to (2) evaluate the general performance of the models in simulating T_{mrt} and other variables relevant to assess human bioclimate. Thereby, we will contribute to the intercomparison and evaluation of these models in a complex urban environment. Finally, we investigate (3) if the models are able to simulate the observed alteration of T_{mrt} in front of the façade greening. In a wider sense the last question addresses if microclimate models are able to represent specific types of urban vegetation such as façade greening.

2. Material and Methods

2.1. Study Site. In order to observe and simulate the effects of façade greening on T_{mrt}, we chose a south-southwest oriented building facade, which is half-covered with *Parthenocissus tricuspidata* while the other part is bare. The façade is located at the campus of the Berlin Institute of Technology, Germany, Hardenbergstaße 38 (52.5112N, 13.3241E, 31–35 m above sea level), in a compact midrise zone (Local Climate Zone 2) [37]. *Parthenocissus tricuspidata* covers the building wall from the bottom to the top (9 m) and nearly half of the building width (11 m). The plants are attaching themselves to the façade without technical climbing support. They rooted in a raised bed on the west oriented side of the building (unsealed area about 6 m^2). The substrate consists of loamy sand. The plants are irrigated in irregular intervals, but we irrigated the cavity before the measurement campaign to guarantee sufficient water supply. The albedo (calculated from observations on 7, 23, 2013, 1000–1600 Central European Time, CET) is 0.36 in front of the bare building wall, 0.28 in front of the façade greening, and 0.18 for the ground surface. The mean depth of the vegetation layer is 0.27 ± 0.08 m (Table 1). The average leaf area density (LAD) of the façade greening is 1.85 m^2/m^3 according to our measurements at one vertical transect of 1 m × 9 m. On 8, 19, 2013, we harvested all leaves at this vertical transect and measured the depth of the vegetation layer and the size of all leaves with an area meter (Model 3100, LI-COR, Inc.).

2.2. Observation. We measured on 7, 23, 2013 (00–23 CET), in front of the building façade. This day was characterized by clear sky conditions and high air temperatures (Figure 1). The measurements comprised mobile integral radiation measurements as well as wind speed, relative humidity, air temperature, and several other variables to initialize ENVI-met, such as soil and indoor temperature (Figure 2).

The mobile measurements quantified T_{mrt} using integral radiation measurements based on three ventilated net radiometers (CNR4, Kipp & Zonen Corp., accuracy ±10% for daily totals) and the calculation of angular factors with the formula by Thorsson et al. [4] ((1) and (2)). Equation (1) summarizes the long- and short-wave radiations from the bottom, the top, and the four cardinal points. The variables were weighted according to the angular factors in order to estimate the shape of a standing person. Afterward T_{mrt} was calculated from mean radiant flux density (S_{str}) with the Stefan-Boltzmann law (2). The net radiometers were oriented along the façade, which means towards north-northeast (NNE) and not towards the main cardinal points:

$$S_{str} = \alpha_k \int_{i=1}^{6} K_i F_i + \varepsilon_p \int_{i=1}^{6} L_i F_i, \quad (1)$$

$$T_{mrt} = \sqrt[4]{\frac{S_{str}}{(\varepsilon_p \sigma)}} - 273.15, \quad (2)$$

where F_i = angular factors for weighting the radiation fluxes (0.06 for up- and downward and 0.22 for the cardinal points), K_i = short-wave radiation (W/m^2), L_i = long-wave radiation (W/m^2), α_k = absorption coefficient of short-wave radiation (0.07), ε_p = the emissivity of the human body (0.97), and σ = the Stefan-Boltzmann constant ($5.67 \cdot 10^{-8}$ W/m^2 K^{-4}).

Table 1: Leaf area density (LAD) and depth of the façade greening based on a vertical transect of (1 m × 9 m).

Height (m)	0-1	1-2	2-3	3-4	4-5	5-6	6-7	7-8	8-9	Mean
LAD (m^2/m^3)	1.91	2.52	2.02	1.90	1.88	1.81	1.77	1.51	1.32	**1.85**
Depth (m)	0.34	0.36	0.30	0.26	0.30	0.34	0.22	0.18	0.13	**0.27**

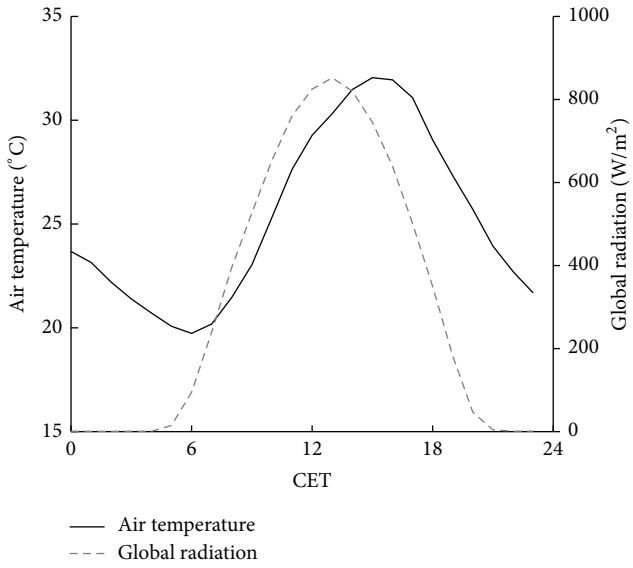

Figure 1: Air temperature in front of the façade and global radiation during the measurement campaign (7, 23, 2013).

The mobile station also included a ventilated temperature and relative humidity sensor (CS215, Campbell Scientific Inc., accuracy ±0.4°C for +5 to +40°C and ±4% for 0 to 100%). The station was set up at a distance of 1.2 m to the building. The measurement height was 1.1 m. We moved the station every 15 min between the greened and the bare site and aggregated the observed data afterwards from a minutely to an hourly resolution for each site (Figure 2).

Additional measurements especially for initializing ENVI-met comprised soil temperatures at a depth of 0.3 m, 0.2 m, and 0.1 m (analog mercury-thermometers), soil humidity (TDR probes) with a resolution of 10 min, and indoor air temperatures averaged over four rooms (Testo 174H, Testo AG, accuracy ±0.5°C for −20 to +70°C) with a 5 min resolution. Furthermore, short-wave transmissivity through the leaves was measured at two heights, each with two pyranometers, one behind and the other one in front of the greening (SP 110, Apogee). Mean transmissivity was 0.28. Off-site observations of global radiation and wind speed were carried out above roof level at the department of ecology (52.4572N, 13.3158E) with a distance of about 6 km to the study site.

2.3. Models and Simulation. For the same day (7, 23, 2013, 00–23 CET), we applied the microclimate models: ENVI-met Version 3.1 Beta 5, ENVI-met Version 4.0 Preview [18, 38], SOLWEIG 2013a [24, 25], and RayManPro [22, 23]. The façade greening was introduced into the models as a flat plant in front of the building with leaves from ground to top. Furthermore, we specified plant parameters (albedo, transmissivity, LAD, etc.) to represent the façade greening as later described for the different models.

In order to analyze the influence of predefined meteorological data from observations and to compare it to the calculations by the models, we performed seven experiments (Table 2). The current version of ENVI-met 3 (E0a) does not support forcing of air temperature and relative humidity and thus additionally the unreleased version 4.0 Preview was applied (E0 unforced and E1 forced). The new version has already been used in other publications [33, 34, 39]. SOLWEIG and RayMan require predefined values of air temperature and relative humidity. Both models can calculate short-wave downward radiation internally, which is the maximum short-wave downward radiation that can be derived at the specific date and location without clouds. These estimated values are used as global radiation to create experiments (R0 and S0) without measurement data of global radiation.

Building data for the input files was generated from the 3D city model of Berlin, which is available in the CityGML data format (http://www.citygml.org). We derived the spatial distribution and the height of vegetation from the Urban and Environmental Information System by the Senate Department for Urban Development and the Environment, Berlin. Terrain is neglected in all simulations because ENVI-met 3 does not support it. Furthermore, we assume its effects to be negligible due to the flat terrain at the study site. Meteorological data for the simulation were derived from on-site observations averaged between the greened and the bare sites in front of the façade for all variables with the exceptions of wind speed, wind direction, and global radiation. To initialize ENVI-met, daily mean values were applied.

2.3.1. ENVI-met. ENVI-met is a CFD model for simulating surface-plant-air interactions from micro- to local scale with a focus on urban environments [18, 38, 40]. It requires intensive computational resources of a personal computer as each of the experiments lasted over 10 days. ENVI-met is, in contrast to RayMan and SOLWEIG, able to simulate the physiological processes of vegetation and to describe vegetation not only as a porous obstacle.

The domain in ENVI-met had a spatial resolution of 1 m × 1 m and consisted of 110 × 80 grid points after removing 30 nesting grid points at each border. The domain size in ENVI-met was limited. Thus, the model domain is smaller than in SOLWEIG and RayMan. We used telescoping grids (factor 15%) starting at 2 m to include the highest building (43 m) because vertical grids were limited to 30 layers. In ENVI-met the wind field and turbulent heat flux were simulated as well. Therefore, the model domain needed to be

Table 2: Overview of the input parameters and model settings in the seven experiments. "X" represents input of times series of meteorological data.

Input parameter	Name	E0a	E0	E1	R0	R1	S0	S1
	Model	ENVI-met 3	ENVI-met 4		RayMan		SOLWEIG	
Meteorological data: initial	Unit							
Wind speed (10 m)	m/s	2.3	2.3	2.3	—	—	—	—
Wind direction (10 m)	deg	57.0	57.0	57.0	—	—	—	—
Potential air temperature (2500 m)	°C	24.85	24.85	24.85	—	—	—	—
Specific humidity (2500 m)	g/kg	8.56	8.56	8.56	—	—	—	—
Relative humidity (2 m)	%	45.8	45.8	—	—	—	—	—
Meteorological data								
Air temperature (1.1 m)	°C	—	—	X	X	X	X	X
Relative humidity (1.1 m)	%	—	—	X	X	X	X	X
Global radiation	W/m^2	—	—	—	—	X	—	X
Soil data								
Initial soil temperature (0–50 cm)	°C	23.10–25.71	23.10–25.71	23.10–25.71	—	—	—	—
Relative soil humidity (0–50 cm)	%	25.00	25.00	25.00	—	—	—	—
Environmental parameter								
Albedo surroundings	—	—	—	—	0.30	0.30	0.36	0.36
Albedo (wall)	—	0.36	0.36	0.36	—	—	—	—
Albedo (roof)	—	0.20	0.20	0.20	—	—	—	—
Albedo (plant)	—	0.28	0.28	0.28	0.28	0.28	—	—
Transmissivity of vegetation	—	—	—	—	—	—	0.28	0.28
Emissivity (ground)	—	—	—	—	—	—	0.95	0.95
Emissivity (walls)	—	—	—	—	—	—	0.90	0.90
Bowen ratio	—	—	—	—	1.00	1.00	—	—
Solar adjustment factor	—	0.85	0.85	0.85	—	—	—	—

Figure 2: Measurement arrangement and study site in Berlin, Germany.

rotated by 30° to avoid unrealistic roughness at the edges of the building walls (Figure 3). With the high resolution vegetation data, we introduced new vegetation classes based on the default plant database of ENVI-met to account for vegetation heights with a resolution of 1 m. The façade greening was also introduced as a new class with the measured LAD values (Table 1). We interpolated the 9 measured levels to 10 relative height levels to adapt to the structure of ENVI-met's plant database (see Table 3). According to on-site experiences, soils beneath vegetation were classified as loamy sand, streets as asphalt, areas beneath buildings as pavement, and nonstreet areas as light brick roads.

Table 3: Measured leaf area density (LAD) profile of façade greening (bold) and assumed parameter for the plant database in ENVI-met.

Plant	Type	Albedo	Height (m)	Root zone (m)	Leaf area density (LAD) at level										Root area density, all levels
					1	2	3	4	5	6	7	8	9	10	
Trees	Deciduous trees	0.28	6–31	2	0	0	0	0.2	0.7	2.2	2.2	2.0	1.7	0.4	0.1
Façade greening	Deciduous trees	0.28	9	1	**1.9**	**2.5**	**2.1**	**1.9**	**1.9**	**1.9**	**1.8**	**1.7**	**1.5**	**1.3**	0.1

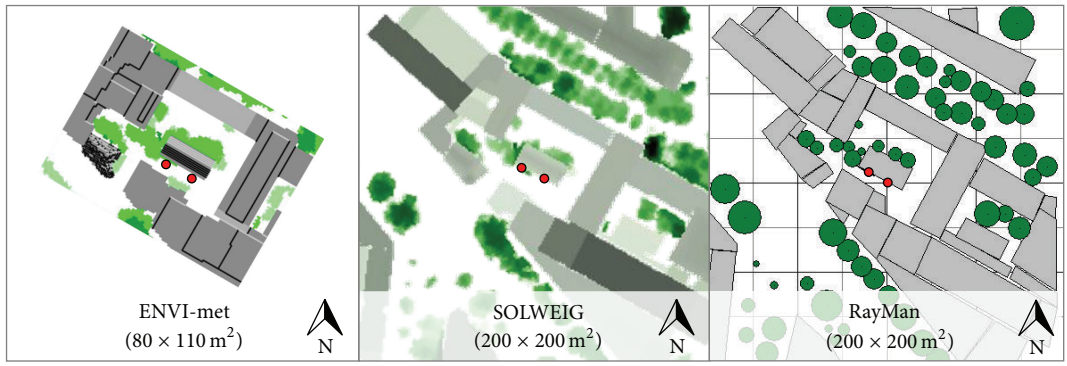

Figure 3: Model domains of the different models. In the domain of SOLWEIG, dark colors represent taller buildings and vegetation compared to pale colors. Red circles indicate the greened and the bare site of observation and analyses.

2.3.2. SOLWEIG. SOLWEIG simulates radiation fluxes and T_{mrt} based on digital surface models [24, 25]. In contrast to ENVI-met and RayMan, SOLWEIG calculates shadow patterns and consequently T_{mrt} for the middle of an hour; thus meteorological input was averaged accordingly. Vegetation and building data were also compiled with a resolution of 1 m. SOLWEIG uses trunk zones to calculate shadow patterns of vegetation, which were about 30% of the vegetation height at the study site. The façade greening was represented as a flat plant without a trunk characterized by the observed values of albedo and transmissivity. In order to generate a SOLWEIG run (S0) without measurement data of global radiation, SOLWEIG1D was used. SOLWEIG1D calculates the maximum global radiation for the geographical location, which SOLWEIG2013a is not able to do.

2.3.3. RayMan. Matzarakis et al. [22] developed the model RayMan (RayMan Pro 2.2) to calculate T_{mrt} and biometeorological indices in complex environments. The building and vegetation data were created manually with the supplied editor on the basis of the digital surface models. Due to this approach, buildings had a flat roof in RayMan. In contrast to SOLWEIG and ENVI-met, RayMan calculates fluxes only for one point of interest. Thus, two obstacle files were used with different center points. Similar to SOLWEIG, RayMan can calculate global radiation itself. Consequently, we did experiments with calculated (R0) and measured global radiation (R1). The façade greening was represented as series of plants in front of the building with a diameter of 1 m, a trunk length of 0 m, and an albedo of 0.28.

2.4. Analyses. The analyses of the simulation results refer to two points in front of the façade in each model domain, the greened site and the bare site (Figure 3). For the model evaluation (Section 3.2), time series plots are only presented for the greened site, but the statistical analysis includes both sites.

The models that did not calculate a specific climate element (e.g., air temperature) were excluded for the section. Long-wave radiation from RayMan and ENVI-met was calculated from surface temperatures using the Stefan-Boltzmann law (with an emissivity of 0.95).

The selected statistical measures for the model evaluation are a combination of generally recommended ones [41, 42] and the ones mostly found in former studies (e.g., coefficient of determination (r^2)). Root-mean-square deviation (RMSD), mean deviation (MD), and mean absolute deviation (MAD) were calculated as described by Schlünzen and Sokhi [42]. For all statistical analyses we used IDL 8.2.2 (2007–2012 Exelis Visual Information Solutions, Inc.) and the library "Coyote" (1996–2014 Fanning Software Consulting, Inc.).

3. Results

3.1. Measuring the Effects of Façade Greening on T_{mrt}. T_{mrt} decreased by 2.13 K (1000–1600 CET, 7, 23, 2014) in front of the greened façade compared to the bare one (Figure 4). The components for calculating T_{mrt} varied slightly between both sites and not only the short-wave radiation reflected and the long-wave radiation emitted from the façade from NNE (Figure 5). Thus, the sums of short-wave and long-wave radiation downward, upward, and from the cardinal points differed between the bare and the greened site (Table 4). Nevertheless, long-wave radiation emitted from the greened site is clearly lower compared to the bare one.

Table 4: Sum (00–23 CET) of long- and short-wave radiation at the greened and the bare site up- and downward (up, down) and from the cardinal points (west-northwest (WNW), east-southeast (ESE), south-southwest (SSW), and north-northwest (NNE) (direction from the façades)) on 7, 23, 2013. F_i is the angular factor used in calculation of mean radiant temperature (0.06 for up- and downward radiation and 0.22 for radiation from the cardinal points).

Direction	Sum of short-wave radiations (MJ d^{-1})				Sum of long-wave radiations (MJ d^{-1})			
	Bare	Greened	$^{\Delta}$Bare-greened	$^{\Delta}$Bare-greened $\times F_i$	Bare	Greened	$^{\Delta}$Bare-greened	$^{\Delta}$Bare-greened $\times F_i$
Down	22.36	20.12	2.24	0.13	36.20	35.88	0.31	0.02
Up	4.35	3.57	0.78	0.05	43.02	42.04	0.99	0.06
WNW	8.67	6.11	2.56	0.56	39.92	39.60	0.33	0.07
ESE	10.93	10.39	0.54	0.12	40.49	39.62	0.87	0.19
SSW	14.27	13.44	0.83	0.18	39.36	38.81	0.55	0.12
NNE	5.03	3.54	1.49	0.33	42.29	39.92	2.37	0.52

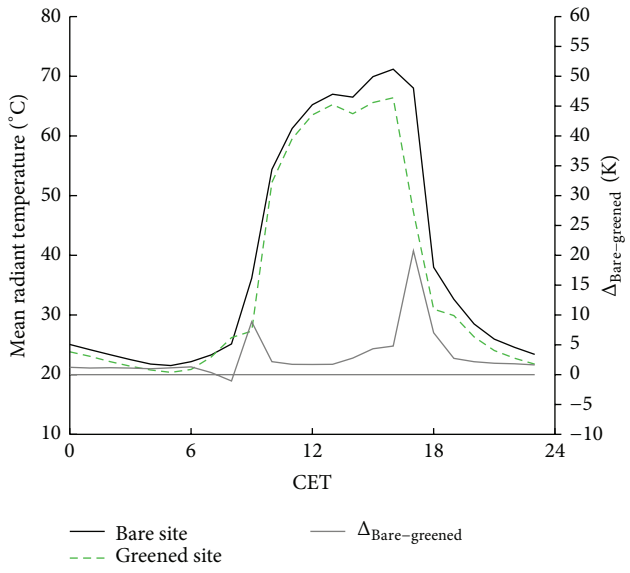

Figure 4: Mean radiant temperature observed at the bare and the greened site in front of the building on 7, 23, 2013.

Table 5: Overview of the performance of the experiments (EXP) in simulating mean radiant temperature on 7, 23, 2013, regarding root-mean-square deviation (RMSD), mean deviation (MD), mean absolute deviation (MAD), and coefficient of determination (r^2).

	Mean radiant temperature (K)			
EXP	RMSD	MD	MAD	r^2
E0a	7.98	−1.26	6.72	0.95
E0	8.30	0.99	6.90	0.94
E1	8.18	1.16	6.87	0.95
R0	7.11	−3.35	5.85	0.90
R1	7.35	−5.53	6.17	0.94
S0	4.63	−2.40	3.40	0.96
S1	4.81	−3.13	3.48	0.96
Mean	6.91	−1.93	5.63	0.94

3.2. Evaluation of ENVI-met, RayMan, and SOLWEIG

3.2.1. Mean Radiant Temperature. The models simulated T_{mrt} reasonably well in pattern and amplitude compared to the observations (Figures 6(a) and 6(b)). Experiments with SOLWEIG showed the lowest normalized standard deviation (Figure 6(b)) and high r^2 (Table 5). Despite high absolute errors in RMSD and MAD, experiments with ENVI-met produced the lowest MD (Table 5).

3.2.2. Long- and Short-Wave Radiation. Short-wave downward radiation in front of the greened and the bare site was simulated with high r^2 and low MD. RMSD showed larger deviation, especially in experiments with ENVI-met. Larger deviation also occurred in the morning and in the evening, which are the transition times between direct sun and shadow (Figure 7(a), Table 6). Simulated short-wave upward radiation differed much more from observations than short-wave downward radiation (Figure 7(b), Table 6). ENVI-met and SOLWEIG are able to compute short-wave upward radiation in contrast to RayMan. ENVI-met produced the amplitude more precisely than SOLWEIG, but SOLWEIG simulated the duration of intensive short-wave downward radiation closer to the observations (Figure 7(a)).

Concerning the long-wave downward radiation, SOLWEIG (S0 and S1) was the closest to the observations (Figures 7(c) and 7(d)). Long-wave upward radiation was underestimated during the night in all models. During the day, the differences between the simulations and observations decreased (Figure 7(c)).

3.2.3. Air Temperature and Specific Humidity. Simulations with RayMan and SOLWEIG are based on predefined air temperatures and specific humidity; only ENVI-met computes these variables itself. ENVI-met captured the diurnal cycle of air temperature, but specific humidity was reproduced with low deviations from observations only in the forced run (E1) (Figures 8(a) and 8(b)). E1 showed lower deviations than E0a and E0 in simulating air temperatures especially in the early morning (Figure 8(a), Table 7). E1 was the closest to the observation for specific humidity as well (Figure 8(b) and Table 7). The unforced experiments E0a and E0 overestimated specific humidity by 1.5 g/kg (RMSD).

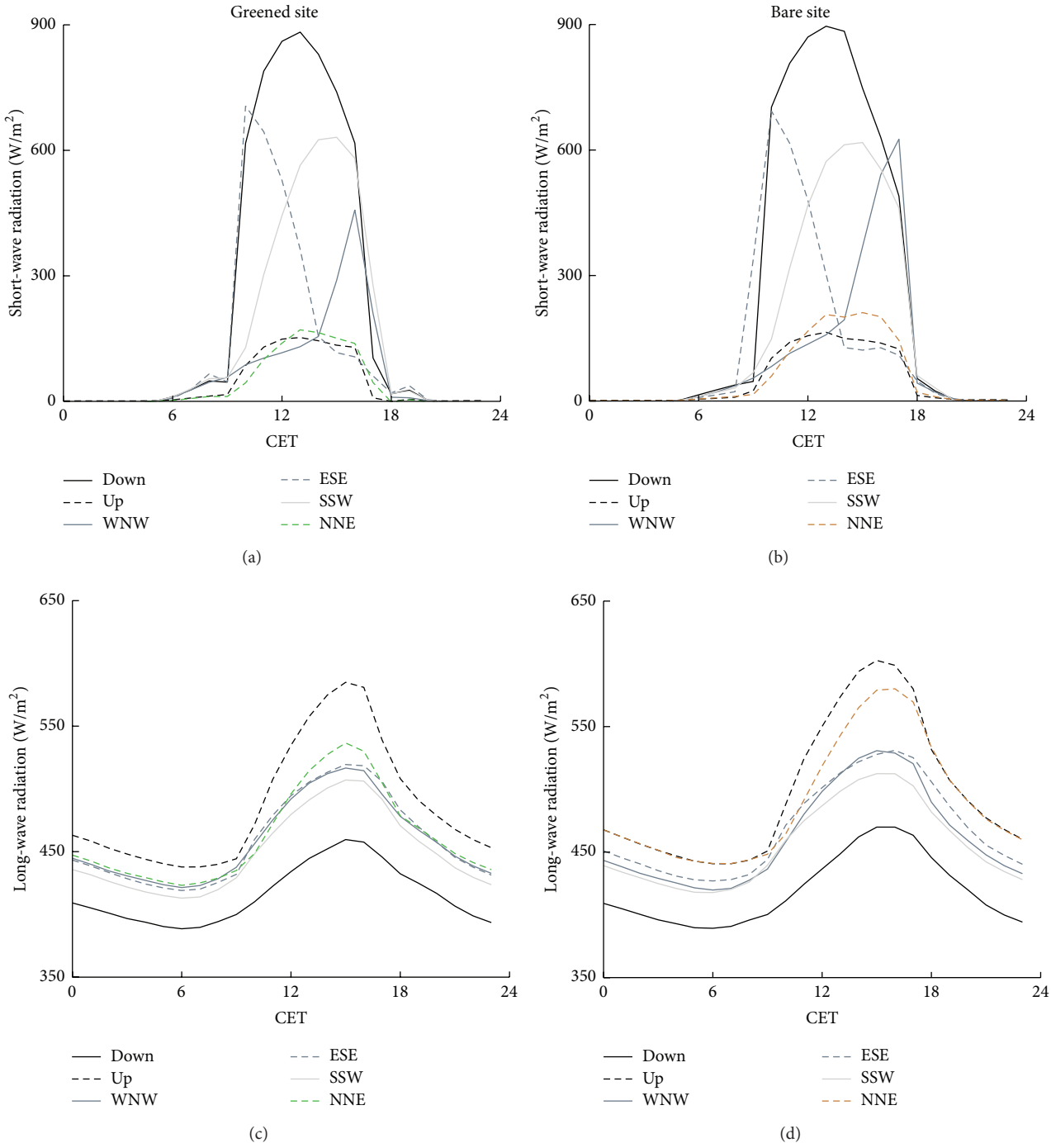

FIGURE 5: Short-wave radiation at the greened (a) and the bare (b) site and long-wave radiation at the greened (c) and the bare (d) site on 7, 23, 2013. All components used to calculate mean radiant temperature are represented, which are up- and downward radiation (up, down) and radiation from the cardinal points (west-northwest (WNW), east-southeast (ESE), south-southwest (SSW), and north-northwest (NNE) (direction from the façades)).

3.3. Comparison of the Observed and Simulated Effects of Façade Greening. The observed differences between the bare and the greened site were not well reproduced by the models (Figure 9 and Table 8). The peaks in the transition times were simulated in all models to different extent. The cooling effect of façade greening, however, was only simulated by S0 and S1, although too small. The experiments with ENVI-met showed a higher T_{mrt} in front of the greened site than in front of the bare site, while R0 and R1 produced no differences between the sites (Table 8). Emitted long-wave radiation from

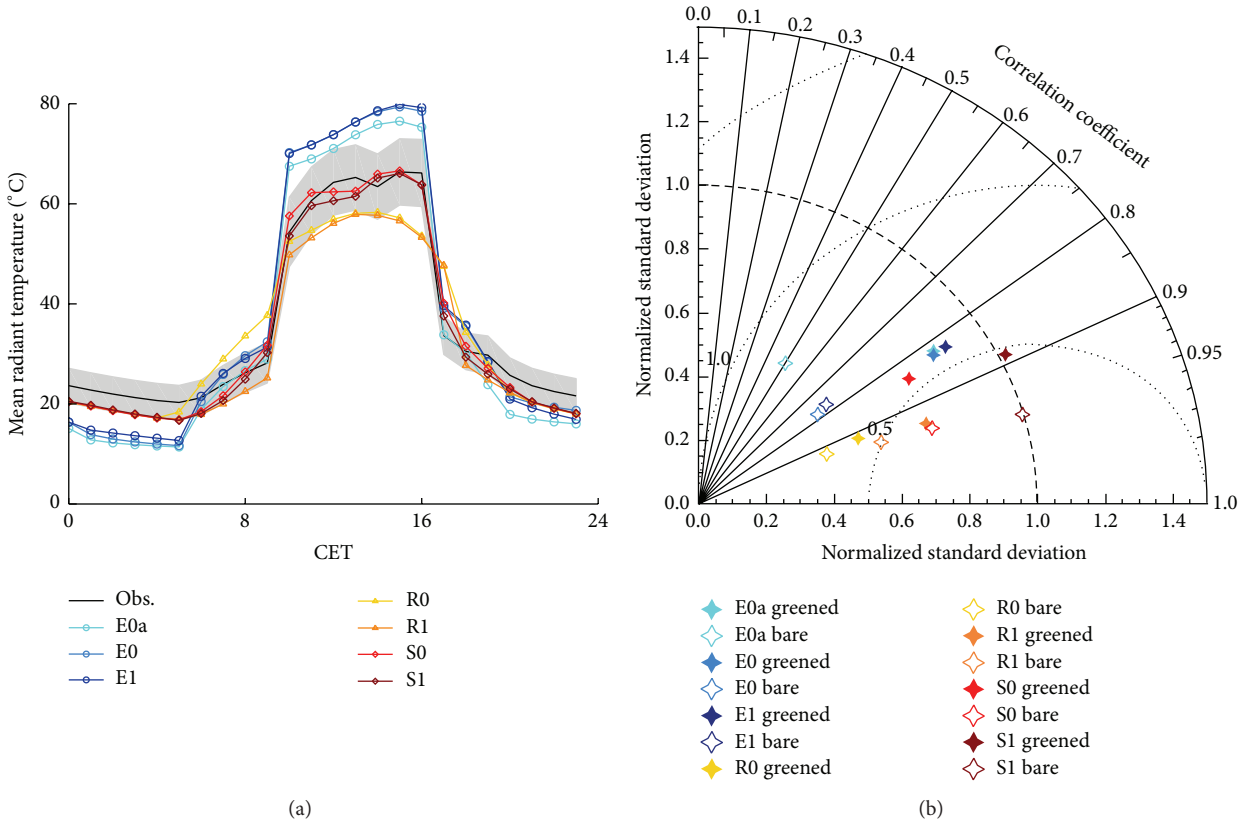

FIGURE 6: Mean radiant temperature on 7, 23, 2013, as observed and simulated (a) at the greened site and (b) Taylor-Diagram for the experiments with ENVI-met 3 (E0a), unforced (E0) and forced ENVI-met 4 (E1), RayMan without (R0) and with global radiation from observation (R1), and SOLWEIG without (S0) and with global radiation from observation (S1). The gray area indicates the accuracy range of the observations.

the greened site was reduced in the experiments with ENVI-met and SOLWEIG (Figure 10(a)), but to a smaller extent (Figure 10(b)).

4. Discussion

4.1. Measuring the Effects of Façade Greening on T_{mrt}. The observed differences in T_{mrt} of 2 K were distinct but lower than the measurement accuracy of about 4 K. Tan et al. [15] detected larger differences of 2 to 13 K between sites with and without façade greening in a tropical environment. They only detected a reduction of T_{mrt} when the façade greening was opposed to direct sunlight and not shaded [15]. In addition, the reduction depended on the distance to the façade and was mainly limited to 1 m. Thus, the small observed differences in this study can be partly explained with the larger distance of the measurement to the façade of 1.2 m. Furthermore, the effects of façade greening on air temperature were found to be small (1.5 K, Djedjig et al. [11], 1 K, Berry et al. [16], 0.25 K, Gross [14], and negligible, Pérez et al. [7]). In this case study façade greening was only attached to one façade wall. Hence, the impact on modified long- and short-wave radiation from the greened façade accounts to only 22% in calculating T_{mrt}(1). Therefore, the impact on T_{mrt} was limited, even though emitted long-wave radiation was clearly reduced in front of the greened façade. The albedo also interferes with T_{mrt} because the light bare wall with its higher albedo reflected more short-wave radiation than the darker greened façade.

Furthermore, the differences in T_{mrt} cannot be reduced to the effects of façade greening exclusively. Boundary conditions were different between both sites regarding times of shadowing (Table 4). The opposing building structure is higher in front of the bare site than in front of the greened site (Figure 3), which leads to different shadowing times. In the evenings, at around 1700 CET, the greened façade was completely shadowed while the bare site still received direct sunlight for another half an hour. In the morning, at around 0900 CET, when the sunlight appeared at the façade, some differences existed as well. Furthermore, the opposing building might also have an influence regarding the reflection of short-wave radiation. With respect to short-wave and long-wave radiation, the greened site received less energy from all directions than the bare one. Consequently, the cooling effect of T_{mrt} was overestimated in the observations. This demonstrates shortcomings in the case study as both sites were not identical regarding the radiation characteristics, which introduces uncertainties when interpreting deviations between the sites. The problem of comparability and usability of case studies to observe the effects of façade greening

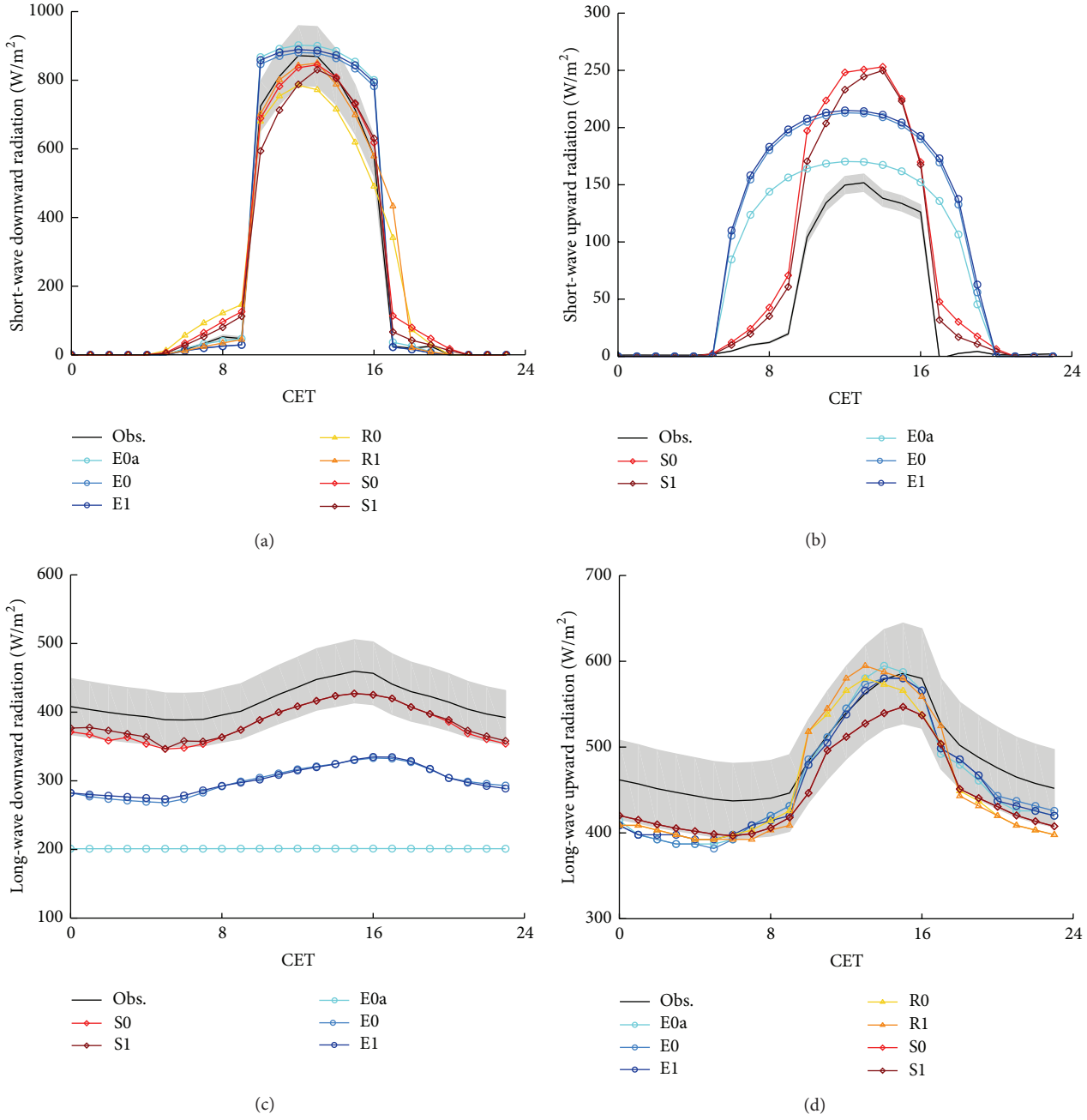

FIGURE 7: Comparison of simulated and observed (a) short-wave downward radiation, (b) short-wave upward radiation, (c) long-wave downward radiation, and (d) long-wave upward radiation on 7, 23, 2013, for the greened site in front of the façade simulated with ENVI-met 3 (E0a), unforced (E0) and forced ENVI-met 4 (E1), RayMan without (R0) and with global radiation from observation (R1), and SOLWEIG without (S0) and with global radiation from observation (S1). The gray areas indicate the accuracy range of the observations.

occurs often as criticized by Hunter et al. [10]. Specifically in complex urban environments optimal study sites are difficult to find. Elaborated assessments (e.g., integral radiation measurements) can reveal such problems in contrast to simple single-variable measurements (e.g., air temperature). Our findings further support the need of reliable model tools in combination with observations to study the effects of façade greening for specific sites and climates.

4.2. Evaluation of ENVI-met, RayMan, and SOLWEIG

4.2.1. Mean Radiant Temperature. Simulated T_{mrt} deviated about 7 K (mean RMSD) from the observation in this and about MD 2–8 K and 2–15 K RMSD in former studies (Table 9). This uncertainty range is reasonable compared to the average accuracy in measurements of about 4 K. The uncertainty, however, varies largely depending on

Table 6: Overview of the performance in simulating downward (a) and upward (b) short-wave and long-wave radiation on 7, 23, 2013. For further explanations refer to Table 5.

(a)

Short-wave downward radiation (W/m^2)				
EXP	RMSD	MD	MAD	r^2
E0a	130.46	46.31	50.33	0.91
E0	124.44	36.96	47.12	0.91
E1	128.17	40.46	49.70	0.91
R0	82.33	−6.15	54.06	0.96
R1	70.50	3.19	25.59	0.96
S0	54.65	−3.20	29.36	0.98
S1	65.86	−16.86	34.64	0.97
Mean	93.77	14.39	41.54	0.94
Long-wave downward radiation (W/m^2)				
EXP	RMSD	MD	MAD	r^2
E0a	209.60	−208.03	208.03	0.01
E0	116.32	−115.83	115.83	0.82
E1	115.27	−114.85	114.85	0.86
R0	—	—	—	—
R1	—	—	—	—
S0	34.89	−34.31	34.31	0.95
S1	31.66	−31.16	31.16	0.95
Mean	101.44	−100.71	100.71	0.71

(b)

Short-wave upward radiation (W/m^2)				
EXP	RMSD	MD	MAD	r^2
E0a	61.86	38.34	39.84	0.60
E0	84.76	58.55	60.04	0.60
E1	87.12	60.50	62.00	0.60
R0	—	—	—	—
R1	—	—	—	—
S0	56.55	32.74	35.11	0.95
S1	51.36	27.94	30.57	0.95
Mean	68.33	43.61	45.51	0.74
Long-wave upward radiation (W/m^2)				
EXP	RMSD	MD	MAD	r^2
E0a	35.19	−26.89	30.96	0.91
E0	33.28	−23.81	27.62	0.92
E1	31.70	−24.88	27.19	0.93
R0	46.23	−35.65	42.69	0.83
R1	46.62	−33.10	43.46	0.86
S0	43.28	−42.09	42.09	0.97
S1	43.30	−42.12	42.12	0.97
Mean	39.94	−32.65	36.59	0.91

Table 7: Overview of ENVI-met's performance in simulating air temperatures and specific humidity on 7, 23, 2013. For further explanations refer to Table 5.

EXP	RMSD	MD	MAD	r^2
Air temperature (K)				
E0a	1.39	0.00	1.13	0.87
E0	1.68	0.06	1.43	0.83
E1	0.96	0.40	0.86	0.98
Mean	1.35	0.16	1.14	0.89
Specific humidity (g/kg)				
E0a	1.44	1.17	1.31	0.10
E0	1.54	1.28	1.40	0.10
E1	0.35	−0.03	0.25	0.91
Mean	1.11	0.81	0.99	0.37

Table 8: Mean (±standard deviation), minimum and maximum difference in T_{mrt} between bare and greened site in observation (OBS) on 7, 23, 2013 (10–16 CET) and experiments (EXP) with ENVI-met 3 (E0a), ENVI-met 4 (E0 and E1), RayMan (R0 and R1) and SOLWEIG (S0 and S1).

EXP	T_{mrt} (Bare – Greened) (K)		
	Mean	Mininum	Maximum
OBS	2.13 ± 1.81	0.02	5.02
E0a	−2.81 ± 2.25	−5.89	0.57
E0	−4.14 ± 1.41	−5.56	−1.82
E1	−4.32 ± 1.44	−5.42	−1.88
R0	0.01 ± 0.04	0.00	0.10
R1	−0.09 ± 0.07	−0.20	0.00
S0	0.96 ± 0.88	−0.57	1.94
S1	1.30 ± 1.01	−0.49	2.28

the selected model and study design (Table 9). Krüger et al. [20] concluded for RayMan that the uncertainty in calculating T_{mrt} depends on different factors, such as morphology, meteorological conditions, and surface properties. For example, correlation coefficients were much higher in this study compared to the investigations of Chen et al. [17]. Such deviations are caused by model specific parameterizations.

Other reasons for deviations in all applied models were discrepancies in building or plant shapes. All experiments produced larger deviations during the transition between shadow and direct radiation, which was also reported by Thorsson et al. [4] and Matzarakis et al. [23]. Such deviations are caused by inaccuracies in building shapes due to the spatial resolution of 1 m or by errors in the basic data of building shapes.

Simulated T_{mrt} differed hardly between the computed and predefined meteorological input data. Consequently, calculated global radiation by RayMan and SOLWEIG was sufficient for simulating T_{mrt}, and observations of global radiations did not enhance the model performance considerably, at least for this nearly cloud-free day. In ENVI-met, the forcing of air temperature and relative humidity showed only minor effects on simulating T_{mrt} as well.

In SOLWEIG, the transmissivity is of importance for calculating T_{mrt} beneath vegetation [25]. We applied an averaged value for the whole model domain because we measured transmissivity only at two points of the façade greening and SOLWEIG does not allow any spatial variations. Nevertheless, the range of deviations in this study is similar

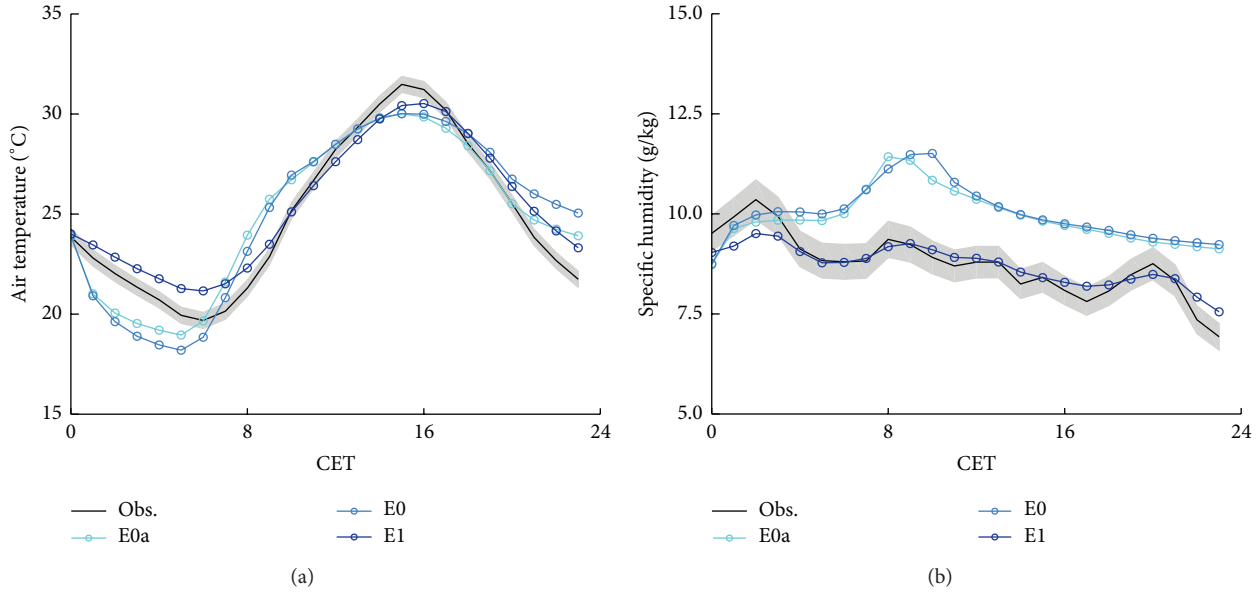

Figure 8: Comparison of simulated and observed (a) air temperatures and (b) specific humidity of the experiments with ENVI-met 3 (E0a) and unforced and forced ENVI-met 4 (E0 and E1) on 7, 23, 2013. The gray area indicates the accuracy range of the observations.

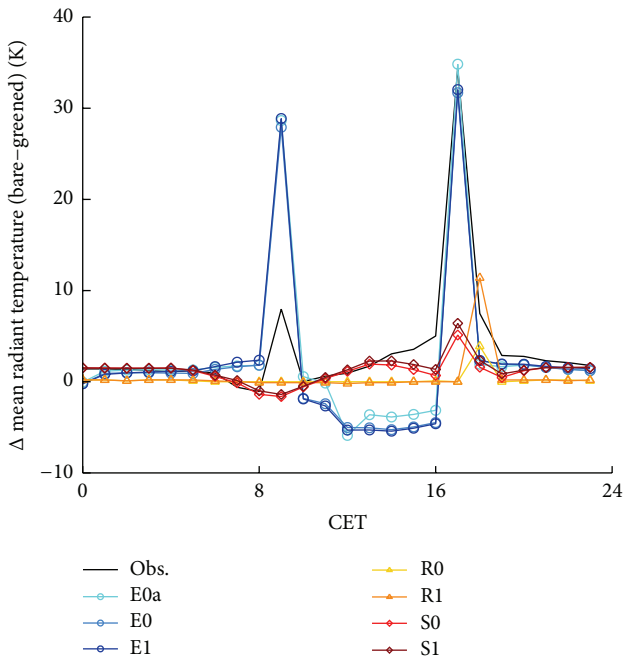

Figure 9: Differences between the bare and greened site in observation and simulations (7, 23, 2013) in experiments with ENVI-met 3 (E0a), unforced (E0) and forced ENVI-met 4 (E1), RayMan without (R0) and with global radiation from observation (R1), and SOLWEIG without (S0) and with global radiation from observation (S1).

Table 9: Overview of deviations in mean radiant temperature between simulations and observations in other studies concerning root-mean-square deviation (RMSD), mean deviation (MD), mean absolute deviation (MAD), and coefficient of determination (r^2). Standard deviations (±) are stated, if more than one analysis is performed per study.

	Mean radiant temperature (K)			
Reference	RMSD	MD	MAD	r^2
		ENVI-met		
[17]	—	—	—	0.09 ± 0.1
[18]	4.13 ± 0.4	—	—	—
E1	8.18	1.16	6.87	0.95
		RayMan		
[17]	—	—	—	0.82 ± 0.0
[19]	—	—	—	0.88
[20]	14.93 ± 3.5	—	12.88 ± 3.5	0.37 ± 0.2
[21]	—	—	—	0.85
[4]	—	8.45 ± 1.7	—	—
[22]	—	—	—	0.77
[23]	1.7 ± 0.5	—	—	0.96 ± 0.5
Mean	8.32 ± 2.0	8.45 ± 1.7	12.88 ± 3.5	0.74 ± 0.23
R1	7.35	−5.53	6.17	0.94
		SOLWEIG		
[17]	—	—	—	0.32
[24]	4.8	2.00 ± 0.3	—	0.94
[25]	3.1	—	2.74	0.91
Mean	3.95	2.00 ± 0.3	2.74	0.72
S1	4.81	−3.13	3.48	0.96

to findings by Lindberg and Grimmond [25], who detected a RMSD of 3.1 K and a MAD of 2.74 K.

RayMan underestimated T_{mrt} in this study probably as a consequence of too low short-wave downward radiation. On the contrary, Krüger et al. [20] examined an overestimation for various cloudiness conditions (RMSD 14.93 K, MAD

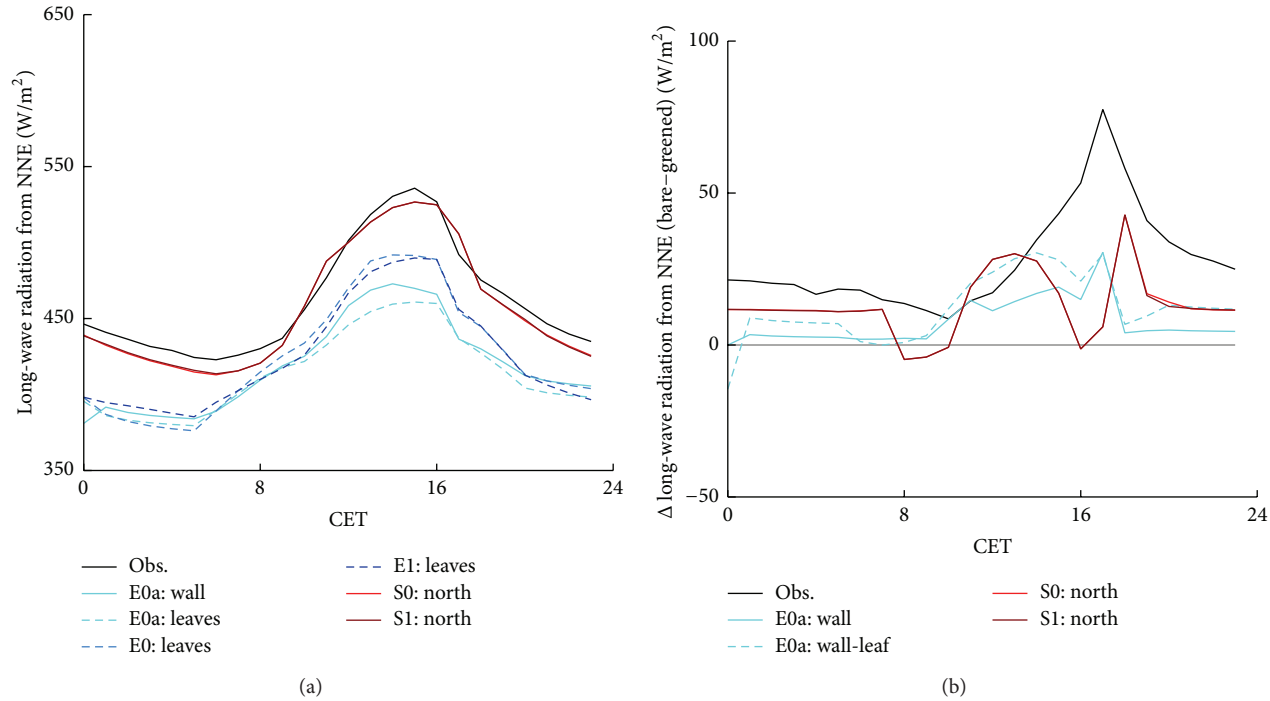

Figure 10: Simulated long-wave radiation (a) emitted from the greened site (wall or leaves) and (b) differences between bare and greened façade in simulations and observation for the experiments with ENVI-met 3 (E0a), unforced (E0) and forced ENVI-met 4 (E1), and SOLWEIG without (S0) and with global radiation from observation (S1) (7, 23, 2014).

12.88 K). Additionally, they detected a higher agreement with observations on clear sunny days compared to cloudy ones [20]. During sunny days the accuracy of SVF has a high influence on the uncertainty in simulating T_{mrt} [20]. Hence, inaccuracies in the building and vegetation shape had a large impact in this study. The deviation in RayMan varies remarkably in this study and other ones [4, 19, 22] (Table 9).

The uncertainty also differs strongly between different studies with ENVI-met. Ali-Toudert [43] detected an underestimation of T_{mrt} during the day and an overestimation during the night. In this study, however, the overestimation of short-wave radiation led to an overestimation of T_{mrt}. Yang et al. [44] also detected an overestimation in ENVI-met due to an overestimation of short-wave downward radiation (without statistical values).

Overall, SOLWEIG simulated T_{mrt} closest to the observation both in this study and in former ones (Table 9). ENVI-met showed the largest deviations in this study. Furthermore, shortcomings in the evaluation of all three models become visible regarding the amount of studies and in comparability due to different statistics to evaluate models uncertainty.

4.2.2. Long- and Short-Wave Radiation. Short-wave downward radiation showed less deviations compared to other radiation components. ENVI-met did not capture the amplitude of global radiation well, partly because only water vapor alternates short-wave radiation [44]. Additionally, Ali-Toudert [43] detected problems in simulating global radiation with ENVI-met and consequently a radiation adjustment factor was introduced to ENVI-met. Here, short-wave downward radiation in ENVI-met was reduced in advance by 25% to match the amplitude of observations (Table 2). Additional deviations in short-wave downward radiation were produced by the resolution of grid points and by inaccuracies of the input data of buildings and vegetation as discussed for T_{mrt}. The small deviation in short-wave downward radiation was a main driver for the sufficient simulation of T_{mrt}.

Short-wave upward radiation has less impact on T_{mrt} due to the generally smaller energy flux density and low F_i in the calculation of T_{mrt}. Thus, the overestimation in all experiments was less decisive for simulating T_{mrt}. ENVI-met overestimated the duration of intense short-wave upward radiation because shadowing effects of the surface are neglected. SOLWEIG captured the duration but overestimated the amplitude of short-wave upward radiation due to a higher albedo. SOLWEIG cannot consider different albedo values of ground surfaces and walls. In future, this problem might be fixed because Lindberg and Grimmond [25] proposed for the next SOLWEIG version the possibility to specify albedo and emissivity spatially.

Long-wave downward radiation was underestimated. The overestimations of short-wave upward radiation and long-wave downward radiation compensate each other and thus the total impact of the inaccuracies on T_{mrt} was reduced. ENVI-met 3 (E0a) failed to simulate the diurnal variation of long-wave downward radiation as it uses averaged emissivity values and surface temperatures to calculate it.

Long-wave upward is underestimated during the night because the models do not consider heat storage of

the buildings sufficiently (ENVI-met 4) or not at all (ENVI-met 3, SOLWEIG, and RayMan). Hwang et al. [19] and Lin et al. [21] discussed these shortcomings in ENVI-met 3 and detected the fact that daytime surface temperature was overestimated and nighttime surface temperature was underestimated. ENVI-met 4 should be able to consider these effects in principle but failed in this case study. Possibly, the heat storage was insufficiently parameterized or the spin-up time was too short. Follow-up studies might acquire a more suitable description of heat storage in the walls. During the night, the underestimation of emitted long-wave radiation also led to undervalued T_{mrt} in all experiments.

Overall, the individual terms of the radiation balance were, with the exception of short-wave downward radiation, not plausibly simulated by all models. Short-wave downward radiation may also show much higher inaccuracies under cloudy conditions as Krüger et al. [20] detected for RayMan. Furthermore, the lack of model evaluation is more apparent for the individual terms of the radiation balance than for T_{mrt} as we detected only three other studies (Table 10), which leads to a high uncertainty regarding the reliability in simulating these variables.

4.2.3. Air Temperature and Specific Humidity. ENVI-met reproduced air temperature close to the observations with a RMSD between 0.9 and 1.6 K and MD between 0.0 and 0.4 K in this case study and with a mean RMSD of 1.9 K and MD −0.65 K in former studies (Table 11). During the day, ENVI-met tended to underestimate air temperature but overestimated it during the night [21, 43]. Berkovic et al. [45], who compared simulations and observations qualitatively, found larger differences during the evenings for air temperatures and relative humidity (about 3 K, 15%). Forcing in E1 clearly decreased the uncertainty compared to E0 especially during the day but showed only minor effects on T_{mrt}.

The uncertainty in simulating air temperature with ENVI-met varies between different studies remarkably (Table 11). A high agreement was achieved by Skelhorn et al. [35] and Srivanit and Hokao [26] after optimization and calibration efforts of different parameters and with a longer spin-up time. Air temperature has been evaluated in several studies. Thus, the simulation seems to be reliable, with an uncertainty of about 1.88 K (RMSD).

Specific humidity was evaluated by Chen et al. [17] with a RMSD of 0.82 g/kg, which is higher than in this study (RMSD = 0.35 g/kg). Forcing (E1) improved the simulation of specific humidity compared to the unforced runs (E0a, E0).

4.3. Comparison of the Observed and Simulated Effects of Façade Greening. The applied models were not able to reproduce the observed effects of façade greening. SOLWEIG was the only model that simulated at least a small reduction of T_{mrt}. The reductions cannot be related to transpirative effects of the plants because such effects are not considered in SOLWEIG. Thus, the decrease in T_{mrt} was produced by radiation changes. Simulated long-wave radiation emitted from the wall was clearly reduced in front of the façade greening (S0, S1).

Table 10: Overview of deviations in short-wave downward radiation between simulation and observation in other studies. For further explanation refer to Table 9.

Short-wave downward radiation (W/m^2)				
Reference	RMSD	MD	MAD	r^2
ENVI-met				
[26]	—	−289.15 ± 8.8	—	—
E1	128.17	40.46	49.70	0.91
SOLWEIG				
[24]	42.1	—	—	0.97
[25]	43.3	—	—	0.97
Mean	42.2	—	—	0.97
S1	65.86	−16.86	34.64	0.97

Table 11: Overview of deviations in air temperature and specific humidity between simulation and observation in other studies. For further explanations refer to Table 9.

Air temperature (K)				
Reference	RMSD	MD	MAD	r^2
[27]	2.79 ± 0.0	0.66 ± 0.1	2.40 ± 0.1	0.70 ± 0.0
[28]	1.45 ± 0.1	−1.29 ± 0.0	1.29 ± 0.0	—
[29]	1.95 ± 0.4	—	—	—
[30]	2.91 ± 0.9	−0.62 ± 1.3	2.45 ± 0.7	0.90 ± 0.1
[18]	1.37 ± 0.4	—	—	—
[31]	1.74 ± 0.3	—	—	—
[32]	—	—	—	0.97
[33]	—	—	—	0.70 ± 0.1
[34]	—	−3.50 ± 0.5	—	0.95 ± 0.0
[35]	—	0.64 ± 0.3	—	0.94
[26]	—	−0.56 ± 0.9	—	—
[26]	—	0.10	—	—
[36]	0.93 ± 0.1	—	—	0.95 ± 0.0
Mean	1.88 ± 0.4	−0.65 ± 0.53	2.05 ± 0.3	0.87 ± 0.4
E1	0.96	0.40	0.86	0.98
Specific humidity (g/kg)				
[36]	0.82 ± 0.0	—	—	0.54 ± 0.0
E1	0.35	−0.03	0.25	0.91

ENVI-met, which is able to simulate transpiration, reproduced higher T_{mrt} in front of the greened site compared to the bare site. Emitted long-wave radiation was reduced in front of the greened façade, but the effect was not permeated to T_{mrt}. Increasing the spin-up time in ENVI-met might amplify the generation of effects of façade greening. Specifically in ENVI-met and RayMan, the inabilities in simulating a reduction of T_{mrt} in front of the greened façade could not be easily traced back because they do not return all relevant components for T_{mrt}.

To conclude, the models showed a limited applicability to façade greening in this study. The small alterations of long- and short-wave radiation due to façade greening were indistinct. Thus, specific types of urban green cannot be included

in these models without further adaptations. Restrictions must be made, however, regarding the complex real-case study site. Moreover, modification of model parameters and settings (e.g., spin-up time) especially for ENVI-met could lead to other results but would go beyond the scope of this study.

5. Conclusions

The effect of façade greening on outdoor human bioclimate was limited in this case study because only a small reduction T_{mrt} in front of the façade greening was detected. Hence, façade greening has only a minor effect in reducing outdoor heat stress. With a façade greening attached to more than one façade in a street canyon or court yard the effect on T_{mrt}, however, might be enlarged.

The general ability of ENVI-met, RayMan, and SOLWEIG to simulate T_{mrt} was reasonable as expected for well-established models. Nevertheless, the deviations from observations vary largely between different studies. Additionally, the deviations from observations for other variables (specific humidity, long-wave downward or short-wave upward radiation) were higher and might impede the models' ability in assessing heat stress. When considering the large differences in complexity and computational time, the good performance of the simple SOLWEIG and RayMan models contrary to the elaborate ENVI-met model is encouraging. ENVI-met, however, offers more opportunities for various issues, such as studies of plant-air interactions or effects of changes in albedo of individual surfaces. It also provides more options for tuning and modifications by the users, which were not completely exhausted in this study. Moreover, we recognized a lack of model evaluations regarding the amount of evaluation studies and the considered variables. An explicit statement of model uncertainties for interpreting the results should be included in every study and not only in rare exceptional cases.

The applied models are helpful for assessing human bioclimate in general due to the acceptable uncertainty in simulating T_{mrt}. In the specific case of façade greening in a complex urban environment, however, their usability is limited in the current set-up. Generic studies or simple environments combined with modified parameterizations might improve the usability. Specific types of vegetation besides trees should not be incorporated in these models without modifications and extensive evaluation. Therefore, new simulation tools or advancements in existing models are desirable to complement observational case studies. The combination of biometeorological microclimate models and observations is helpful in order to complement benefits of each method. More effort in bridging the gaps between case studies and large-scale applications of countermeasures is needed to detect an effective countermeasure against heat stress risks in cities.

Conflict of Interests

The authors declare that there is no conflict of interests regarding the publication of this paper.

Acknowledgments

The authors wish to thank their colleagues for the great support during the measurement campaign and the enriching discussions. The study is part of the Research Unit 1736 "Urban Climate and Heat Stress in Mid-Latitude Cities in View of Climate Change (UCaHS)" (http://www.UCaHS.org) funded by the Deutsche Forschungsgemeinschaft (DFG) under the codes SCHE 750/8-1, SCHE 750/9-1, and WE 1125/30-1.

References

[1] D. Scherer, U. Fehrenbach, T. Lakes, S. Lauf, F. Meier, and C. Schuster, "Quantification of heat-stress related mortality hazard, vulnerability and risk in Berlin, Germany," *Die Erde*, vol. 144, no. 3-4, pp. 238–259, 2013.

[2] A. M. Rizwan, L. Y. C. Dennis, and C. Liu, "A review on the generation, determination and mitigation of Urban Heat Island," *Journal of Environmental Sciences*, vol. 20, no. 1, pp. 120–128, 2008.

[3] M. Georgescu, P. E. Morefield, B. G. Bierwagen, and C. P. Weaver, "Urban adaptation can roll back warming of emerging megapolitan regions," *Proceedings of the National Academy of Sciences of the United States of America*, vol. 111, no. 8, pp. 2909–2914, 2014.

[4] S. Thorsson, F. Lindberg, I. Eliasson, and B. Holmer, "Different methods for estimating the mean radiant temperature in an outdoor urban setting," *International Journal of Climatology*, vol. 27, no. 14, pp. 1983–1993, 2007.

[5] N. Kántor and J. Unger, "Benefits and opportunities of adopting GIS in thermal comfort studies in resting places: an urban park as an example," *Landscape and Urban Planning*, vol. 98, no. 1, pp. 36–46, 2010.

[6] M. Köhler, "Green facades—a view back and some visions," *Urban Ecosystems*, vol. 11, no. 4, pp. 423–436, 2008.

[7] G. Pérez, L. Rincón, A. Vila, J. M. González, and L. F. Cabeza, "Green vertical systems for buildings as passive systems for energy savings," *Applied Energy*, vol. 88, no. 12, pp. 4854–4859, 2011.

[8] E. A. Eumorfopoulou and K. J. Kontoleon, "Experimental approach to the contribution of plant-covered walls to the thermal behaviour of building envelopes," *Building and Environment*, vol. 44, no. 5, pp. 1024–1038, 2009.

[9] R. M. Pulselli, F. M. Pulselli, U. Mazzali, F. Peron, and S. Bastianoni, "Emergy based evaluation of environmental performances of living wall and grass wall systems," *Energy and Buildings*, vol. 73, pp. 200–211, 2014.

[10] A. M. Hunter, N. S. G. Williams, J. P. Rayner, L. Aye, D. Hes, and S. J. Livesley, "Quantifying the thermal performance of green façades: a critical review," *Ecological Engineering*, vol. 63, pp. 102–113, 2014.

[11] R. Djedjig, E. Bozonnet, and R. Belarbi, "Experimental study of the urban microclimate mitigation potential of green roofs and green walls in street canyons," *International Journal of Low-Carbon Technologies*, 2013.

[12] T. Koyama, M. Yoshinaga, H. Hayashi, K.-I. Maeda, and A. Yamauchi, "Identification of key plant traits contributing to the cooling effects of green façades using freestanding walls," *Building and Environment*, vol. 66, pp. 96–103, 2013.

[13] R. W. F. Cameron, J. E. Taylor, and M. R. Emmett, "What's 'cool' in the world of green façades? How plant choice influences the cooling properties of green walls," *Building and Environment*, vol. 73, pp. 198–207, 2014.

[14] G. Gross, "Effects of different vegetation on temperature in an urban building environment. Micro-scale numerical experiments," *Meteorologische Zeitschrift*, vol. 21, no. 4, pp. 399–412, 2012.

[15] C. L. Tan, N. H. Wong, and S. K. Jusuf, "Effects of vertical greenery on mean radiant temperature in the tropical urban environment," *Landscape and Urban Planning*, vol. 127, pp. 52–64, 2014.

[16] R. Berry, S. J. Livesley, and L. Aye, "Tree canopy shade impacts on solar irradiance received by building walls and their surface temperature," *Building and Environment*, vol. 69, pp. 91–100, 2013.

[17] Y.-C. Chen, T.-P. Lin, and A. Matzarakis, "Comparison of mean radiant temperature from field experiment and modelling: a case study in Freiburg, Germany," *Theoretical and Applied Climatology*, vol. 118, no. 3, pp. 535–551, 2014.

[18] S. Huttner, *Further development and application of the 3D microclimate simulation ENVI-met [Ph.D. thesis]*, Johannes Gutenberg-Universität Mainz, 2012.

[19] R.-L. Hwang, T.-P. Lin, and A. Matzarakis, "Seasonal effects of urban street shading on long-term outdoor thermal comfort," *Building and Environment*, vol. 46, no. 4, pp. 863–870, 2011.

[20] E. L. Krüger, F. O. Minella, and A. Matzarakis, "Comparison of different methods of estimating the mean radiant temperature in outdoor thermal comfort studies," *International Journal of Biometeorology*, vol. 58, no. 8, pp. 1727–1737, 2013.

[21] T.-P. Lin, A. Matzarakis, and R.-L. Hwang, "Shading effect on long-term outdoor thermal comfort," *Building and Environment*, vol. 45, no. 1, pp. 213–221, 2010.

[22] A. Matzarakis, F. Rutz, and H. Mayer, "Modelling radiation fluxes in simple and complex environments—application of the RayMan model," *International Journal of Biometeorology*, vol. 51, no. 4, pp. 323–334, 2007.

[23] A. Matzarakis, F. Rutz, and H. Mayer, "Modelling radiation fluxes in simple and complex environments: basics of the RayMan model," *International Journal of Biometeorology*, vol. 54, no. 2, pp. 131–139, 2010.

[24] F. Lindberg, B. Holmer, and S. Thorsson, "SOLWEIG 1.0—modelling spatial variations of 3D radiant fluxes and mean radiant temperature in complex urban settings," *International Journal of Biometeorology*, vol. 52, no. 7, pp. 697–713, 2008.

[25] F. Lindberg and C. S. B. Grimmond, "The influence of vegetation and building morphology on shadow patterns and mean radiant temperatures in urban areas: model development and evaluation," *Theoretical and Applied Climatology*, vol. 105, no. 3-4, pp. 311–323, 2011.

[26] M. Srivanit and K. Hokao, "Evaluating the cooling effects of greening for improving the outdoor thermal environment at an institutional campus in the summer," *Building and Environment*, vol. 66, pp. 158–172, 2013.

[27] W. T. L. Chow and A. J. Brazel, "Assessing xeriscaping as a sustainable heat island mitigation approach for a desert city," *Building and Environment*, vol. 47, no. 1, pp. 170–181, 2012.

[28] W. T. L. Chow, R. L. Pope, C. A. Martin, and A. J. Brazel, "Observing and modeling the nocturnal park cool island of an arid city: horizontal and vertical impacts," *Theoretical and Applied Climatology*, vol. 103, no. 1-2, pp. 197–211, 2011.

[29] R. Emmanuel and H. J. S. Fernando, "Urban heat islands in humid and arid climates: role of urban form and thermal properties in Colombo, Sri Lanka and Phoenix, USA," *Climate Research*, vol. 34, no. 3, pp. 241–251, 2007.

[30] B. C. Hedquist and A. J. Brazel, "Seasonal variability of temperatures and outdoor human comfort in Phoenix, Arizona, U.S.A," *Building and Environment*, vol. 72, pp. 377–388, 2014.

[31] A. Middel, K. Häb, A. J. Brazel, C. A. Martin, and S. Guhathakurta, "Impact of urban form and design on mid-afternoon microclimate in Phoenix Local Climate Zones," *Landscape and Urban Planning*, vol. 122, pp. 16–28, 2014.

[32] N. Müller, W. Kuttler, and A.-B. Barlag, "Counteracting urban climate change: adaptation measures and their effect on thermal comfort," *Theoretical and Applied Climatology*, vol. 115, no. 1-2, pp. 243–257, 2014.

[33] E. Ng, L. Chen, Y. Wang, and C. Yuan, "A study on the cooling effects of greening in a high-density city: an experience from Hong Kong," *Building and Environment*, vol. 47, no. 1, pp. 256–271, 2012.

[34] L. L. H. Peng and C. Y. Jim, "Green-roof effects on neighborhood microclimate and human thermal sensation," *Energies*, vol. 6, no. 2, pp. 598–618, 2013.

[35] C. Skelhorn, S. Lindley, and G. Levermore, "The impact of vegetation types on air and surface temperatures in a temperate city: a fine scale assessment in Manchester, UK," *Landscape and Urban Planning*, vol. 121, pp. 129–140, 2014.

[36] X. Yang, L. Zhao, M. Bruse, and Q. Meng, "Evaluation of a microclimate model for predicting the thermal behavior of different ground surfaces," *Building and Environment*, vol. 60, pp. 93–104, 2013.

[37] I. D. Stewart and T. R. Oke, "Local climate zones for urban temperature studies," *Bulletin of the American Meteorological Society*, vol. 93, no. 12, pp. 1879–1900, 2012.

[38] M. Bruse and H. Fleer, "Simulating surface-plant-air interactions inside urban environments with a three dimensional numerical model," *Environmental Modelling and Software*, vol. 13, no. 3-4, pp. 373–384, 1998.

[39] N. H. Wong, A. Y. Kwang Tan, Y. Chen et al., "Thermal evaluation of vertical greenery systems for building walls," *Building and Environment*, vol. 45, no. 3, pp. 663–672, 2010.

[40] M. Bruse, *Die Auswirkungen kleinskaliger Umweltgestaltung auf das Mikroklima [Ph.D. thesis]*, Universität Bochum, 1999.

[41] C. J. Willmott, S. G. Ackleson, R. E. Davis et al., "Statistics for the evaluation and comparison of models," *Journal of Geophysical Research*, vol. 90, no. 5, pp. 8995–9005, 1985.

[42] K. H. Schlünzen and R. S. Sokhi, "Overview of tools and methods for meteorological and air pollution mesoscale model evaluation and user training," WMO Joint Report COST Action 728 GURME, 2008.

[43] F. Ali-Toudert, *Dependence of outdoor thermal comfort on street design in hot and dry climate [Ph.D. thesis]*, Universität Freiburg, Freiburg im Breisgau, Germany, 2005.

[44] F. Yang, S. S. Y. Lau, and F. Qian, "Thermal comfort effects of urban design strategies in high-rise urban environments in a sub-tropical climate," *Architectural Science Review*, vol. 54, no. 4, pp. 285–304, 2011.

[45] S. Berkovic, A. Yezioro, and A. Bitan, "Study of thermal comfort in courtyards in a hot arid climate," *Solar Energy*, vol. 86, no. 5, pp. 1173–1186, 2012.

Hindawi Publishing Corporation
Advances in Meteorology
Volume 2015, Article ID 987576, 8 pages
http://dx.doi.org/10.1155/2015/987576

Research Article

Temporal Differences of Urban-Rural Human Biometeorological Factors for Planning and Tourism in Szeged, Hungary

Ronja Vitt,[1] Ágnes Gulyás,[2] and Andreas Matzarakis[1]

[1]*Albert-Ludwigs-University Freiburg, 79085 Freiburg, Germany*
[2]*Department of Climatology and Landscape Ecology, University of Szeged, P.O. Box 653, Szeged 6701, Hungary*

Correspondence should be addressed to Ronja Vitt; ronja_vitt@gmx.de

Received 16 December 2014; Revised 12 March 2015; Accepted 17 March 2015

Academic Editor: Panagiotis Nastos

Heat load and cold stress can provoke annoyance and even health issues. These climatic situations should be avoided by tourists and locals to prevent negative experiences. Thermal comfort indices are required, as they combine meteorological and thermophysiological parameters. The Physiologically Equivalent Temperature (PET) is easy to understand and interpret also for nonexperts like tourists or decision-makers. The Hungarian Meteorological Service and the University of Szeged run an urban and a rural weather station close to Szeged, which build the basis for the human biometeorological analysis for a twelve-year period between 2000 and 2011. The maximum, mean, and minimum air temperature of both stations were compared to detect the differences of thermal dynamics. Heat and cold stress are quantified by analyzing the PET frequencies at 14 CET. The air temperature of urban areas is on average 1.0°C warmer than rural areas (11.4°C). Heat stress is more frequent in urbanized areas (6.3%) during summer months at 14 CET, while thermal acceptance is more frequent for surrounding rural areas (5.9%) in the same period. The Climate-Tourism/Transfer-Information-Scheme is a possibility to present the meteorological and human biometeorological data which is interesting for decision-making and tourism in a well-arranged way.

1. Introduction

Tourism is an important economic sector in Hungary representing 11% of the Hungarian GDP [1]. In 2011 about 9.8% of the total employments were directly or indirectly related to the tourism sector. The tourism potential of a region arises from several influencing criteria, such as landscape, flora, fauna, geographical position, topography, culture, leisure opportunities, weather, and climate [2, 3]. One of the crucial factors for tourists choosing a certain holiday destination is the climatic conditions, followed by scenery and nature [4].

The climatic conditions vary between urbanized and rural districts and therefore have to be investigated separately. The urban climate is altered through the construction of artificial structures and surfaces [5]. Every city has individual thermal dynamics, which form a very heterogeneous microclimate, depending on surface structure, height of the buildings, street width, and numerous other factors. One of the most important effects is the increased heat storage of buildings, which can cause heat stress for human beings during summer as well as a negative impact on recreation and well-being. The heat wave in Europe 2003 recorded predominant human deaths of about 14 802 in France, 2 045 in the United Kingdom, and 2 099 in Portugal [6]. The knowledge of climate information is required for a better tourism planning and for tourism industries. It should help travellers to prepare and adapt to the climatic situation, and it will protect tourists from negative climatic effects like heat stress [7, 8]. Therefore it is crucial to ascertain the temporal distribution of heat stress situations. Both city-planning and tourism derive advantage from investigations of the urban and rural climatic conditions [9]. It must be pointed out that it is insufficient to evaluate the climatic variables separately. The thermal sensation of humans is a combination of air temperature, wind velocity, water vapour, and radiation fluxes [10–12]. There are applicable human-biometeorological indices which combine not only these meteorological parameters but also several personal parameters [13–15]. In this study,

the biometeorological conditions of a mid-sized city in the south of Hungary and its rural surroundings are analyzed in terms of urban planning and vacation issues. The mean, minimum, and maximum air temperature for urban and rural areas around Szeged are presented. In order to quantify thermal stress conditions, the frequencies of PET classes, as well as the precipitation conditions, for each ten-day interval of the year were analyzed. The Climate-Tourism/Transfer-Information-Scheme gives a clearly arranged overview of the most important meteorological and human-biometeorological factors which influence tourism potential and recreation. This paper offers a bioclimatic information scheme developed for tourism purposes for the medium-sized Hungarian city of Szeged that could be used also for urban planning. It compares thermal and climatic differences between the city and its surroundings. Meteorological data comes from one urban and one rural station and covers the period from 2000 to 2011.

2. Materials and Methods

In this study, meteorological and human-biometeorological conditions of Szeged were analyzed. The city is located in the south of Hungary in a huge plain, the so-called Carpathian/Pannonian basin (Figure 1). Szeged is a mid-sized city with 170 000 inhabitants and has a circuit street system. The data for the period 2000–2011 is provided by the Hungarian Meteorological Service and the University of Szeged and has a time resolution of one hour [16, 17]. The rural synoptic weather station is surrounded by grassland and is located in the west of the city center of Szeged (Figure 1(c)). The climate station in the heavily built-up city center is separated; some measurement tools are located on the top of the roof of a university building, while the Stevenson screen is situated on a lawn beneath the roof station, in order to conform to international regulations.

Evaluating the influence of meteorological parameters on human beings, various thermal indices have been established, which can be classified into three categories: elementary, bioclimatic, and combined indices. Elementary indices usually attach single parameters such as air temperature, sunshine duration, and precipitation. The required synthetic values do not have any thermophysiological relevance and are mostly unproven [7]. Bioclimatic and combined indices, such as the Tourism Climate Index (TCI) or the Physiologically Equivalent Temperature (PET), take account of several climatological parameters and also combine their effects. The TCI developed by Mieczkowski [19] includes seven climatological factors: two of them are in a bioclimatic combination (Daytime comfort index and Daily comfort index) and three are independent (precipitation, sunshine, and wind velocity). The weak point of this index is that it does not rely on the human energy balance. Recognising this weakness, Kovács and Unger [20, 21] have aimed and presented methods to replace the air temperature and relative humidity values as the basis of Daytime and Daily comfort indices of the TCI with the human-biometeorological index PET. In addition to TCI, there are indices which include the effects of short- and longwave radiation fluxes on the human body, such as Predicted Mean Vote (PMV) [22], Standard Effective Temperature (SET*) [23], Universal Thermal Climate Index (UTCI) [24], or Physiologically Equivalent Temperature (PET) [25–27]. The parameter used in this study is PET, which is defined as the assessed air temperature under complex outdoor conditions, at which the human energy budget is balanced at typical indoor conditions. In order to calculate PET, several parameters such as air temperature, wind velocity, relative humidity, or vapour pressure and global radiation are needed. PET is an indicator for thermophysiological stress and its values are given in °C, which makes it easy to interpret and understand also for nonexperts (Table 1) [26]. The calculations for PET have been done by the use of RayMan model [28, 29]. For analyzing the annual distribution, a PET frequency diagram at 14 CET (Central European Time) for the urban station was made for 10-day periods, as this time span comes very close to the mean vacation duration [30, 31]. In addition, the average maximum, mean, and minimum air temperature in urbanized and rural areas were analyzed.

Table 1: Threshold values of Physiologically Equivalent Temperature (PET) for thermal sensation and the physiological stress level of human beings [18].

PET (°C)	Thermal sensation	Physiological stress level
	Very cold	Extreme cold stress
4		
	Cold	Strong cold stress
8		
	Cool	Moderate cold stress
13		
	Slightly cool	Slight cold stress
18		
	Comfortable	No thermal stress
23		
	Slightly warm	Slight heat stress
29		
	Warm	Moderate heat stress
35		
	Hot	Strong heat stress
41		
	Very hot	Extreme heat stress

More detailed information about tourism relevant to climatological and bioclimatological parameters can be illustrated in the Climate-Tourism/Transfer-Information-Scheme (CTIS). The threshold for the included thermal, aesthetic, and physical facets is chosen as follows [30, 32, 33]:

Thermal Facet

(i) thermal acceptance (18.0°C < PET < 29.0°C),

(ii) heat stress (PET > 35.0°C),

(iii) cold stress (PET < 4.0°C).

Aesthetic Facet

(i) cloudiness (cloud cover < 4),

(ii) fog (relative humidity > 93%).

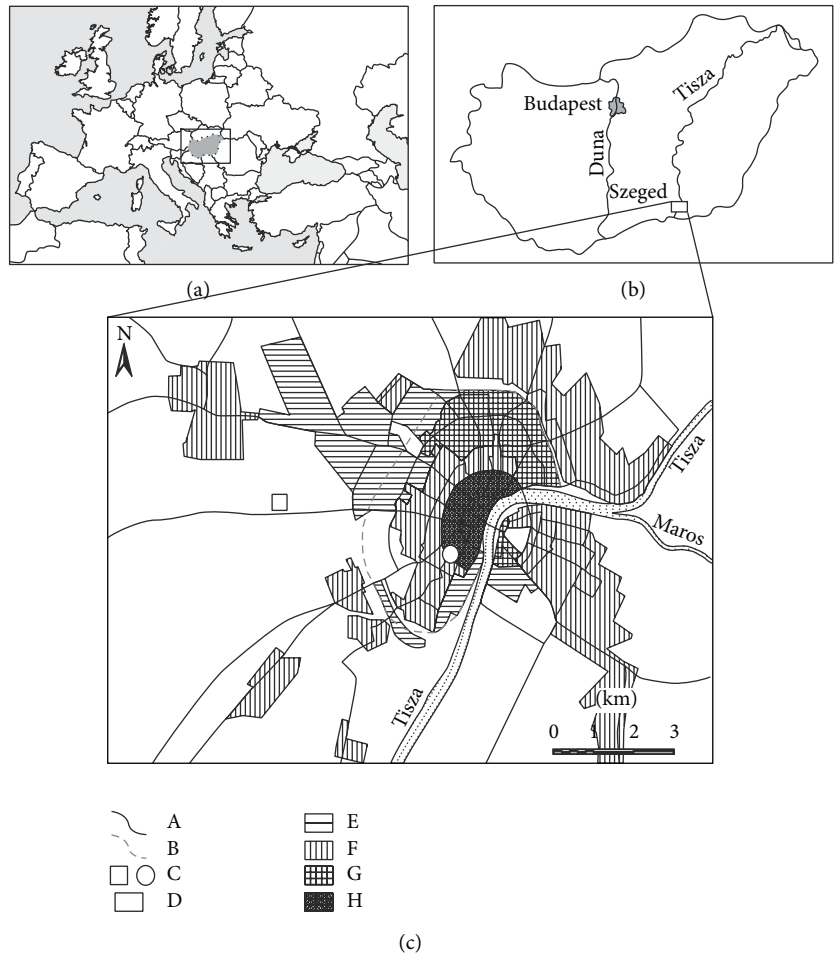

Figure 1: Geographical location of Hungary in Europe (a) and of Szeged in Hungary (b) and characteristic land-use types and road network of Szeged (c); A: road; B: circle dike; C: measuring point in the city centre (○) and in the rural area (□); D: agricultural area; E: industrial area; F: 1-2-storey detached houses; G: 5–11-storey apartment buildings; H: historical city core with 3–5-storey buildings (modified after [36]).

Physical Facet

(i) sultriness (vapour pressure > 18 hPa),

(ii) windy (wind velocity > 8 m/s),

(iii) dry days (precipitation < 1 mm),

(iv) wet days (precipitation > 5 mm).

In CTIS, the absolute frequencies and probabilities of these factors are given in 10-day intervals. To make the information easier to understand for tourists and the tourism industry, each factor given in CTIS can be ranked as positive or negative and will be categorized in seven classes from "very poor" to "ideal." As heat stress, cold stress, fog, sultriness, windy, and wet days are not favourable for tourism, these factors are ranked as negative. On the other hand, thermal acceptance, cloudiness, and dry days are presumed to be beneficial for tourism. This means that a high probability of heat stress is categorized as "very poor," whereas a high probability of thermal acceptance is evaluated as "ideal."

3. Results

3.1. Annual Course of the Maximum, Mean, and Minimum Air Temperature. The annual courses of the maximum, mean, and minimum air temperature in rural and urbanized areas are shown in Figure 2 for each ten-day interval of the year. Rural areas show marginal lower air temperature than urban areas from November until May and become higher from June to October. In the city of Szeged, $T_{a,\max}$ is up to 0.8°C higher in April and up to 0.5°C lower in September and October compared to its surroundings. In general, $T_{a,\max}$ of urban areas ranges from 2.5°C to 29.1°C and in rural areas ranges from 2.1°C to 29.3°C. The lowest $T_{a,\max}$ occurs in December and January, and the highest $T_{a,\max}$ occurs in July. The annual mean air temperature of urban areas is 12.4°C, while rural areas in the region of Szeged are 1.0°C cooler. The coldest period of the urban and rural areas is the first ten-day interval of January with 0.1°C and −0.8°C, and the warmest period occurs in the second ten-day interval of July with 23.9°C and 22.9°C, respectively. In the winter months (December to February), the urban areas have an average

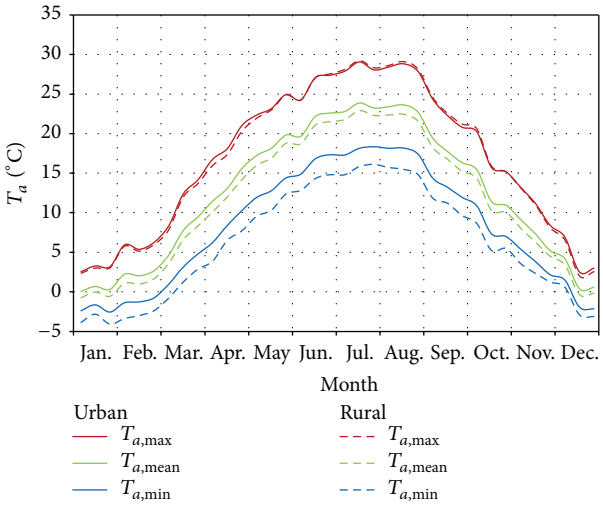

Figure 2: Mean annual course of the maximum, mean, and minimum air temperature for urban and rural areas of Szeged.

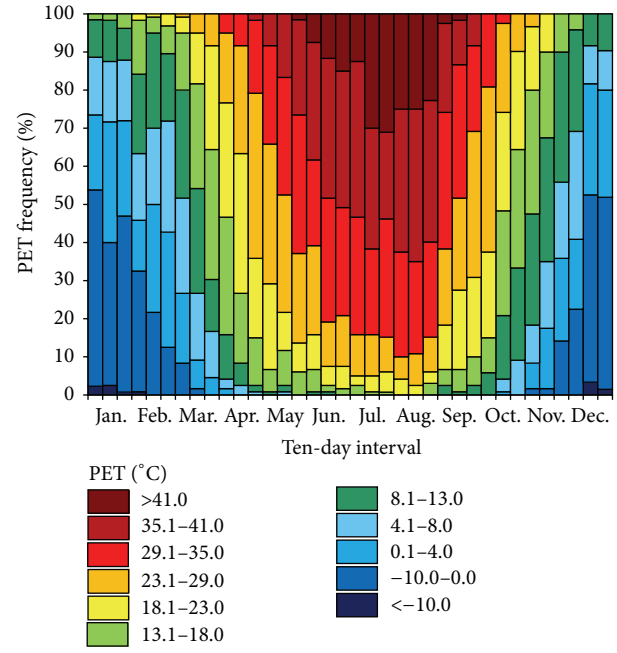

Figure 3: Frequency diagram of PET at 14 CET based on ten-day intervals for urban areas.

$T_{a,\text{mean}}$ of 1.5°C, which is about 0.9°C warmer than in rural areas. In summer (June to August), it is even 1.1°C warmer, with an average $T_{a,\text{mean}}$ of 22.7°C. The highest differences of $T_{a,\text{mean}}$ between urban and rural areas occur during summer and add up to 1.4°C. The average minimum air temperature of rural areas compared to the city of Szeged is 1.5°C lower in winter and 2.6°C lower in summer. It varies from −2.5°C to 18.5°C in urban areas and for rural areas $T_{a,\min}$ varies from −4.1°C to 16.0°C. The lowest values of $T_{a,\min}$ occur in January and the highest values occur in July for both areas.

3.2. Physiologically Equivalent Temperature for Urban Areas at 14 CET. The values of PET in the urbanized areas at 14 CET are grouped into the classes of thermal sensation and physiological stress level (Figure 3). The class frequencies are shown for each ten-day interval of the year. Due to this well-arranged diagram, it is easy to detect the occurrence and probability of thermal comfort, heat, and cold stress. In the urbanized area the mean annual PET is 19.3°C, with maximum values up to 48.9°C and minimum values up to −15.8°C. The range of PET values for the rural surroundings ranges from −20.5°C up to 50.6°C, with an average of 17.8°C. Expressed in the thermal sensation scale, the meteorological conditions in Szeged and its outer conurbation area go from "very cold" to "very hot," which are the upper extremes of the scale.

Between the first ten-day interval of November and the first ten-day interval of May, cold stress (PET < 4.0°C) can occur. The probability of cold stress increases rapidly from 8.3% in the first ten-day interval of November to 35.8% in the third ten-day interval of November. In December the occurrence triples and up to four of five days show PET values < 4.0°C. In winter (December until February) cold stress dominates at almost two-thirds of the days. In December and January the PET values do not exceed 18.0°C, whereas in February the first comfortable days (18.0°C < PET < 29.0°C) can occur. During winter months the urbanized areas of Szeged have an average PET value of 2.4°C at 14 CET. While in February thermal acceptance has a probability of 1.9%, which is about one day every second year: it increases during spring (March until May) with at least 40% of the days. The second ten-day interval of April shows the highest probability of thermal acceptance (65.0%) and neither cold nor heat stress occurs. At an average of 18 days in April thermal acceptance is expected and the probability of heat and cold stress is less than 1%. In March, there is still a slight chance of cold stress, while in May almost every fifth day produces heat stress. In spring the mean PET at 14 CET is thermally comfortable in general, with an average of 20.5°C.

Heat stress (PET > 35.0°C) may occur between the third ten-day interval of April and the third ten-day interval of August. During summer months (June until August) heat stress occurs on average every second day (54.8%), while there is a minor chance of thermal acceptance (16.0%). The average value of PET at 14 CET during summer is 34.9°C. The highest risk of heat stress is given in August with an average of 62.4% and accordingly about 19 days, while there are only 3 days which are thermally comfortable. In autumn (September until November) the number of comfortable days increases rapidly. Thermal acceptance already dominates in September with 45.3% compared to 15.8% of heat stress. Neither heat stress nor cold stress occurs in October and every second day (50.3%) is expected to be thermally comfortable. Per year there are about 67 days of cold stress and 61 days of heat stress in the city of Szeged, while at least 84 days are thermally comfortable. The majority of the comfortable days are detected in spring and autumn. The frequencies of PET classes are very similar for rural areas and therefore not shown in a figure separately. In general, cold stress is more frequent (78 days per year) and heat stress occurs less

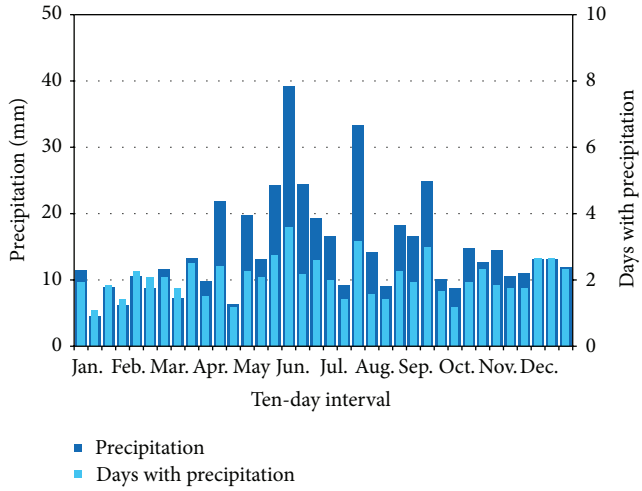

Figure 4: Total amount of precipitation and amount of days with precipitation (RR > 1 mm) per ten-day interval at the urban station.

frequently (53 days per year), while there is no difference for thermally comfortable days between urban and rural areas.

3.3. Precipitation in Szeged. In Szeged there are on average 73 days with precipitation per year at a total amount of 520 mm. Most of the precipitation falls during summer, with a maximum of 82 mm in June falling within 8 days (Figure 4). Compared to 25 mm within 5 days in January, the winter precipitation events are less intensive than during summer. Between May and July precipitation events occur during 24% of the days. There are only marginal differences of precipitation between the urban and the rural station, due to the relatively short horizontal distance between the stations and the homogeneous area.

3.4. Climate-Tourism/Transfer-Information-Scheme. In Figure 5, the probability of thermal acceptance, heat and cold stress, cloudiness, fog, sultriness, wind, and dry and wet days at the urban station are shown for 14 CET for each ten-day interval. In April and October, up to 70% of the days are thermally comfortable, while during summer there are only on average 5 days per month with high thermal comfort. Regarding the difference between the urban and the rural station (Figure 6), it is noticeable that during spring and autumn the probability of thermal acceptance is up to 20% lower in the city than at the rural station, but there is a higher chance during summer months.

Heat stress is possible from May until September, with the highest probabilities in July and August, when PET exceeds 29.0°C for almost two-thirds of the days. In rural areas heat stress occurs less frequently than in urban areas. Between October and April cold stress might occur; in the second ten-day interval of December 84% of the days cause cold stress. In general, two out of three days show a PET below 4.0°C during winter months. At the rural station, the possibility of cold stress is slightly higher than at the urban station (Figure 6).

Mean annual cloud cover of Szeged is 5 octas, with small differences between the seasons. During summer it is up to 40% less cloudy than during winter months. Sultriness can occur in May and October, with the highest probability of 30% in July and August. Wind and fog seem to have almost no impact on the human well-being in the region of Szeged, as they hardly exceed the given threshold values.

Generally eight out of ten days are presumed to be dry days, with less than 1 mm of precipitation per day. About 33 days of the year are wet days with more than 5 mm of precipitation. There are only little annual differences in the amount of dry and wet days.

4. Discussion

The differences of the air temperature and PET between the urban and the rural area are a result of the anthropogenic urban structures. The energy balance in urbanized areas is influenced by the composition, degree of sealing, surface roughness, street orientation, and thermal characteristics. Due to the alteration of land surfaces in cities, the materials absorb and accumulate short-wave radiation, which will be emitted as heat radiation. Weak wind conditions in cities facilitate the development of the UHI, which occurs especially in winter and summer during nighttime [34]. Therefore the mean annual air temperature at the urban station is about 1.0°C higher than at the rural station. Regarding PET, the rural station shows a mean value of 8.1°C and the urban station shows a mean value of 9.8°C.

The urban and rural human-biometeorological conditions of Szeged were compared by using the Thermohygrometric Index THI, the Relative Strain Index RSI, and the number of beer garden days for a 3-year period [35]. On the scale of THI, 6% of the year was "hot" in urban areas, while in rural areas it was only 1%. Cold conditions occurred for 54% and 66% in urban and rural areas, respectively. Beer garden days occur almost twice as often as in urban areas between May and October. Gulyás et al. [36] and Gulyás and Unger [37] made further studies about the human-biometeorological situation in Szeged, using hourly PET frequencies over a 10-year period from 1999 until 2008. The mean annual PET value for urban areas is 2.9°C higher than for rural areas. While the maximum PET values are insignificantly higher (0.9°C), the minimum PET values are 10.6°C higher in urban areas compared to rural areas. Thermal acceptance occurs almost twice as often in urban areas. Findings were that rural areas have a higher frequency of extreme cold and extreme heat stress. The heat wave of 2003 was investigated separately [17]. The examined period was March until November 2003, concluding that extreme heat stress occurs more frequently in rural areas due to direct radiation, which decreases in urbanized areas. Even though the average annual PET value is 14% higher in urban areas, thermal acceptance occurs twice as often. The difference in PET is the highest after sunset, when the urban areas are 7-8°C warmer due to the decreased cooling effect. These studies coincide with our results.

The human thermal differences in Budapest, Hungary, expressed with the PET were investigated by comparing

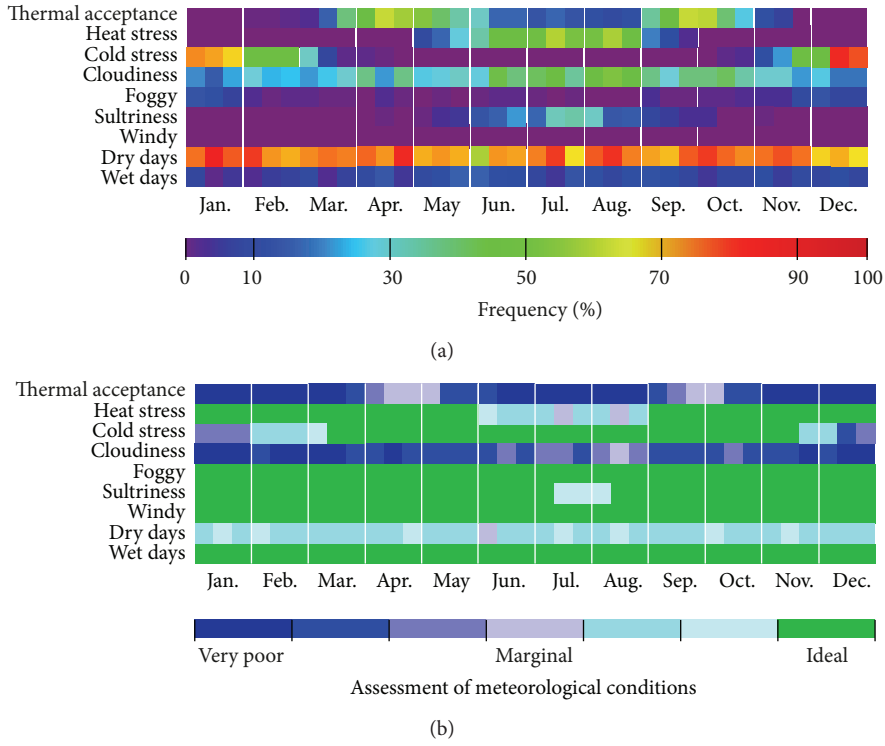

Figure 5: Climate-Tourism/Transfer-Information-Scheme (CTIS) for the urban station at 14 CET shown in relative frequencies (a) and as evaluated parameters (b).

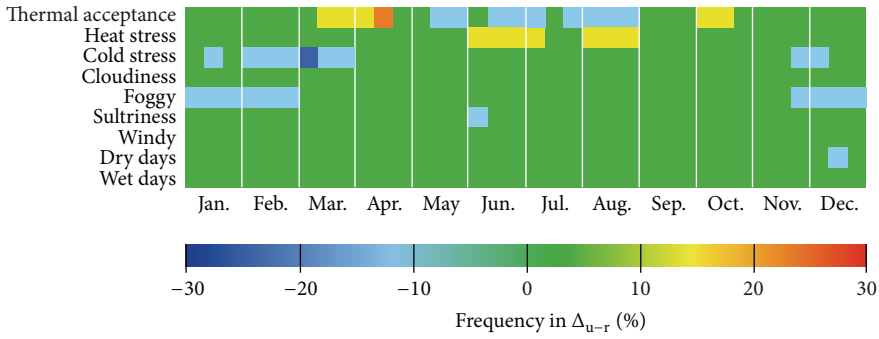

Figure 6: Difference of frequency between the urban and the rural station at 14 CET.

measurements of weather stations situated in the central and the suburban area [38]. They found that the PET differences are the same in all characteristic diurnal observation times (0, 6, 12, and 18 UTC) in the periods 1961–1990 and 1981–2010: the heat load is stronger and the cold stress level is less in the city centre than in the suburbs. During the period from 2001 until 2010 the average PET value is higher by 3°C in the city centre. The maximum PET is only slightly higher (0.9°C) here, but the difference in the minimum value is much higher, about 5°C. The tendencies are similar to those in Gulyás et al. [36] and Gulyás and Unger [37].

The biometeorological comfort of rural urban and urban forest in Erzurum, Turkey, were determined by using the THI [39]. Erzurum has a continental climate and a population of about 361 235. Unlike this study, they stated that the urban area is most advantageous for human comfort, followed by the urban forest and rural area. It has to be considered that the THI is based only on air temperature and relative humidity. The cooling effect of wind is not involved, which is usually higher in rural areas than in urban areas, due to urban structures. The differences of urban, suburban, and rural districts over Greater Cairo in Egypt, which has a subtropical climate, were investigated [40]. As well as Balogun et al. [41], Robaa [40] ascertained that the urban areas are in general warmer than its surroundings.

In our study a more complex system was used; hence, it is of higher significance. Not only the difference of air temperature between urban and rural areas but also PET was compared. We analyzed the mean, maximum, and minimum air temperature, the frequency of PET classes

at 14 CET, and arranged the most important meteorological information for planning and tourism in a Climate-Tourism-Information-Scheme. Tourists can easily ascertain favourable and unfavourable conditions to plan their vacation for their individual needs. Zaninović and Matzarakis [31] designed a bioclimate leaflet, which includes climatological and bioclimatological information of a city or region for tourists. It is an application to assist the tourism industry and stakeholders in decision-making, as well as tourists themselves. The information which is contained could help tourist planners in order to extend the tourist season, and it could help tourists to find the best individual period for their vacation. The design of the leaflet is easy to understand and gives a broad and compact overview of the climatological conditions of the destination.

5. Conclusion

In this study, meteorological and human-biometeorological parameters of urban and rural areas of Szeged were analyzed and the temporal differences of thermal conditions were discovered. There are differences for PET values during the day, as in summer heat stress occurs more frequently in urban areas at 14 CET, and thermal acceptance is more probable in the rural surroundings. On the contrary, cold stress is more frequent in rural areas during winter, due to the absence of heat storage of buildings and low wind speed. Based on the little horizontal distance between the urban and the rural station, there are marginal differences of precipitation.

Single weather parameters, usually presented on a monthly basis, are not appropriate for planning in tourism and urban structures. The Climate-Tourism-Information-Scheme visualizes the most important weather and climate information which is useful for tourism and recreation. It might be helpful for planning a vacation and to know more about the climatic conditions than the usually given meteorological forecast. Information about biometeorological conditions can detect the risk of heat or cold stress whereby the tourists can adapt. The CTIS is user-friendly and easy to understand also for nonexperts like tourists and it gives an overview about the most important climatic and biometeorological parameters.

Conflict of Interests

The authors declare that there is no conflict of interests regarding the publication of this paper.

References

[1] World Travel and Tourism Council, Eds., *Travel and Tourism*, Economic impact 2012 Hungary, 2012.

[2] D. R. Hall, "The challenge of international tourism in eastern Europe," *Tourism Management*, vol. 13, no. 1, pp. 41–44, 1992.

[3] D. R. Hall, "Tourism development and sustainability issues in Central and South-eastern Europe," *Tourism Management*, vol. 19, no. 5, pp. 423–431, 1998.

[4] W. Lise and R. S. J. Tol, "Impact of climate on tourist demand," *Climatic Change*, vol. 55, no. 4, pp. 429–449, 2002.

[5] A. Matzarakis, *Die thermische Komponente des Stadtklimas*, vol. 6, Berichte des Meteorologischen Institutes der Universität Freiburg, 2001.

[6] World Health Organization Europe, *Heat-Waves: Risks and Responses. Health and Global Environmental Change*, Series No. 2, World Health Organization, Regional Office for Europe, Copenhagen, Denmark, 2004.

[7] A. Matzarakis, "Weather- and climate-related information for tourism," *Tourism and Hospitality Planning & Development*, vol. 3, no. 2, pp. 99–115, 2006.

[8] A. Matzarakis, "Climate, thermal comfort and tourism," in *Climate Change and Tourism: Assessment and Coping Strategies*, B. Amelung, K. Blazejczyk, and A. Matzarakis, Eds., pp. 139–154, 2007.

[9] C. R. de Freitas, "Tourism climatology: Evaluating environmental information for decision making and business planning in the recreation and tourism sector," *International Journal of Biometeorology*, vol. 48, no. 1, pp. 45–54, 2003.

[10] A. Matzarakis, "Entwicklung einer Bewertungsmethodik zur Integration von Wetter und Klimabedingungen im Tourismus," *Berichte des Meteorologischen Institutes der Universität Freiburg*, vol. 16, pp. 73–80, 2007.

[11] K. Büttner, *Physikalische Bioklimatologie*, Akademische Verlagsgesellschaft, Leipzig, Germany, 1938.

[12] N. E. Davis, "An optimum weather index," *Weather*, vol. 23, no. 8, pp. 305–317, 1968.

[13] P. R. Höppe, "Heat balance modelling," *Experientia*, vol. 49, no. 9, pp. 741–746, 1993.

[14] P. Höppe, "Aspects of human biometeorology in past, present and future," *International Journal of Biometeorology*, vol. 40, no. 1, pp. 19–23, 1997.

[15] H. Mayer, "Urban bioclimatology," *Experientia*, vol. 49, no. 11, pp. 957–963, 1993.

[16] Á. Gulyás and A. Matzarakis, "Seasonal and spatial distribution of PET—physiologically equivalent temperature (PET) in Hungary," *Időjárás*, vol. 113, no. 3, pp. 221–231, 2009.

[17] Á. Gulyás, A. Matzarakis, and J. Unger, "Differences in the thermal bioclimatic conditions on the urban and rural areas in a southern Hungarian city (Szeged)," in *Berichte des Meteorologischen Institutes der Universität Freiburg*, H. Mayer and A. Matzarakis, Eds., vol. 18, pp. 229–234, 2009.

[18] A. Matzarakis and H. Mayer, "Another kind of environmental stress: thermal stress," in *WHO Collaborating Centre for Air Quality Management and Air Pollution Control*, vol. 18, pp. 7–10, 1996.

[19] Z. Mieczkowski, "The tourism climatic index: a method of evaluating world climates for tourism," *The Canadian Geographer*, vol. 29, no. 3, pp. 220–233, 1985.

[20] A. Kovács and J. Unger, "Modification of the tourism climatic index to central European climatic conditions—examples," *Quarterly Journal of the Hungarian Meteorological Services*, vol. 118, no. 2, pp. 147–166, 2014.

[21] A. Kovács and J. Unger, "Analysis of tourism climatic conditions in Hungary considering the subjective thermal sensation characteristics of the South-Hungarian residents," *Acta Climatologica et Chorologica*, vol. 47-48, pp. 77–84, 2014.

[22] P. O. Fanger, *Thermal Comfort*, McGraw-Hill, New York, NY, USA, 1972.

[23] A. P. Gagge, A. P. Fobelets, and L. G. Berglund, "A standard predictive index of human response to the thermal environment," *ASHRAE Transactions*, vol. 92, pp. 709–731, 1986.

[24] G. Jendritzky, R. de Dear, and G. Havenith, "UTCI—why another thermal index?" *International Journal of Biometeorology*, vol. 56, no. 3, pp. 421–428, 2012.

[25] P. Höppe, "The physiological equivalent temperature—a universal index for the biometeorological assessment of the thermal environment," *International Journal of Biometeorology*, vol. 43, no. 2, pp. 71–75, 1999.

[26] A. Matzarakis, H. Mayer, and M. G. Iziomon, "Applications of a universal thermal index: physiological equivalent temperature," *International Journal of Biometeorology*, vol. 43, no. 2, pp. 76–84, 1999.

[27] H. Mayer and P. Höppe, "Thermal comfort of man in different urban environments," *Theoretical and Applied Climatology*, vol. 38, no. 1, pp. 43–49, 1987.

[28] A. Matzarakis, F. Rutz, and H. Mayer, "Modelling radiation fluxes in simple and complex environments—application of the RayMan model," *International Journal of Biometeorology*, vol. 51, no. 4, pp. 323–334, 2007.

[29] A. Matzarakis, F. Rutz, and H. Mayer, "Modelling radiation fluxes in simple and complex environments: basics of the RayMan model," *International Journal of Biometeorology*, vol. 54, no. 2, pp. 131–139, 2010.

[30] A. Matzarakis, "Transferring climate information for application and planning—the Climate-Tourism/Transfer-Information-Scheme," in *Advances in Meteorology, Climatology and Atmospheric Physics*, C. G. Helmis and P. Nastos, Eds., vol. 1 of *Springer Atmospheric Sciences*, pp. 591–597, Springer, Berlin, Germany, 2013.

[31] K. Zaninović and A. Matzarakis, "The bioclimatological leaflet as a means conveying climatological information to tourists and the tourism industry," *International Journal of Biometeorology*, vol. 53, no. 4, pp. 369–374, 2009.

[32] A. Matzarakis, "Assessment method for climate and tourism based on daily data," in *Developments in Tourism Climatology*, A. Matzarakis, C. R. de Freitas, and D. Scott, Eds., pp. 52–58, 2007.

[33] A. Matzarakis, "Transfer of climate data for tourism applications—the climate-tourism/transfer-information-scheme," *Sustainable Environmental Research*, vol. 24, no. 4, pp. 273–280, 2014.

[34] J. Unger, "Modelling of the annual mean maximum urban heat island using 2D and 3D surface parameters," *Climate Research*, vol. 30, no. 3, pp. 215–226, 2006.

[35] J. Unger, "Comparisons of urban and rural bioclimatological conditions in the case of a Central-European city," *International Journal of Biometeorology*, vol. 43, no. 3, pp. 139–144, 1999.

[36] Á. Gulyás, A. Matzarakis, and J. Unger, "Comparison of the urban-rural thermal comfort sensation in a city with warm continental climate," in *Berichte des Meteorologischen Instituts der Universität Freiburg*, A. Matzarakis, H. Mayer, and F.-M. Chmielewski, Eds., vol. 20, pp. 473–478, 2010.

[37] Á. Gulyás and J. Unger, "Analysis of bioclimatic loads inside and outside the city in a long-term and an extremely short-term period (Szeged, Hungary)," *Urban Climate News*, vol. 37, pp. 11–14, 2010.

[38] A. Kovács and Á. Németh, "Tendencies and differences in human thermal comfort in distinct urban areas in Budapest, Hungary," *Acta Climatologica et Chorologica*, vol. 46, pp. 115–124, 2012.

[39] S. Toy, S. Yilmaz, and H. Yilmaz, "Determination of bioclimatic comfort in three different land uses in the city of Erzurum, Turkey," *Building and Environment*, vol. 42, no. 3, pp. 1315–1318, 2007.

[40] S. M. Robaa, "Urban-suburban/rural differences over Greater Cairo, Egypt," *Atmósfera*, vol. 16, no. 3, pp. 157–171, 2003.

[41] A. A. Balogun, I. A. Balogun, and Z. D. Adeyewa, "Comparisons of urban and rural heat stress conditions in a hot–humid tropical city," *Global Health Action*, vol. 3, pp. 1–5, 2010.

Hindawi Publishing Corporation
Advances in Meteorology
Volume 2015, Article ID 792172, 14 pages
http://dx.doi.org/10.1155/2015/792172

Research Article

Contribution of Greening and High-Albedo Coatings to Improvements in the Thermal Environment in Complex Urban Areas

Bonggeun Song[1] and Kyunghun Park[2]

[1]*National Institute of Ecology, 1210 Geumgang-ro, Maseo-myeon, Seocheon-gun, Chungcheongnam-do 325-813, Republic of Korea*
[2]*Changwon National University, 20 Changwondaehak-ro, Uichang-gu, Changwon-si, Gyeongsangnam-do 641-773, Republic of Korea*

Correspondence should be addressed to Kyunghun Park; landpkh@changwon.ac.kr

Received 13 October 2014; Accepted 5 February 2015

Academic Editor: Marialena Nikolopoulou

The aim was to identify microclimate characteristics in relation to ground cover in green areas and the reflectivity of building coating materials. Furthermore, microclimate modeling of temperatures was conducted using ENVI-met, to analyze the effects of improved thermal environments based on increased green areas and increased reflectivity of exterior coatings. The accuracy of ENVI-met was validated through comparisons with field temperature measurements. The RMSE deviation of the predicted and actual field temperature values was 3–6°C; however, the explanatory power was as high as 60%. ENVI-met was performed for commercial and single residential areas that have high densities of artificial cover materials, before and after changes related to development of green areas and to increase in the reflectivity of coating materials. The results indicated that both areas exhibited distinct temperature reductions due to the creation of green spaces. When the reflectivity of the coating material was increased, a temperature increase was observed in all land-use types. Therefore, in order to improve the thermal environment of complex urban areas, it is necessary to improve green-area development and to use high-reflectivity ground and building cover materials, while taking into account the spatial characteristics of land-use types and their surrounding areas.

1. Introduction

Urban areas consist of a variety of land covers and geometrical structures of various heights, characteristics that result in a unique climate. The albedo (reflectance) of land cover is mostly determined by its color. This characteristic has a significant impact on the radiation accumulated within the ground surface and thus on the surface temperature as well [1, 2]. Moreover, urban green areas have the function of lowering the surface temperature of surrounding areas and are thus effective in improving the urban thermal environment [3, 4]. However, because artificial ground covers like asphalt and concrete, which have low reflectivity, are increasing in urban areas while green areas and water surfaces are decreasing, a great deal of heat is constantly accumulating in our cities [5]. For this reason, issues related to urban thermal environments and urban heat-island effect (urban temperatures clearly higher than outskirts) [6, 7] are of growing concern. Recently, climate change has caused record-breaking heat waves that have become a serious environmental issue in urban areas all over the world. This in turn has increased interest in space-environment engineering for improving the thermal outdoor comfort of city dwellers and for minimizing the accumulation of heat in artificial structures [8–11].

Many recent studies have revealed that the thermal environment of urban areas can be improved through methods such as developing green areas and greening the roofs of buildings [3, 12–21]. Other studies have focused on ways to reduce surface and air temperature by increasing the albedo of roof and land covers and at the same time reducing the energy consumption of buildings [22–34]. Studies have also been conducted on how to adjust the dimensions, configurations, and placement of buildings (urban form and design) to improve the thermal environment. This is

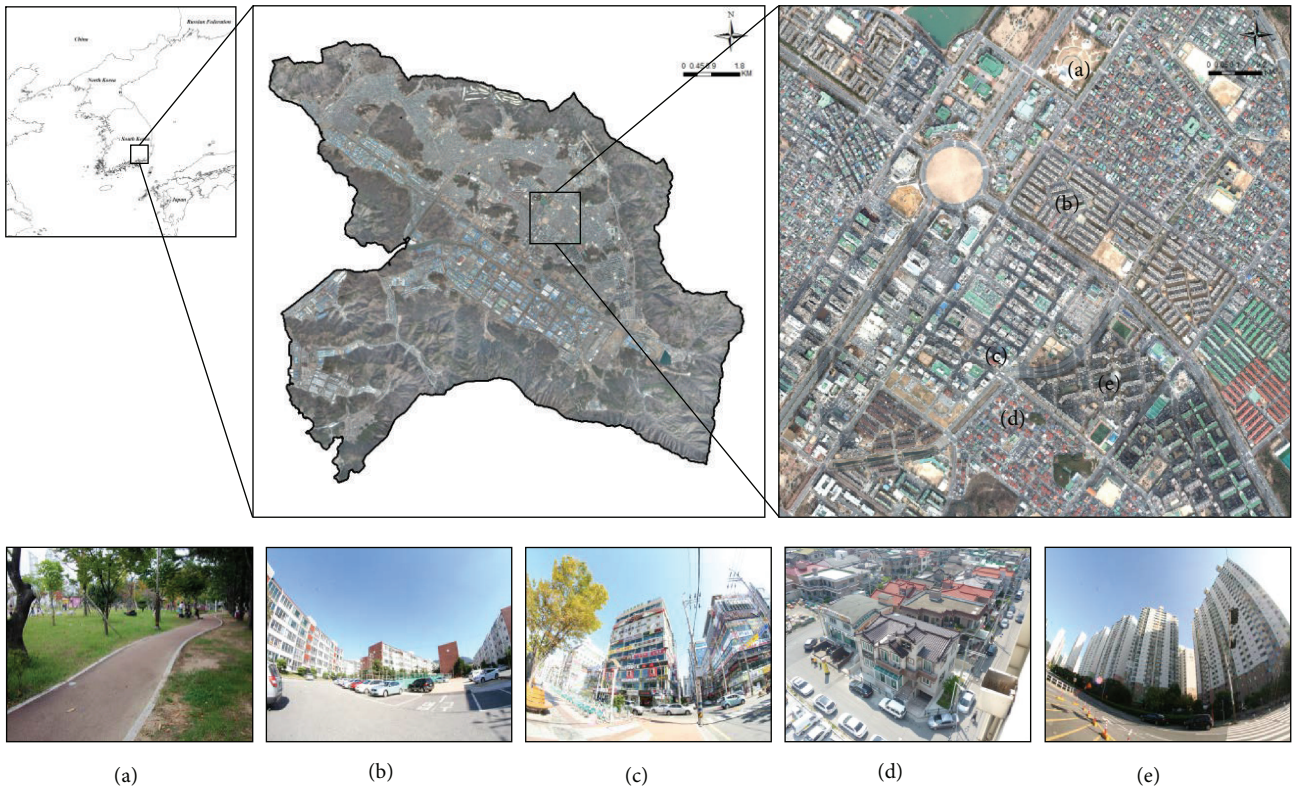

Figure 1: Five analysis areas encompassing different urban landscapes and land-use types in Changwon City, namely, (a) an urban park, (b) a low-rise apartment area, (c) a commercial area, (d) a single residential area, and (e) a high-rise apartment area.

accomplished by making systematic provisions for shade [26, 35–38].

Various studies focused on urban form and design (building dimensions) are being conducted to improve the thermal environment. However, there are too few studies involving complex high-density urban areas. These typically consist of various types of buildings and cover materials, feature extensive land development, and involve complicated land-use types. In recent years, urban areas in South Korea have exhibited increases in power usage and frequent power-supply interruptions, due to a growing number of heat-wave days in summer. These urban areas also face other problems in connection with heat waves, such as increases in disease and death rates [38]. Hence, it is necessary to provide plans for improvement of the outdoor thermal environment that take into account the diverse and complex land-use types, as well as the spatial arrangement, of urban areas in South Korea.

It was the goal of this study to identify microclimate characteristics, in relation to green-area development and the reflectivity of exterior coating materials, using field measurements of temperature in the urban area of Changwon City, South Korea. Furthermore, the effects from improving the thermal environment were identified for various land-use types, and their characteristics were determined. This was accomplished by analyzing the effects from additional green-area development and from the application of high-reflectivity cover materials to existing space. For this analysis, the climate model ENVI-met was used. Based on this investigation, a plan for optimal space design to improve the thermal environment was provided at the level of urban environment planning.

2. Materials and Methods

2.1. Target Study Area. The urban area of Changwon City (35°14′01.02″N, 128°41′19.95″E) in South Korea is a basin-form city surrounded by mountains, with a population of approximately 50 million [39, 40]. Because it is the first planned city in South Korea, the land-use types there are distinct. These include densely distributed residential, commercial, and public facilities, but large-scale national industrial complexes are also located in the vicinity. The average annual temperature is approximately 15°C. Warmer weather is experienced in summer, which lasts from June to September (average temperature of ~24°C) [41].

Five different urban land-use types in Changwon City were selected as targets for analysis. These include urban park, low-rise apartment, commercial, single-detached residential, and high-rise apartment areas (Figure 1). The urban park area consists mostly of trees and grass, as well as landscape arrangements such as marble stones and sculpture. The area surrounding the urban park consists of roads, public offices, and single residential areas. The low-rise apartment area consists of relatively low-rise buildings (up to five floors), and the buildings are densely distributed. The land surface in this area is mostly covered with asphalt. Trees are present in

Table 1: Characteristics of land cover at the measure points.

Site	Land cover
Urban park (9 points)	(1) Granite
	(2) Brick
	(3) Brick
	(4) Lawn
	(5) Urethane
	(6) Wooden board
	(7) Brick
	(8) Granite
	(9) Lawn
Low-rise APT (6 points)	(10) Asphalt
	(11) Sand
	(12) Asphalt
	(13) Asphalt
	(14) Concrete
	(15) Asphalt
Commercial area (3 points)	(16) Asphalt
	(17) Brick
	(18) Gravel
Single residential (4 points)	(19) Asphalt
	(20) Asphalt
	(21) Gravel
	(22) Asphalt
High-rise APT (5 points)	(23) Sand
	(24) Brick
	(25) Brick
	(26) Tile
	(27) Brick

the spaces between the edges of the apartment complex and the buildings. The commercial area consists of very densely distributed high-rise buildings (height > 30 m) that are all 10 m wide. The ground is covered with asphalt. Moreover, the commercial area includes resting places for citizens in the form of a fountain square and a small green park. The single residential area consists of buildings with two floors. The buildings are densely distributed and form a block of approximately 10 houses. The interval between the blocks is approximately 5 m, and the land surface is covered with asphalt. Retail shops (20 m in width) and parking lots covered by asphalt are situated in the area. The high-rise apartment area comprises vast areas of greenery with a spacious square covered in tiles; the building density in this area is not high.

2.2. Field Measurements. Field measurements were conducted in summer between June and August, under clear weather conditions (almost no clouds, less than 10% coverage). Daytime measurements were conducted on 29 June 2013 and 09 August 2013, whereas nighttime measurements were conducted over three days starting from 14 August 2013. Daytime measurements were conducted from 1:00 p.m. to 3:30 p.m. (UTC+9), whereas nighttime measurements were conducted from midnight to 2:30 a.m. (UTC+9), and each round of measurements took approximately 2.5 h. These measurement intervals should have captured the maximum and minimum daily temperatures. As shown in Figure 2 and Table 1, 27 points (urban park: 9, low-rise apartment area: 6, commercial area: 3, single residential area: 4, and high-rise apartment area: 5) were selected as the measurement points based on the three-dimensional (3D) spatial characteristics of the buildings and the reflectivity of the ground and building cover materials. The temperatures of bricks, lawn, and granite were measured in the urban park. Most of the temperatures measured in the low-rise apartment, commercial, and single residential areas were for asphalt and concrete. The temperatures measured in the high-rise apartment area were mostly for bricks. The distance from the urban park to the high-rise apartment area is approximately 5 km.

At each study site, three researchers used a mobile meteorological measuring device (Davis Vantage Pro2, accuracy of ±0.5°C) set at a height of 1.2 m (see Figure 3). The measurements were then taken by fixing the device in a horizontal position, relative to the ground surface, for 2 min. Measurement start and end times, as well as the surface temperatures at each measurement point, were recorded in a field book. Each cycle of measurements occurred in the following order: urban park area → low-rise apartment area → high-rise commercial area → single residential area → high-rise apartment area. In the urban park area, the granite material located in the northern section was selected as the measurement point. Since temperature changes as time passes, corrections must be made based on specific time. This study corrected the time to 2 p.m. for daytime measurement and 1 a.m. for nighttime measurement and set the final point of measurement to be equal to the starting point, correcting it through

$$\alpha = \frac{\left\{\left(X_f - X_s\right)/X_f\right\}}{\left(T_f - T_s\right)},$$
$$Y = X - X \times \left(T - T_s\right) \times \alpha. \quad (1)$$

For (1), X_f is the measurement value of the end point, X_s is the measurement value of the start point, T_f is the measurement time of the end point, T_s is the measurement time of the start point, α is the correction factor, X is the measured value, T is the measured time, and Y is the corrected value.

2.3. ENVI-Met Model. In this study, thermal-improvement effects were compared by considering outdoor space design using the ENVI-met model version 3.1. This is a microclimate analysis program that simulates meteorological factors (e.g., distribution of air currents, flow fields of fluids, temperature, humidity, and radiation energy) in 3D, based on input information that includes land surface, structures, and vegetation of urban spaces in grid form [21, 42]. This program has a spatial resolution of 0.5–10 m, temporal resolution of 10 s, and can simulate time frames of 24–48 h [18, 43].

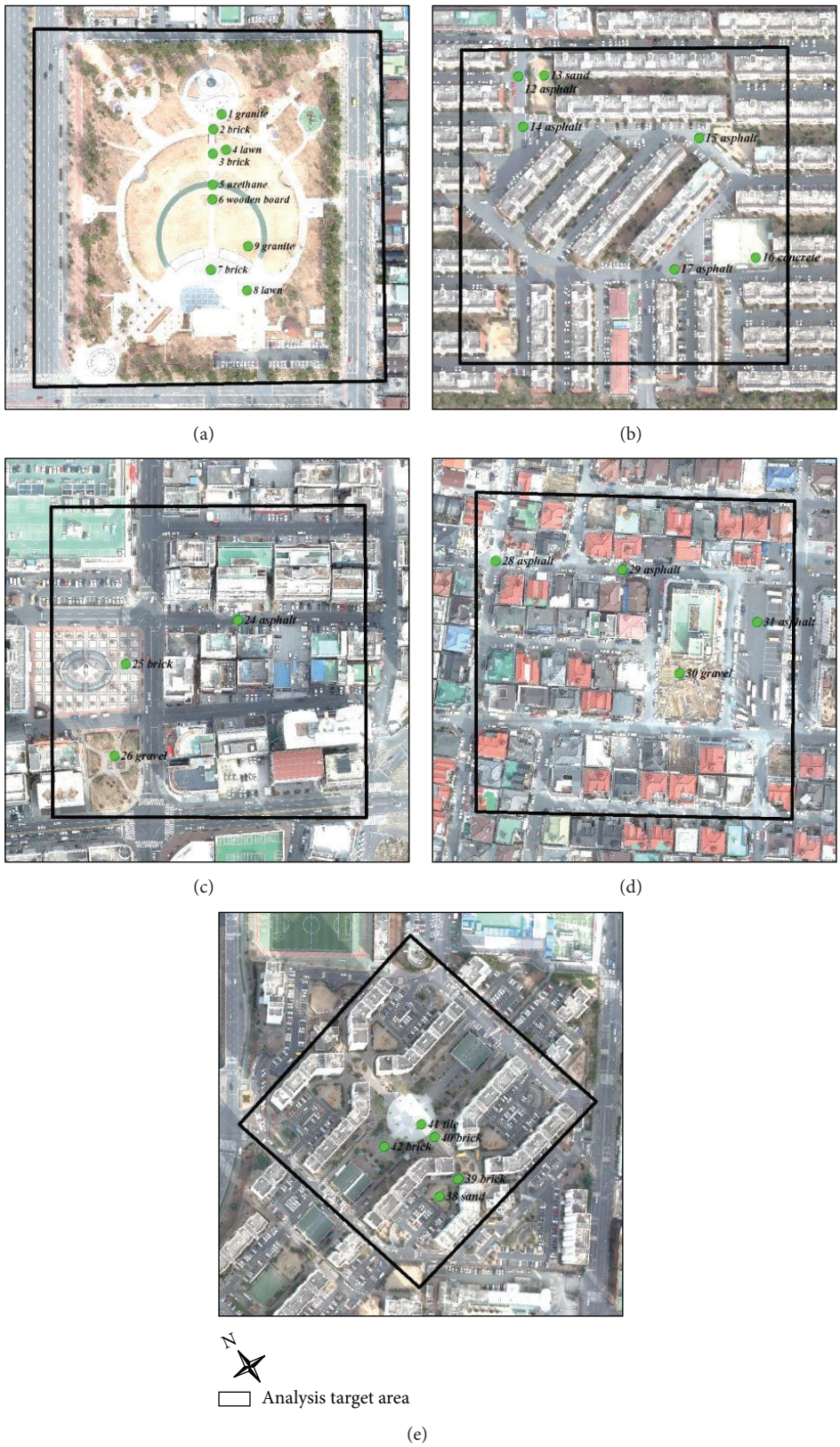

Figure 2: Field measurement points in the analysis target sites: (a) urban park area (9 points), (b) low-rise apartment area (6 points), (c) high-rise commercial area (3 points), (d) single residential area (4 points), and (e) high-rise apartment area (5 points).

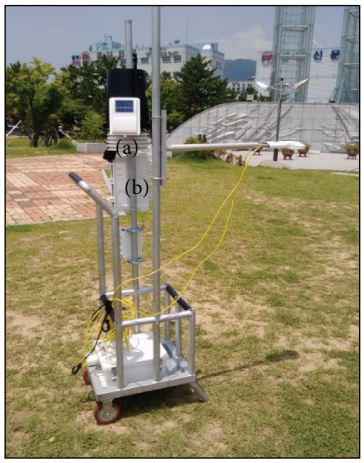

Figure 3: Portable measurement equipment: (a) meteorological measuring device, (b) data logger box.

For this work, the input data consisted of an area input file (∗.in) and a configuration file (∗.cf). The former included representations of the geographic location, building arrangement and height, type of ground cover, or type of vegetation of the target area, whereas, the latter includes the initial simulation of weather conditions. The information for each area input file was compiled based on surface fabric classification, geographic information systems (GIS) data, emissivity and reflectivity of coating materials, and a field survey based on the study by Song [44]. The horizontal grid resolution was set at 4 m after considering the area of each site, and the vertical grid resolution was set at 1 m. The number of grids was 60 × 60 × 30 grids for the urban park area, 52 × 52 × 30 grids for the low-rise apartment area, 50 × 50 × 30 grids for the high-rise commercial area, 34 × 34 × 30 grids for the single residential area, and 52 × 52 × 30 grids for the high-rise apartment area. Moreover, buildings were rotated vertically or horizontally to accurately express the building shape. The rotation degree was set at 35° for the urban park area, low-rise apartment area, high-rise commercial area, and single residential area but set at 78° for high-rise apartment area. A receptor was positioned at the same location as the field measurement point.

The data for factors such as temperature, wind speed, wind direction, and humidity were obtained from an automatic weather-measuring device, which managed the information on weather conditions from the configuration file. This device was installed at the Changwon Disaster Prevention and Countermeasures Headquarters, located near the target area. Ng et al. [18] stated that the best time to start a simulation is at sunrise and that the total running time should be longer than 6 h, in order to overcome the influence of the initialization. The simulation start time in this study was 06:00 on 29 June, 09 August, and 13 August 2013. The simulation duration was set to 24 h, and the data was stored at 10 min intervals. Moreover, the albedo of walls was set to 0.2, and the albedo of roofs was set to 0.3 (Table 2).

For ENVI-met, analysis data was assumed to be measured from a height of 2 m and at 2 p.m. (daytime) or 1 a.m. (nighttime), which is equivalent to the actual site measurements. The distribution of the ENVI-met results was analyzed using the ArcGIS 9.3 program.

Table 2: ENVI-met model configuration-file settings.

Category	Test dates		
	29/06/2013	09/08/2013	14/08/2013
Simulation setting			
Start simulation day (dd.mm.yyyy)	29.06.2013	09.08.2013	13.08.2013
Start simulation time (hh.mm.ss)	06:00:00	06:00:00	06:00:00
Total simulation time in hours (h)	24	24	24
Save model state (min)	10	10	10
Meteorological inputs			
Wind speed in 10 m above ground (m/s)	1.0	0	0.9
Wind direction (°)	135	112.5	225
Initial temperature atmosphere (K)	293.4	301.2	300.1
Specific humidity in 2500 m (g/kg)	3.48	3.52	3.52
Relative humidity in 2 m (%)	81.3	88.5	74.7
Albedo of walls		0.2	
Albedo of roofs		0.3	

Since information on soil ingredients and vegetation used as input data for ENVI-met analysis (infrared and visible range and calculations of radiation) was all measured using the values or formulas provided by the program, there are considerable gaps between the target areas. The accuracy of the models utilized must be validated using actual field data. There have been a number of recent tests [18, 36, 37, 45–47] of the accuracy of the ENVI-met model. For this study, the results of the ENVI-met model were validated by comparison with field data generated at a receptor installed at the measurement points.

2.4. Space Design. Space design was established by considering green-area development and increases in the reflectivity of each target area (Table 3). The green areas were developed by growing broad-leaf trees to a height of 2 m or by growing grass 10 cm high in parking lots and squares distributed within the target areas. On rooftops, green areas were expanded using 1.5 m high trees. Design changes intended to increase albedo have been studied actively in previous research using ENVI-met [48]. Based on these previous results, an albedo increase of 0.2 was added to the ground cover data provided by the ENVI-met program, mostly by applying them to parking facilities or building roofs.

Following analysis of the target areas, the urban park area was found to consist of scattered sections covered by marble and granite. Green ground cover was set up in these areas (U-1, Table 3) by growing grass, which increased their reflectivity

Table 3: Space design plan for each target area.

Site	Space design	
	Green space formation	Covering material replacement
Urban park	 <U-1>	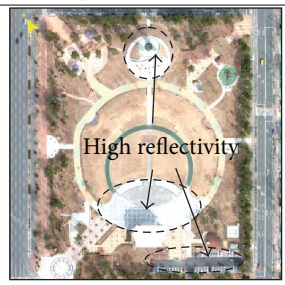 <U-2>
Low-rise apartment	 <L-1>	 <L-2>
	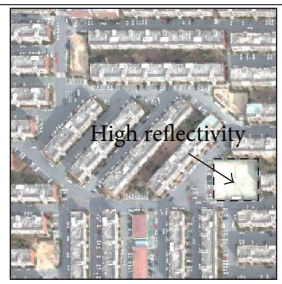 <L-3>	 <L-4>
Commercial area	 <C-1>	 <C-2>
	 <C-3>	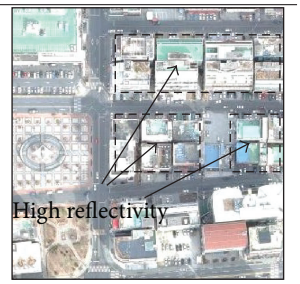 <C-4>
Single residential	 <S-1>	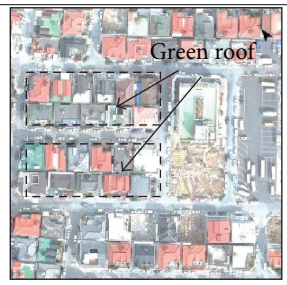 <S-2>
	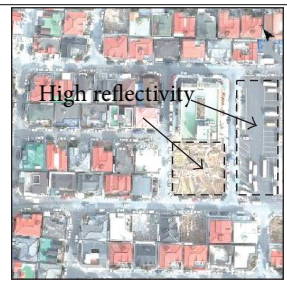 <S-3>	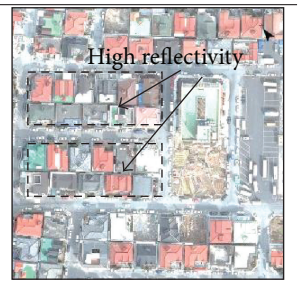 <S-4>
High-rise apartment	 <H-1>	 <H-2>
	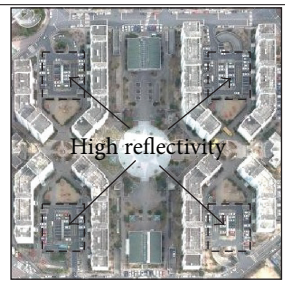 <H-3>	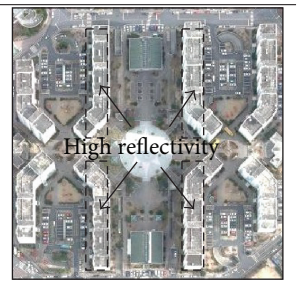 <H-4>

(U-2, Table 3). In the low-rise apartment area, the parking lot was equipped (L-1, Table 3) with trees and the roof cover was replaced (L-3, Table 3) with high-reflectivity material. Furthermore, for each of the four buildings located at the center of the analysis area, a green roof (1.5 m high) was built (L-2, Table 3) and the reflectivity of the roof was increased by applying (L-4, Table 3) high-reflectivity roof-cover materials. In the commercial area, a green area was formed (C-1, Table 3). In the fountain square, green roofs (C-2, Table 3) were built on the high-rise buildings, and their reflectivity was increased (C-4, Table 3). The reflectivity of the coating materials in the parking lot was also increased (C-3, Table 3) by 0.2. In the single residential area, plants were grown (S-1, Table 3) in the parking facilities, and its reflectivity was increased (S-3, Table 3). Green plants were placed on the roofs of approximately 20 households (S-2, Table 3), and their reflectivity was increased (S-4, Table 3). In the high-rise apartment area, greenery was added (H-1, Table 3) to tile-covered squares; for the four buildings located at the center, rooftop greening (H-2, Table 3) and reflectivity (H-4, Table 3) were increased. Furthermore, the asphalt material of the parking lot located between the buildings was replaced (H-3, Table 3) with a high-reflectivity material.

Simulations were conducted for each target area using the ENVI-met model, considering the plan adopted for the space design. Improvements in the thermal environment were equated by comparing the spatial changes in climate according to the space designs, using ArcGIS 9.3. The ENVI-met model time was set as 09 August 2013, which corresponded to the highest recorded field measured temperature. The comparisons were done using the simulated 14 h results.

3. Results and Discussion

3.1. Field Measurement Results. Table 4 shows the field temperature values by measurement point. The average temperature (29.5°C) occurred on 29 June 2013, reaching the highest average (35.4°C) on 09 August 2013. On 14 August 2013, the average nighttime temperature was 29.5°C. Among the different measurement areas, the high-rise commercial and single residential areas had high average temperatures (29 June: 30.0°C, 09 August: 35.8°C, and 14 August: 29.2°C). These two areas also had a high density of artificial structures composed of asphalt and concrete. The high-rise apartment area had relatively more greenery and shade due to the presence of taller buildings. This area had lower average temperatures than the others (29 June: 29.4°C, 09 August: 34.7°C, and 14 August: 28.4°C). The measurement points (points 1–4, Table 4) in the northern part of the urban park area were strongly affected by the surrounding area. During the field analysis, moderate winds (1-2 ms^{-1}) were experienced, resulting in considerably lower temperatures than at other measurement points.

3.2. Accuracy of the ENVI-Met Model. Figure 4 shows the results of modeled temperature and measured temperature in each measurement area. Measured temperatures turned out to be higher than modeled temperatures. A scatter plot was examined to determine the accuracy of the modeled temperature, and the result is shown in Figure 5. The temperatures of points 1–4 (Table 4), corresponding to the urban park area, were excluded because they were severely affected by the surrounding area. The coefficient of determination was very high on 09 August 2013 (0.627) and on 14 August 2013 (0.613). Ng et al. [18] and Yang et al. [49] found the coefficient of determination to be 0.6–0.7 and 0.94. The former was a bit higher and the latter much higher, than the values determined in the present study (Figure 5). In previous studies, the daily variations at each measurement point of the model and field data were compared. In the present study, the data at the same time were compared for the various points.

Table 4: Field temperature measurement (°C).

ID	Surface cover	06/29/2013	08/09/2013	08/14/2013
	Urban park			
1	Granite	28.3	37.0	28.4
2	Brick	28.7	37.3	29.1
3	Brick	28.9	36.9	29.0
4	Lawn	29.0	35.9	28.9
5	Urethane	29.1	35.4	28.8
6	Wooden board	29.2	35.3	28.7
7	Brick	29.1	34.8	28.6
8	Granite	29.1	34.7	28.5
9	Lawn	29.2	34.6	28.4
	Mean	**29.0**	**35.7**	**28.7**
	Low-rise APT			
10	Asphalt	29.8	35.0	28.4
11	Sand	29.9	35.1	28.5
12	Asphalt	29.9	35.2	28.5
13	Asphalt	30.0	35.4	28.5
14	Concrete	30.3	35.4	28.6
15	Asphalt	30.4	35.4	28.6
	Mean	**30.1**	**35.3**	**28.5**
	Commercial area			
16	Asphalt	29.9	35.6	29.1
17	Brick	30.1	35.8	29.2
18	Gravel	30.0	35.9	29.2
	Mean	**30.0**	**35.8**	**29.2**
	Single residential			
19	Asphalt	29.8	35.6	29.1
20	Asphalt	29.9	35.8	28.9
21	Gravel	30.0	35.8	28.8
22	Asphalt	29.9	35.9	28.7
	Mean	**29.9**	**35.8**	**28.9**
	High-rise APT			
23	Sand	29.5	34.7	28.4
24	Brick	29.5	34.7	28.4
25	Brick	29.3	34.7	28.4
26	Tile	29.3	34.6	28.4
27	Brick	29.3	34.6	28.4
	Mean	**29.4**	**34.7**	**28.4**

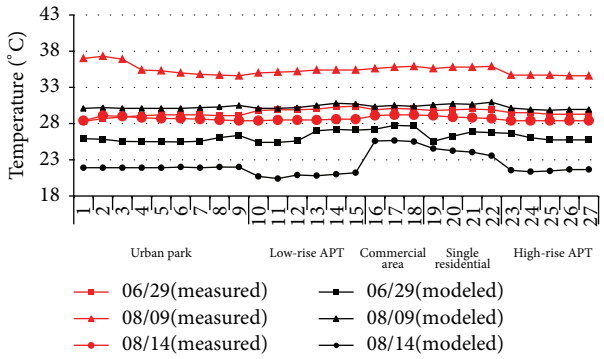

Figure 4: Comparison of modeled and measured temperatures at each measurement point.

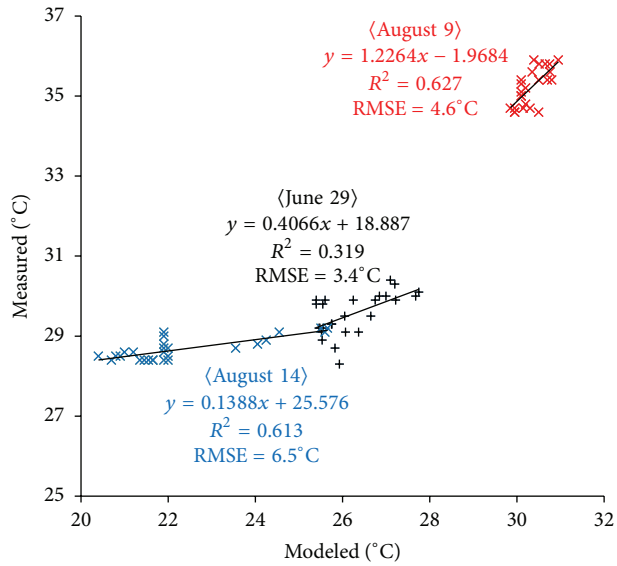

Figure 5: Comparison of the 2013 ENVI-met modeled and field measured temperatures for the following: 29 June: lower left set (x), 09 August: central set (+), and 14 August: upper right set ($*$).

Therefore, direct comparison of these results with those of earlier studies is not possible. Nevertheless, the temperature data from the model and field measurements showed high correlation, and it was determined that the ENVI-met results were suitable. The root-mean-square error (RMSE) showed a difference of 3.4°C on 29 June 2013, 4.6°C on 09 August 2013, and 6.5°C on 14 August 2013. The field measurement data were consistently higher. The mean difference between the ENVI-met model and field measurements reported by Middel et al. [37], Yang et al. [49], and Chow et al. [45] were 1.4–2.0, 1.01, and 1.53°C, respectively. In sharp contrast, a study by Park [50] showed a mean difference of 7.0–11.0°C. However, the remaining literature, showed a temperature difference of approximately 3°C between the model and field measurements over the course of 14 h. This is in agreement with the findings of this study. Therefore, it was found that the difference between the model and field measurements in this study was not significant, compared to previous studies, and that the correlation was very high. Thus, it was concluded that the accuracy of the model was sufficient.

3.3. Thermal Environment Improvement Effect. Table 5 and Figure 6 show the results of the analysis of temperature changes according to space design, using the ENVI-met model. Table 6 shows the changes in surface temperature at the measurement points.

3.3.1. Urban Park. The temperature provided by the ENVI-met model for 09 August 2013, at 14:00, on the road east of the park was >31°C, whereas that for the inner park was lower (<30.4°C). When the artificial material covering the ground inside the park was replaced with grass (U-1), the average temperature increased by 0.05°C. Considering the uncertainty level of the model, this change was considered insignificant. Moreover, the temperature increased by 0.15°C when the reflectivity was increased (U-2). However, unlike in the unaltered park space, a road located in the eastern part of the park exhibited lower temperatures. This was because of changes in the microclimate after the material covering of the ground was replaced (Figure 5). Therefore, in the urban park area, establishing grass as the ground cover in place of artificial coverings, or increasing the reflectivity of the ground

Table 5: Changes in temperature by space design.

Site	Temperature changes (°C)			
Urban park	U-1	U-2		
	+0.05	+0.15		
Low-rise apartment	L-1	L-2	L-3	L-4
	+0.15	−0.05	+0.15	+0.18
Commercial area	C-1	C-2	C-3	C-4
	−0.21	−0.07	+0.15	+0.17
Single residential	S-1	S-2	S-3	S-4
	−0.28	−0.01	+0.18	+0.11
High-rise apartment	H-1	H-2	H-3	H-4
	+0.08	+0.46	+0.06	+0.06

cover, resulted in an increase in the average temperatures. However, these alterations decreased the temperatures of the surrounding areas.

3.3.2. Low-Rise Apartment Area. The results of the temperature distribution analysis, given the space design of the low-rise apartment area, showed that the initial temperature in the parking lot was 30.8–31.0°C, whereas, in the south the temperature was comparatively high, measuring 31.0–31.2°C. Conversely, the analysis showed that the temperature was less than 30.6°C in most areas. When the concrete material of the parking lot was replaced (L-1) with grass, the surface temperature decreased significantly (8.6°C); however, the average temperature increased by 0.15°C and the temperature of the parking lot increased to 31.0–31.2°C. As roof-top greening was applied to the buildings (L-2), the average temperature decreased by 0.05°C, and the surface temperature of the surrounding area decreased by 1.7–5.0°C. Once the reflectivity of the cover materials (L-3) of the parking lot

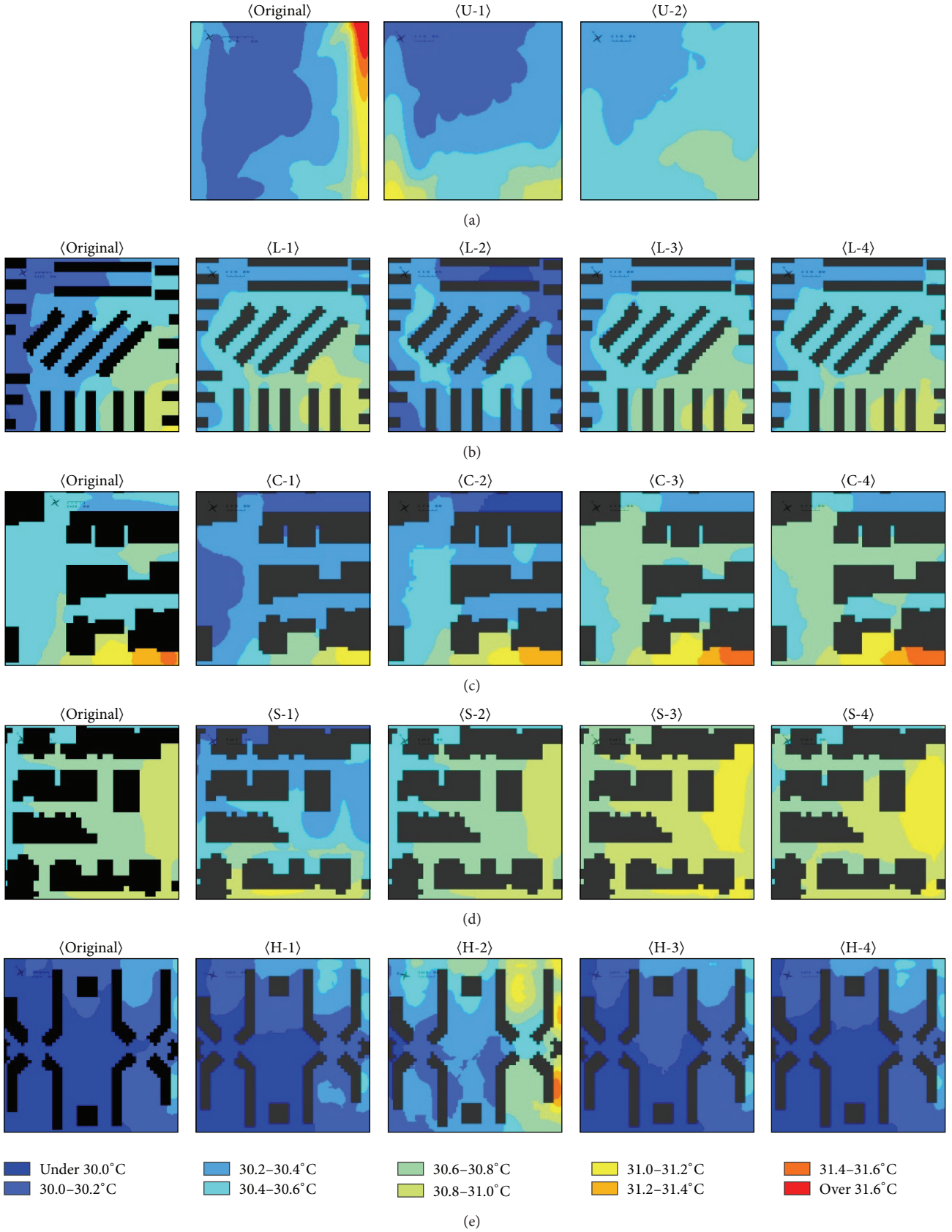

Figure 6: Changes in temperature distribution according to the scenario settings: (a) urban park area, (b) low-rise apartment area, (c) high-rise commercial area, (d) single residential area, (e) high-rise apartment area.

Table 6: Differences in surface temperature of existing spaces and space design.

Point	Scenario																	
	Urban park		Low-rise apartment				Commercial area				Single residential				High-rise apartment			
	U-1	U-2	L-1	L-2	L-3	L-4	C-1	C-2	C-3	C-4	S-1	S-2	S-3	S-4	H-1	H-2	H-3	H-4
Urban park																		
1	+6.6	+12.1																
2	−2.4	−1.7																
3	+2.9	−1.7																
4	+1.3	+1.9																
5	+12.5	+8.3																
6	+2.9	−0.7																
7	+2.3	−2.3																
8	−4.7	−0.8																
9	+0.4	+1.3																
Low-rise apartment																		
10			−4.4	−1.7	−3.1	−4.0												
11			+0.1	+1.1	+0.7	+0.8												
12			−5.0	−5.0	−5.1	−5.0												
13			+1.6	+1.4	+1.6	+1.6												
14			−8.6	+2.7	+0.7	+3.0												
15			−4.2	−5.1	−4.8	−4.8												
Commercial area																		
16							−1.2	−0.6	−0.3	−0.2								
17							−11.0	+2.8	+2.5	+2.6								
18							+0.0	+8.8	+13.5	+13.7								
Single residential																		
19											−0.4	+0.1	+2.5	+2.4				
20											−0.5	−0.1	+1.8	+1.5				
21											−7.1	−0.1	+10.2	+12.0				
22											−20.6	−3.4	−2.5	−3.8				
High-rise apartment																		
23															+0.2	+0.6	+0.2	+0.2
24															+0.1	+0.9	+0.0	+0.0
25															+0.6	+1.6	+0.7	+0.7
26															−3.9	+3.2	+10.8	+0.4
27															+1.6	+1.8	+1.6	+1.4

and the building rooftop (L-4) was increased, the average temperature increased by 0.15 and 0.18°C, respectively. It was also observed that the temperature around the parking lot and building increased from 30.4 to 30.8°C and that the temperature of the existing space rose by the same amount (from 30.2 to 30.6°C, for an increase of 0.4°C in both cases).

3.3.3. Commercial Area. In the commercial area, the temperature in the southern section was generally higher than 31.0°C. For C-1 (Figure 5), which was designed with a green park, the average temperature decreased by 0.21°C, compared with the existing space, and the temperature was found to be less than 30.4°C in most areas. The surface temperature of the measure points with green areas decreased by about 11°C. When the green spaces of the commercial area were developed, a distinct temperature reduction effect was confirmed. Following rooftop greening (C-2), the surface temperature of the surrounding area increased slightly; however, the average temperature decreased by 0.07°C. Most areas showed a lower temperature distribution (30.2–30.6°C) than that of the existing space (30.4–30.6°C). As the reflectivity of the cover material (C-3) of the parking lot and building rooftop (C-4) was increased, the average temperature increased by 0.15 and 0.17°C, respectively, compared with the existing space; many of the areas were observed to be within the temperature range of 30.6 to 30.8°C.

3.3.4. Single Residential Area. The existing single residential area mostly showed a temperature distribution ranging between 30.6 and 31.0°C. When green covering was added to the parking lot (S-1), the average temperature decreased by 0.28°C, and the surface temperature range was between

7.1 and 20.6°C, showing a significant decrease. After the rooftop greening was applied (S-2), the average temperature decreased by 0.01°C, which is insignificant considering the existing space. Moreover, the surface temperatures around the buildings decreased slightly. When the reflectivity of the materials in the parking lot (S-3) and the building rooftop (S-4) were increased, the average temperature increased by 0.18 and 0.11°C, respectively. As the reflectivity of the parking lot was increased, the surface temperature at the measurement point adjacent to the building increased by 10.2°C, whereas the surface temperature decreased by 2.5°C at a measurement point far away from the building. Similarly, when the reflectivity of the rooftop was increased, the surface temperature at the measurement point adjacent to the building increased by 12.0°C, but the surface temperature decreased by 3.8°C at the measurement point far away from the building.

3.3.5. High-Rise Apartment Area. The temperatures in the existing space of the high-rise apartment area were typically below 30.0°C. Following the space design, the average temperatures increased, but there were no significant differences (H-1 +0.08°C, H-3 +0.06°C, and H-4 +0.06°C) except after rooftop greening was performed (H-2 +0.46°C). The surface temperature at H-3, where the reflectivity of the cover materials of the parking lot was increased, showed a significant increase in temperature of 10.8°C compared to the surface temperature of the existing space. An increase in surface temperature was observed at all measurement points except for H-1, which was designed with trees.

3.4. Discussion. When a green area was developed near trees in the space design plan, commercial and single residential area land-use types that were mostly covered in artificial materials, such as asphalt and concrete, showed significant decreases in temperature. The urban park, low-rise apartment, and high-rise apartment areas, all of which had comparatively rich green areas, exhibited low surface temperatures; however, after similar changes were applied the temperatures increased. After rooftop greening was performed, the decrease in temperature was not as significant as it was when a green park was formed. The temperatures were slightly lower in the low-rise apartment and commercial areas than in the single residential area. The formation of green areas resulted in different effects depending on the spatial characteristics of the surrounding area. Furthermore, it was revealed that the temperature-reducing effect of green areas became more distinct as the density of artificial structures within the space increased.

When the reflectivity of the cover material was increased, an increase in temperature was observed; the surface temperature increased as the distance between the measurement point and the building decreased. Taha et al. [51] compared surface temperatures with reflectivity for a variety of cover materials. White elastomeric coatings (albedo of 0.72) exhibited surface temperatures that were 45°C lower than black coating (albedo of 0.08). Furthermore, Li et al. [25] examined the temporal changes in reflectivity in relation to the colors of cover materials such as concrete and asphalt. They observed that surface temperature decreased as reflectivity increased. This is because when reflectivity is increased, the amount of net-radiative energy accumulating on the surface decreases. However, the analytical results of the present study showed that surface temperatures increased slightly even when reflectivity increased. It was concluded that the reflected radiation energy was absorbed by the surrounding buildings and was consequently reradiated to the surface from the building. The observed low surface temperatures at the measurement points in the park (without buildings) and at a distance from the buildings confirm this conclusion. Additionally, studies by Lau and Yang [24], Lin et al. [26], and Wang et al. [32] showed that although surface temperature decreased as reflectivity increased, it had a negative effect on the physical and mental health of pedestrians. Yang et al. [33] showed that when the reflectivity of the land surface was increased to 0.4, the physiological equivalent temperature increased by 5–7°C, thereby reducing the level of overall outdoor thermal comfort. A number of studies [27, 29, 34, 52–54] have demonstrated that a reduction in building energy and mitigation of the urban heat-island effect can be achieved by increasing the reflectivity of roof surfaces. However, these studies have not shown that thermal comfort is improved in outdoor spaces with a high density of buildings; therefore, it is necessary to establish the reflectivity of cover materials, which is one aspect of the space design plan, while considering the arrangement of the surrounding buildings.

4. Conclusions

In this study, an effective application plan was established for improving the thermal environment in the urban areas of Changwon City, South Korea. The plan was based on space design, and it included the development of a green area and increasing the reflectivity of ground and building cover materials for various types of land use. The results from analysis of the changes caused by this plan are summarized below.

The results of the field measurements showed that the highest temperature occurred on 09 August 2013, (35.4°C), while on 29 June 2013 the temperature was 29.5°C. The average nighttime temperature (28.7°C) was recorded on 14 August 2013. Based on the accuracy of the ENVI-met model, it was concluded that the temperatures exhibited a high RMSE; however, analysis showed that the coefficient of determination of the linear regression on 09 August 2013 and 14 August 2013 exceeded 0.6, thereby increasing the explanatory power of the ENVI-met model. The analysis of the temperature changes (according to the space design), taking into account increases in reflectivity and development of green areas for different types of land use, showed distinct temperature reduction effects due to creation of green spaces in areas where buildings and artificial cover materials were densely distributed (i.e., commercial and single residential areas). The urban park, low-rise apartment, and high-rise apartment areas, with relatively many green areas, were predicted to exhibit temperature increases. When the reflectivity of the cover materials was increased, those areas exhibited

increases in temperature; when the reflectivity in areas with high building density was increased, the surface temperature increased.

The results suggest that the effects of thermal improvement due to green area development and increasing reflectivity differ depending on land use. This is because different land uses have different building arrangements and proportions of cover materials. To achieve the optimal thermal environment improvement effect at an urban and environmental planning level, it is necessary to consider the spatial characteristics of the land-use types and the surrounding areas appropriately. For example, the single residential or apartment areas, which had copious green space, showed an insignificant decrease in temperature even after rooftop greening and creation of a park. Therefore, in order to improve the thermal environment, it is more beneficial to increase the effect of shading by varying the arrangement of buildings, rather than by developing a green area. Furthermore, areas with a high density of artificial cover materials and of buildings displayed increases in air and surface temperatures after increasing the reflectivity of cover materials. Furthermore, this study showed that in spaces where artificial cover materials and buildings are concentrated the increased reflectivity of cover materials rather led to an increase in temperature. To clarify the temperature reduction effect according to cover materials of high reflectivity, it is also necessary to consider urban geometry (e.g., the sky-view factor), as well as the reflectivity or emissivity of building walls. These should be considered in future research.

In order to validate the accuracy of the model, the results of the ENVI-met model were compared with temperatures measured in the field, and a high correlation was found. However, there was a significant difference in the RMSE. This is because the ENVI-met model only takes into consideration the geographical location and initial weather conditions, without accounting for seasonal impacts. To solve this problem, a method must be utilized that can simulate the changes in climate for longer periods. In addition to temperature, other factors (e.g., radiation flux, wind speed, humidity, and surface temperature) also affect the thermal environment; therefore, it is necessary to consider the validity of the model with respect to these various factors. It is believed that an optimal space design plan for the improvement of the thermal environment can be provided, at the urban and environmental planning level, by taking into account a wider range of factors.

Conflict of Interests

The authors declare that there is no conflict of interests regarding the publication of this paper.

Acknowledgment

This research was supported by the Basic Science Research Program through the National Research Foundation of Korea (NRF) funded by the Ministry of Education, Science and Technology (no. 2013-0095-0000).

References

[1] Y. Gao, J. Xu, S. Yang et al., "Cool roofs in China: policy review, building simulations, and proof-of-concept experiments," *Energy Policy*, vol. 74, pp. 190–214, 2014.

[2] R. Levinson and H. Akbari, "Potential benefits of cool roofs on commercial buildings: conserving energy, saving money, and reducing emission of greenhouse gases and air pollutants," *Energy Efficiency*, vol. 3, no. 1, pp. 53–109, 2010.

[3] L. Shashua-Bar and M. E. Hoffman, "Vegetation as a climatic component in the design of an urban street: an empirical model for predicting the cooling effect of urban green areas with trees," *Energy and Buildings*, vol. 31, no. 3, pp. 221–235, 2000.

[4] F. Wilmers, "Effects of vegetation on urban climate and buildings," *Journal of Energy and Building*, vol. 15, no. 3-4, pp. 507–514, 1990.

[5] M. Taleghani, M. Tenpierik, A. van den Dobbelsteen, and D. J. Sailor, "Heat in courtyards: a validated and calibrated parametric study of heat mitigation strategies for urban courtyards in the Netherlands," *Solar Energy*, vol. 103, pp. 108–124, 2014.

[6] I. Eliasson, "Urban nocturnal temperatures, street geometry and land use," *Atmospheric Environment*, vol. 30, no. 3, pp. 379–392, 1996.

[7] T. R. Oke, *Boundary Layer Climates*, Methuen, London, UK, 2nd edition, 1987.

[8] H. Akbari and S. Konopacki, "Energy effects of heat-island reduction strategies in Toronto, Canada," *Energy*, vol. 29, no. 2, pp. 191–210, 2004.

[9] Y. Kim, H. Lee, J. Hong, and E. Son, "A study on the effect of anthropogenic heat flux and land-use on thermal environment in Pusan," *Journal of Korean Society for Atmospheric Environment*, vol. 16, no. 4, pp. 363–372, 2000.

[10] M. Kolokotroni, X. Ren, M. Davies, and A. Mavrogianni, "London's urban heat island: impact on current and future energy consumption in office buildings," *Energy and Buildings*, vol. 47, pp. 302–311, 2012.

[11] E. Lim, W. Lee, C. Choi, B. Song, and S. Jung, "An evaluation of thermal comfort on urban neighborhood park for improving thermal environment," *Journal of the Korean Association of Geographic Information Studies*, vol. 16, no. 4, pp. 153–170, 2013.

[12] H. Akbari, M. Pomerantz, and H. Taha, "Cool surfaces and shade trees to reduce energy use and improve air quality in urban areas," *Solar Energy*, vol. 70, no. 3, pp. 295–310, 2001.

[13] D. E. Bowler, L. Buyung-Ali, T. M. Knight, and A. S. Pullin, "Urban greening to cool towns and cities: a systematic review of the empirical evidence," *Landscape and Urban Planning*, vol. 97, no. 3, pp. 147–155, 2010.

[14] P. Cohen, O. Potchter, and A. Matzarakis, "Daily and seasonal climatic conditions of green urban open spaces in the Mediterranean climate and their impact on human comfort," *Building and Environment*, vol. 51, pp. 285–295, 2012.

[15] I. Eliasson, "The use of climate knowledge in urban planning," *Landscape and Urban Planning*, vol. 48, no. 1-2, pp. 31–44, 2000.

[16] J. N. Georgi and D. Dimitriou, "The contribution of urban green spaces to the improvement of environment in cities: case study of Chania, Greece," *Building and Environment*, vol. 45, no. 6, pp. 1401–1414, 2010.

[17] S. Hamada and T. Ohta, "Seasonal variations in the cooling effect of urban green areas on surrounding urban areas," *Urban Forestry and Urban Greening*, vol. 9, no. 1, pp. 15–24, 2010.

[18] E. Ng, L. Chen, Y. Wang, and C. Yuan, "A study on the cooling effects of greening in a high-density city: an experience from Hong Kong," *Building and Environment*, vol. 47, no. 1, pp. 256–271, 2012.

[19] S. Oliveira, H. Andrade, and T. Vaz, "The cooling effect of green spaces as a contribution to the mitigation of urban heat: a case study in Lisbon," *Building and Environment*, vol. 46, no. 11, pp. 2186–2194, 2011.

[20] M. Robitu, M. Musy, C. Inard, and D. Groleau, "Modeling the influence of vegetation and water pond on urban microclimate," *Solar Energy*, vol. 80, no. 4, pp. 435–447, 2006.

[21] C. Yu and W. N. Hien, "Thermal benefits of city parks," *Energy and Buildings*, vol. 38, no. 2, pp. 105–120, 2006.

[22] S. E. Bretz and H. Akbari, "Long-term performance of high-albedo roof coatings," *Energy and Buildings*, vol. 25, no. 2, pp. 159–167, 1997.

[23] A. M. Coutts, E. Daly, J. Beringer, and N. J. Tapper, "Assessing practical measures to reduce urban heat: green and cool roofs," *Building and Environment*, vol. 70, pp. 266–276, 2013.

[24] S. S. Y. Lau and F. Yang, "Introducing healing gardens into a compact university campus: design natural space to create healthy and sustainable campuses," *Landscape Research*, vol. 34, no. 1, pp. 55–81, 2009.

[25] H. Li, J. Harvey, and A. Kendall, "Field measurement of albedo for different land cover materials and effects on thermal performance," *Building and Environment*, vol. 59, pp. 536–546, 2013.

[26] T.-P. Lin, A. Matzarakis, and R.-L. Hwang, "Shading effect on long-term outdoor thermal comfort," *Building and Environment*, vol. 45, no. 1, pp. 213–221, 2010.

[27] D. S. Parker and S. F. Barkaszi Jr., "Roof solar reflectance and cooling energy use: field research results from Florida," *Energy and Buildings*, vol. 25, no. 2, pp. 105–115, 1997.

[28] A. H. Rosenfeld, H. Akbari, S. Bretz et al., "Mitigation of urban heat islands: materials, utility programs, updates," *Energy and Buildings*, vol. 22, no. 3, pp. 255–265, 1995.

[29] J. R. Simpson and E. G. McPherson, "The effects of roof albedo modification on cooling loads of scale model residences in Tucson, Arizona," *Energy and Buildings*, vol. 25, no. 2, pp. 127–137, 1997.

[30] H. Taha, "Urban climates and heat islands: albedo, evapotranspiration, and anthropogenic heat," *Energy and Buildings*, vol. 25, no. 2, pp. 99–103, 1997.

[31] H. Takebayashi and M. Moriyama, "Surface heat budget on green roof and high reflection roof for mitigation of urban heat island," *Building and Environment*, vol. 42, no. 8, pp. 2971–2979, 2007.

[32] B.-L. Wang, T. Takigawa, Y. Yamasaki, N. Sakano, D.-H. Wang, and K. Ogino, "Symptom definitions for SBS (sick building syndrome) in residential dwellings," *International Journal of Hygiene and Environmental Health*, vol. 211, no. 1-2, pp. 114–120, 2008.

[33] F. Yang, S. S. Y. Lau, and F. Qian, "Thermal comfort effects of urban design strategies in high-rise urban environments in a sub-tropical climate," *Architectural Science Review*, vol. 54, no. 4, pp. 285–304, 2011.

[34] M. Zinzi and S. Agnoli, "Cool and green roofs. An energy and comfort comparison between passive cooling and mitigation urban heat island techniques for residential buildings in the Mediterranean region," *Energy and Buildings*, vol. 55, pp. 66–76, 2012.

[35] H. Chen, R. Ooka, H. Huang, and T. Tsuchiya, "Study on mitigation measures for outdoor thermal environment on present urban blocks in Tokyo using coupled simulation," *Building and Environment*, vol. 44, no. 11, pp. 2290–2299, 2009.

[36] E. L. Krüger, F. O. Minella, and F. Rasia, "Impact of urban geometry on outdoor thermal comfort and air quality from field measurements in Curitiba, Brazil," *Building and Environment*, vol. 46, no. 3, pp. 621–634, 2011.

[37] A. Middel, K. Häb, A. J. Brazel, C. A. Martin, and S. Guhathakurta, "Impact of urban form and design on mid-afternoon microclimate in Phoenix Local Climate Zones," *Landscape and Urban Planning*, vol. 122, pp. 16–28, 2014.

[38] Korea Center for Disease Control and Prevention, "Annual report on the notified patients with heat-related illness in Korea," Public Health Weekly Report, 2013.

[39] B. G. Song and K. H. Park, "Analysis of heat island characteristics considering urban space at nighttime," *Journal of the Korean Association of Geographic Information Studies*, vol. 15, no. 1, pp. 133–143, 2012.

[40] B. Song and K. Park, "Validation of ASTER surface temperature data with in situ measurements to evaluate heat islands in complex urban areas," *Advances in Meteorology*, vol. 2014, Article ID 620410, 12 pages, 2014.

[41] Gyeongnam Green Environment Center, "Establishment of rainwater management master plan," Gyeongnam Green Environment Center Research Report, 2014.

[42] W. T. L. Chow, R. L. Pope, C. A. Martin, and A. J. Brazel, "Observing and modeling the nocturnal park cool island of an arid city: horizontal and vertical impacts," *Theoretical and Applied Climatology*, vol. 103, no. 1, pp. 197–211, 2011.

[43] M. Bruse and H. Fleer, "Simulating surface-plant-air interactions inside urban environments with a three dimensional numerical model," *Environmental Modelling and Software*, vol. 13, no. 3-4, pp. 373–384, 1998.

[44] B. G. Song, *Development of environmental planning methodology for mitigation of climate change and heat island effect in urban area [Ph.D. dissertation]*, Changwon National University, Changwon, Republic of Korea, 2014.

[45] W. T. L. Chow, R. L. Pope, C. A. Martin, and A. J. Brazel, "Observing and modeling the nocturnal park cool island of an arid city: horizontal and vertical impacts," *Theoretical and Applied Climatology*, vol. 103, no. 1, pp. 197–211, 2011.

[46] W. T. L. Chow and A. J. Brazel, "Assessing xeriscaping as a sustainable heat island mitigation approach for a desert city," *Building and Environment*, vol. 47, no. 1, pp. 170–181, 2012.

[47] M. Samaali, D. Courault, M. Bruse, A. Olioso, and R. Occelli, "Analysis of a 3D boundary layer model at local scale: validation on soybean surface radiative measurements," *Atmospheric Research*, vol. 85, no. 2, pp. 183–198, 2007.

[48] A. Middel, N. Chhetri, and R. Quay, "Urban forestry and cool roofs: assessment of heat mitigation strategies in Phoenix residential neighborhoods," *Urban Forestry & Urban Greening*, 2014.

[49] X. Yang, L. Zhao, M. Bruse, and Q. Meng, "Evaluation of a microclimate model for predicting the thermal behavior of different ground surfaces," *Building and Environment*, vol. 60, pp. 93–104, 2013.

[50] S. Park, *Human-urban radiation exchange simulation model [Ph.D. thesis]*, University of Victoria, Victoria, Canada, 2012.

[51] H. Taha, D. Sailor, and H. Akbari, "High albedo materials for reducing cooling energy use," Tech. Rep. 31721 UC-350, Lawrence Berkeley Laboratory, 1992.

[52] H. Akbari, S. Bretz, D. M. Kurn, and J. Hanford, "Peak power and cooling energy savings of high-albedo roofs," *Energy and Buildings*, vol. 25, no. 2, pp. 117–126, 1997.

[53] A. Shariah, B. Shalabi, A. Rousan, and B. Tashtoush, "Effects of absorptance of external surfaces on heating and cooling loads of residential buildings in Jordan," *Energy Conversion and Management*, vol. 39, no. 3-4, pp. 273–284, 1998.

[54] A. Synnefa, M. Santamouris, and H. Akbari, "Estimating the effect of using cool coatings on energy loads and thermal comfort in residential buildings in various climatic conditions," *Energy and Buildings*, vol. 39, no. 11, pp. 1167–1174, 2007.

Hindawi Publishing Corporation
Advances in Meteorology
Volume 2015, Article ID 423508, 11 pages
http://dx.doi.org/10.1155/2015/423508

Research Article

Investigating Thermal Comfort and User Behaviors in Outdoor Spaces: A Seasonal and Spatial Perspective

Kuo-Tsang Huang,[1] Tzu-Ping Lin,[2] and Hsiao-Chi Lien[3]

[1]*Department of Bioenvironmental Systems Engineering, National Taiwan University, 1 Section 4, Roosevelt Road, Taipei 106, Taiwan*
[2]*Department of Architecture, National Cheng Kung University, 1 University Road, Tainan 701, Taiwan*
[3]*Program of Landscape and Recreation, National Chung Hsing University, 250 Kuo Kuang Road, Taichung 402, Taiwan*

Correspondence should be addressed to Tzu-Ping Lin; lin678@gmail.com

Received 22 September 2014; Accepted 17 March 2015

Academic Editor: Julio Diaz

Numerous studies have examined the correlation between the number of attendants in a given outdoor environment and thermal indices to understand how the environmental planning has an impact on the users. However, extensive observations should be conducted to examine the detailed static and dynamic behavior patterns of users. We conducted dynamic observations at a stepped plaza to perform on-site measurements of the physical environment and observations of users behaviors, including their resting positions, movements, and stay durations. The results indicated that more people rested on the steps during the cool season than hot season. Compared to neutral temperatures, people demonstrated higher heat tolerance to the hot season. The results indicated that more than 75% of users preferred to remain in shaded areas and stayed longer than in the sunlight. The people tended to engage in static activities in environments that exhibit sufficient shading. The shaded areas were conducive to static activities as the summer grew hotter. The results verified that the people of Taiwan would avoid sunlight and desire shaded spaces based on their previous climate experiences and expectations, which can serve as a reference for outdoor space design to improve the usability and quality of open urban spaces.

1. Introduction

Requiring leisure and recreation space, people in urban environments use public outdoor spaces, such as parks and plazas, for their activities; this directly exposes them to the external climate. Thermal comfort, which is governed by temperature, humidity, wind speed, and radiation, closely relates to perceptions and preferences towards the way people use outdoor spaces. Because the success of a public space can be judged by the number of people using it [1], numerous studies have examined the number of people using specific spaces and how this variable relates to the thermal indices of the environment. Such studies have investigated locations in diverse countries and climate zones, such as Canada [2], UK [3], Sweden [4, 5], Japan [6], Taiwan [7, 8], Greece [9], Hungary [10], and Netherland [11]. These findings indicate a significant relation between the number of people using a space and the thermal environment of that space, depending on the climate conditions.

Studies have analyzed and compared the numbers of people and the thermal environments in locations that exhibit distinct spatial patterns (e.g., various degrees of shading) within a surveyed area. The results indicate that environmental design, for example, shading levels, would influence the thermal environments and the number of people gathering in outdoors [12, 13].

However, the number of people using a space alone cannot detail how that space is being used. Therefore, detailed observations should be conducted to examine user behavioral patterns and describe how the thermal environment affects space usage. These observations assess the personal attributes of users (e.g., age, sex, purpose, and clothing), their resting positions (in the shaded or unshaded area), staying characteristics (location selection, movement, and stay

duration), and behavior patterns (e.g., reading, discussing, or resting).

To obtain detailed information regarding users' behavior patterns for verifying the relation between behavior and the thermal environment, researchers must firstly determine appropriate observation methods and select an appropriate site. Regarding observational methods, similar studies in the past focused on numbers of attendants and the distributions of their locations. Therefore, researchers typically use visual methods to count the number of attendants and record their locations by using static photographs as supplementary information sources during analyzing.

However, to document users' behavior patterns in detail, long-term observation is needed. It is often done by means of scrutinizing continuous dynamic images filming from video camera. For example, Gómez-Martín and Martínez-Ibarra [14] used webcams to observe the number of people on beaches, employing quantitative visual estimation to determine the number and the density of people at various regions and timeframes. In their study, only users' location distribution and the density were analyzed due to the limitation of webcam's footage resolution; therefore, the behavior patterns of users were not assessed. Regarding the site selection, actual measurements must be conducted in spaces that are able to demonstrate diversifying thermal environments to further analyse the association between the thermal environment and the user behavior patterns. When using dynamic video recording, the locations of positioning recording device should be carefully selected to ensure that an unobstructed full view of the space is captured.

Digital video camera was used for dynamic observations toward a stepped square situated at the outdoor public recreational garden of National Museum of Natural Science (NMNS) in Taichung City, Taiwan. The chosen square exhibits diversifying thermal environments, which is partially shrouded by various thicknesses of tree canopies and partially sky open, and is considered an ideal place to perform on-site thermal measurements and observations. The objectives of this study are as follows:

(a) to observe the number of space users during various seasons and determine the histogram of the number of users against various temperature ranges;

(b) to investigate the user's prior selection of activity locations and the amount of time that people remained at their chosen locations;

(c) to analyze the relation between the thermal environment characteristics and the user behavior patterns.

The findings elucidated space use behaviors in response to thermal environments, which would help facilitate decision determining of outdoor space planning and design in the future.

2. Methods

2.1. Observational Subjects. As previously mentioned, the observation location requires a varied thermal environment that comprises unobstructed observation spots for placing video camera to elucidate how microclimates would influence the usage of recreation spaces, thermal comfort, and adaptive behaviors. Therefore, a stepped plaza at the outdoor garden of the NMNS was chosen for long-term observation. Figure 1 shows that the stepped plaza is located at 24°08′ N, 120°40′ E with an altitude of 26 m. The area is approximately 12.5 m in width, 4 m in depth, and the observational height range of the space is approximately 2.7 m. The area comprises four levels of steps. A lawn is positioned at the front of the steps with the two sides being turf and shading trees. The primary users of the space arrive after visiting the museum or attend the NMNS park for walking or resting. Most people remain in the plaza for less than 30 minutes. People use the plaza with various behaviors, including movements, talking, and reading.

Taichung City exhibits a hot and humid climate. The average observed climate data from 1991–2010 recorded by the Central Weather Bureau of Taiwan indicated that the monthly mean air temperature is highest in July at 28.5°C and lowest in January at 16.2°C. Furthermore, the mean monthly relative humidity is held constantly around 80% all the year, suggesting a humid climate. Since cool air temperature only exists from December to February, this research defines this period as the "cool season" and the remaining months (March to November) as the "hot season," which is in accordance with the definition of previous local studies [7, 12, 15, 16].

2.2. Shading Characteristics of the Stepped Plaza. The shading characteristics of an outdoor space would affect the thermal environment [15, 16]. Therefore, the shading characteristics of the evaluated stepped plaza must be quantitatively described. Because trees are mainly located at the south and north sides of the steps, the degree of shade varies along the steps. The sky view factor (SVF) was introduced herein to represent the shading level in an outdoor environment. The SVF can be defined as the percentage of free sky at specific location with the value ranging from totally obstructed (SVF = 0) to totally free spaces (SVF = 1) [17, 18].

A small SVF value indicates that a high amount of shade is present and the range of the visible sky is limited. Figure 2 shows fisheye photos shot in cool season 15:00 of the external appearance of the stepped plaza and the 10 corresponding positions. The SVF distribution ranged from position B1, which exhibited a high level of shade (SVF = 0.09), to A4, which was relatively open (SVF = 0.57). This indicates that various locations within the stepped plaza demonstrated distinct levels of solar insolation depending on the season, and the plaza exhibited varying thermal environmental characteristics. The SVF values of each location are similar whether in hot or cool season due to the surrounding evergreen trees planted in the stepped plaza.

2.3. Data Obtainment. Thermal environment measurements and user behavior observations were performed simultaneously. Physical quantities of microclimatic parameters measurements including the air temperature, relative humidity, globe temperature, and wind speed were measured with two identical sets of instruments with which one was placed

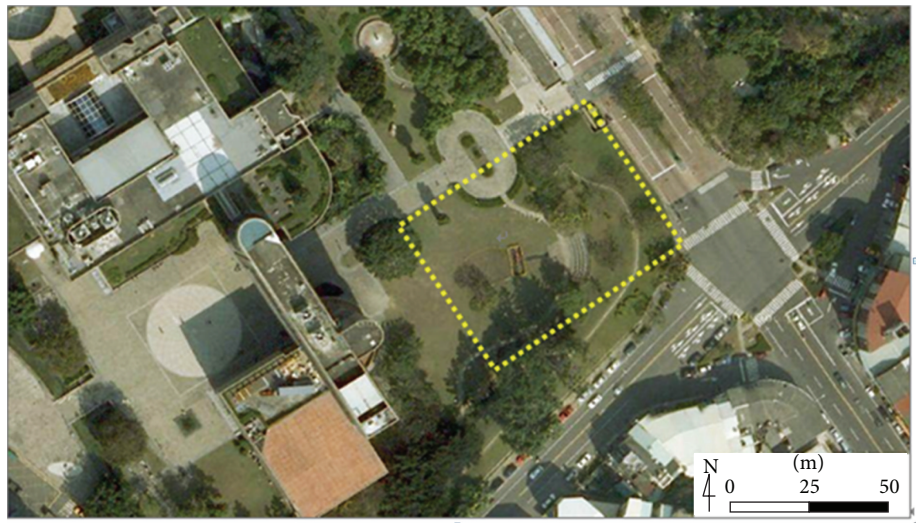

Figure 1: Aerial photograph of the NMNS location.

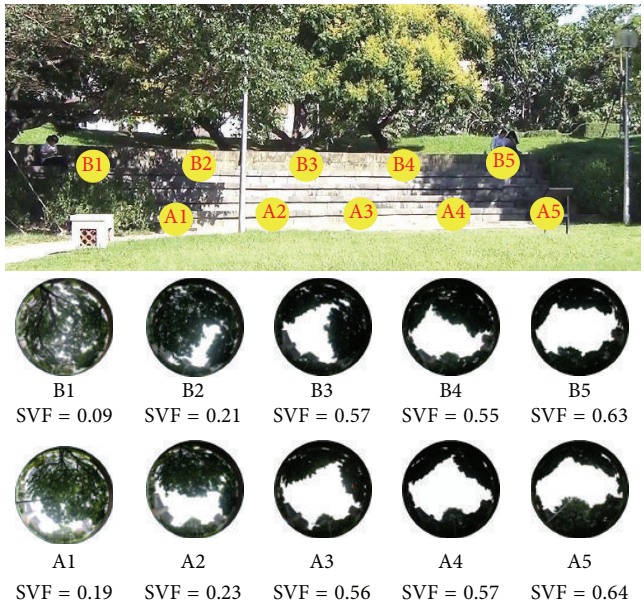

Figure 2: Panorama of the steps and fisheye diagrams of the measuring points. (Cool season 15:00).

under the tree shaded area and the other was placed totally unshaded as counterpart. A location with a dense tree canopy was considered a "shaded" location, whereas a location without shading from nearby buildings or trees was considered as an "unshaded" location. The resolution and accuracy of the instruments for each parameter are 0.1°C and ±0.3°C for air temperature and globe temperature, 0.1% and ±2.5% for relative humidity, and 0.01 m/s and ±0.2 m/s for wind speed. Both instruments were mounted on tripods that were 1.1 m above the ground and the parameters were automatically recorded once per minute from 1400 to 1700 hours simultaneously on the day the instruments were deployed.

The shaded and unshaded locations where the two sets of instruments were placed would vary day by day according to the position of the sun, resulting in various degrees of shading levels for each duration of time, and are dependent on seasons. The "shaded" and "unshaded" locations were not fixed and could vary according to the sun's movement. Nevertheless, the sunlight in the "shaded" locations by definition must be fully blocked, whereas the "unshaded" locations must be exposed to direct sunlight at all times without obstructions. The method of selecting shaded and unshaded measurement locations was similar to that used in a previous park study in Taiwan [12]. The hourly meteorological observations, such as the wind direction, horizontal solar insolation, and the amount of cloud, were obtained from the nearby Taichung Park weather station.

To record the basic characteristics and behaviors of users in the observation area, a high-resolution digital video camera was deployed approximately 25 m away from the steps and 1 m above ground to conduct nonstop snapshots. The time of appearance and departure, movements, and adaptive behaviors of the users were documented by scrutinizing the recorded footage. Although children were present in the observation area, we did not include them in the analysis because their activities/behaviors would possibly be restricted by their guarding parents.

2.4. Thermal Comfort Index Calculation. This study applied physiologically equivalent temperature (PET) to evaluate the thermal environment objectively. PET is defined as the air temperature at which, in a typical indoor setting (air temperature = mean radiant temperature; vapor pressure = 12 hPa; wind velocity = 0.1 m/s), the heat budget of the human body is in equilibrium, with the same core and skin temperatures as those under complex outdoor conditions [19–21]. To calculate PET, this study adopted the RayMan model [22, 23]. The value of mean radiant temperature was calculated from the measured globe temperature using formulas proposed by ISO

(a) 15:32

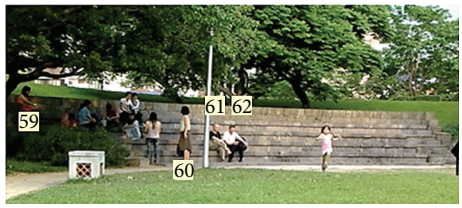

(b) 15:34

(c) 15:35

Figure 3: Image sample from the video.

standard 7726 [24] initially and subsequently corrected by the parallel measurements of both the globe thermometer and the six-direction short- and long-wave radiation flux measurement system previously conducted in Taiwan [25].

2.5. Video Image Interpretation and Encoding. To establish an observation record table for facilitating analysis, the dynamic digital image recordings were interpreted and encoded. First, we encoded the observed subjects, assigning a number to each individual (e.g., 001 and 002). Second, we visually interpreted the basic characteristics (gender, age, number of companions, and amount of wearing clothing) and behavioral characteristics of the subjects (primary activity, choice of sunny or shaded area, number of people within an area, the amount of time between arriving to and departing from an area, total time spent within an area, and other thermal related adaptive behaviors) to facilitate subsequent quantitative statistical analyses. One specific researcher interpreted all the images to ensure consistency. Finally, we linked the thermal environmental measurements (each physical parameter and the integrated thermal comfort index PET) to each of subjects, establishing a complete database containing records of the subject codes, basic and behavioral characteristics, and thermal environmental parameters.

An example of how the video image is interpreted and encoded is expounded as follows. Figure 3 shows that subjects numbers 59–62 formed a four-member group. Their staying and moving patterns can be divided into three periods. (a) Subjects numbers 59 and 60 were women; at 15:32, they walked into the semishaded area on the left side of the steps and sat down. Subjects numbers 61 and 62 were men; they stood and talked on the lawn approximately 2 m from the stairs. (b) After 2 min, at 15:34, subjects numbers 61 and 62 walked to the steps and sat in the sunlight. At the same time, subjects numbers 59 and 60 stood up and considered sitting in a position covered by dense shade. (c) After 1 min, at 15:35, subjects numbers 59 and 60 moved toward the shade and sat. Subjects numbers 61 and 62 remained sitting and talking in their original position.

In this way, we were able to track the users through each image footage, enabling us to establish a complete database of the association between user behavioral characteristics and the thermal environment to facilitate subsequent analyses.

2.6. Measurement Process. This study performed a total of 19 measurements and observations from April of 2012 to February of 2013. All measurements were conducted between 13:00 and 18:00 on Saturday or Sunday, which is the most visited period for local users. The observation days were divided into two seasons, hot seasons (March to November) and cool seasons (December to February), based on Taiwan's climate characteristics, as stated in Section 2.1.

To prevent the observation from influencing users' behavior, we carefully installed the instruments in inconspicuous locations instead of intervening in the user activities by conducting questionnaires or interviews. Before the measurements were conducted, the consent from the NMNS authority was acquired. The privacy of the filmed people during identification, analysis, and processing was also ensured.

3. Results

3.1. Number of Users. As the number of users is the most basic information regarding the space use, the number of subjects accompanied with their corresponding PET thermal index measurements from the 19 observations was illustrated. The mean air temperature was 32.9°C during the hot season and 24.1°C during the cool season. The mean radiant temperature was 39.6°C during the hot season and 30.6°C during the cool season. The PET was 36.7°C during the hot season and 27.1°C during the cool season. The relation between PET and the number of participants is shown in Figure 4. In June and July (hot season), the PET was as high as approximately 45°C, and the number of users was consistently less than 10. In November and December (cool season), the PET decreased to approximately 20°C and the number of users was as high as 59. This indicates that, during the hot season, the number of users decreased as the PET increased. During the cool season, the number of users increased as the temperature increased. These data are consistent with the results of similar study previously conducted in Taiwan, addressing the relation between the thermal comfort range and number of users. As Taiwan is located in a subtropical hot-and-humid climate zone, the temperatures during the hot season are inversely proportional to the number of plaza users [7].

To elucidate the relation between the use of the stepped plaza and the PET variation in outdoor thermal environment, the number of users observed from all 19 observations was lumped and grouped against each PET range based on

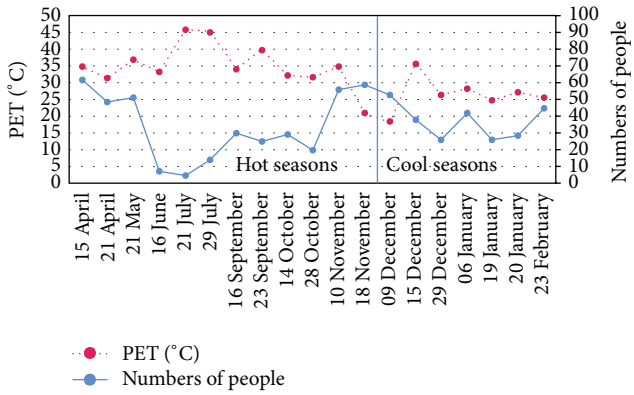

Figure 4: Relation between the PET and number of participants.

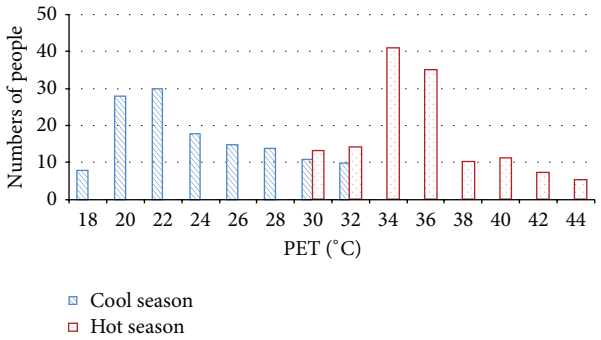

Figure 5: Relation between the annual PET and mean number of participants.

a temperature increment of 2°C PET, as illustrated in Figure 5. During the hot season, the results indicate that the mean number of space users was the highest (41 people) when the PET was 34°C. The number of people decreased as temperatures increased, and only 5 users were present when the PET reached 44°C. During the cool season, the mean number of space users was the highest (30 people) when the PET was 22°C. The number of people decreased to 10 as temperature increased.

3.2. Location Selection and Movement. When engaging in outdoor activities, people choose a staying location based on their past experiences of the current or a similar location/space from thermal perspective. When people feel thermally dissatisfied with their first location choice, they may move. These choices may be closely associated with microclimate perception, experiences, and expectations. For example, Kántor and Unger [10] examined microclimate perception regarding plazas in Netherlands; the results indicated that people do not go to a location only after determining that the climate is suitable. Instead, they use their past experiences and awareness to judge the current environment and decide. For example, when users observe shade under trees, they may speculate that the shaded area is cooler based on their past experiences and move to this location. Therefore, first choices of location are psychological representations of environmental experiences. Subsequent movements are responses caused by the combination of physiological exposure and psychological expectations. In other words, people exhibit appropriate adaptive behaviors based on their microclimate expectations and preferences, in addition to changes in physiological heat balance caused by exposure to the microclimate. Thus, people move to other locations because their perceptions of the heat level differ from their psychological experiences and expectations.

To explore this phenomenon, we recorded the first locations chosen by users when interpreting and encoding the images. These locations reflected differences in the thermal environment, comprising (a) sunny areas, (b) shaded areas, and (c) boundaries between the two. The time at which users arrived at and departed from these locations was recorded. The location types and the arrival and departure time for the first and second movements of users were also recorded in the same fashion. Thus, the stay duration for each location type of every user movement could be calculated and recorded.

This section addresses staying and moving location types (the stay duration is addressed in Section 3.3). We calculated the number and percentage of people who stayed in various types of locations (sunny area, shaded area, and the boundary area between the two) within the stepped plaza during the hot and cool seasons (Figure 6). During the hot season, 74% of users first chose shaded areas, whereas 22% first chose sunny areas. Subsequently, 5% moved to shaded areas and 3% moved to sunny areas, indicating that most people first chose shaded areas as resting locations during the hot season. Only a minority selected sunny areas as their resting locations. Most who initially chose shaded areas remained in their original locations, whereas some who firstly chose sunny areas moved to shaded areas.

During the cool season, 87% of users first selected shaded areas, whereas 13% selected sunny areas. Subsequently, 1% moved to shaded areas and none moved to sunny areas, indicating that most people initially chose shaded areas for resting during the cool season. Likewise in hot seasons, only a minority selected sunny areas for resting. In a statistics regarding the second movement, 99% of people stayed in their original positions and only 1% moved to shaded areas.

In both the hot and cool seasons, users tended to select shaded areas as their first choices. This indicates that people prefer to engage in outdoor leisure activities in areas containing shade-providing trees or canopies, avoiding direct exposure to intense solar irradiance. As previously described, most people perceived that shaded areas would exhibit relatively low temperatures based on their past experiences and expectations and considered these places would be more comfortable. As a result, most people preferred engaging in activities in shaded areas. Few people had made their second movement, indicating that few people were affected by increased physiological heat loads. Thus, people relied on their experiences, expectations, and other psychological factors rather than on physiological factors when displaying thermal adaptive behaviors.

3.3. Stay Duration. The amount of time that users spend on activities in outdoor spaces can reflect their satisfaction

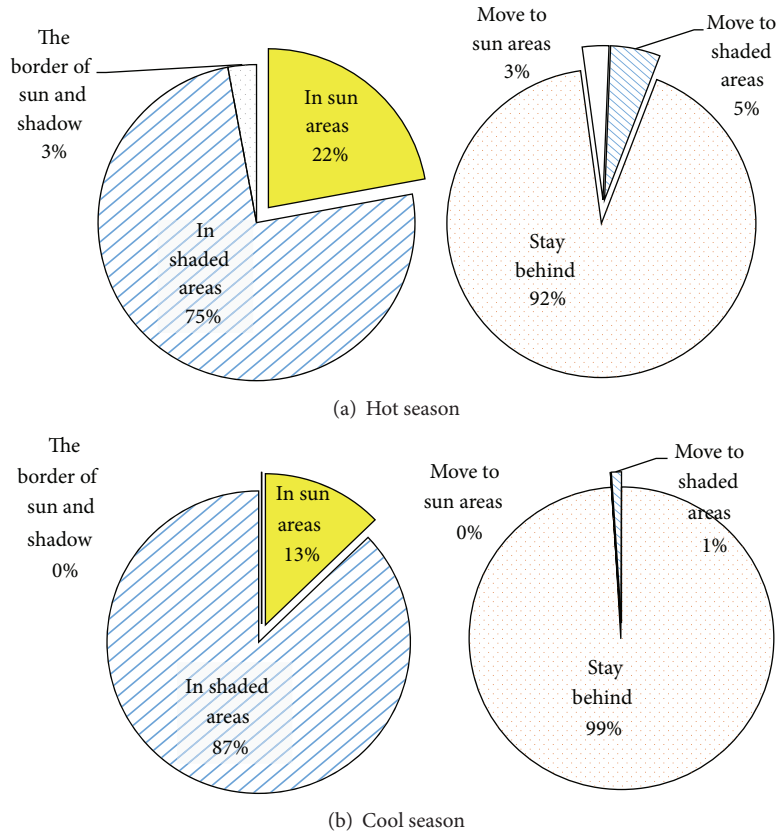

Figure 6: User choices of resting locations and movements during the hot and cool seasons.

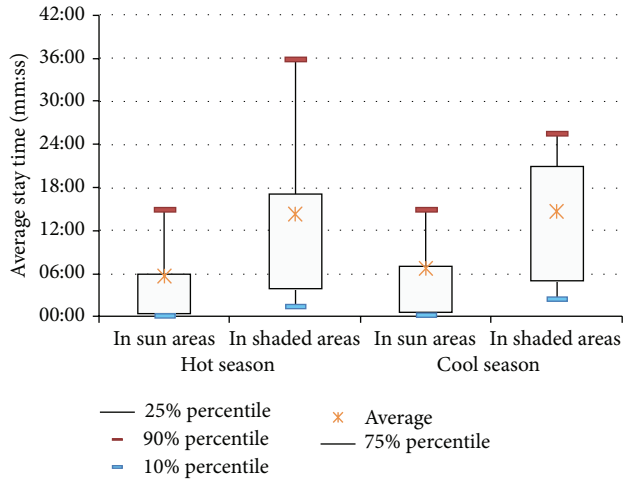

Figure 7: User time spent in sunny and shaded areas during the cool and hot seasons.

with the environment. When encoding the images, we recorded the location types, arrival and departure time for the first location choices, and the subsequent movements. This enabled calculating the amount of time users spent in sunny and shaded areas. The box plot shown in Figure 7 reveals the distribution of the duration that users spent in sunny and shaded areas, and the differences between the two. The results indicate that the mean stay duration during the hot season was 5 min, 41 s in sunny areas and 14 min, 18 s in shaded areas. During the cool season, the mean stay duration was 6 min, 45 s in sunny areas and 14 min, 41 s in shaded areas.

Figure 7 apparently indicates that the stay duration was longer in shaded areas than it was in sunny areas during both seasons. Despite the low air temperatures during the cool season, people did not move to sunny areas for enhancing their thermal comfort but rather tended to avoid solar insolation, showing a likewise preference for shaded and cool areas as in hot seasons. The classical physiological thermal balance failed to explain these behavioral patterns.

It is worthy to mention that the 90th percentile of stay duration in shaded areas was 35 min, 55 s during the summer. Few users spent approximately half an hour, which is longer than that in the cool season, in shaded areas during the hot season. It suggests that users would be willing to increase their stay duration in open spaces if shaded recreation areas were provided in hot outdoor environments.

To elaborate the variations in stay duration under various thermal comfort conditions, cases observed in the hot season were used as an example to calculate changes in mean stay durations under sunny and shaded areas at fixed intervals against the PET thermal comfort index (e.g., 2°C PET). Figure 8 shows that users in shaded areas stayed longest (17 min 7 s) when the PET was 31°C. The stay duration

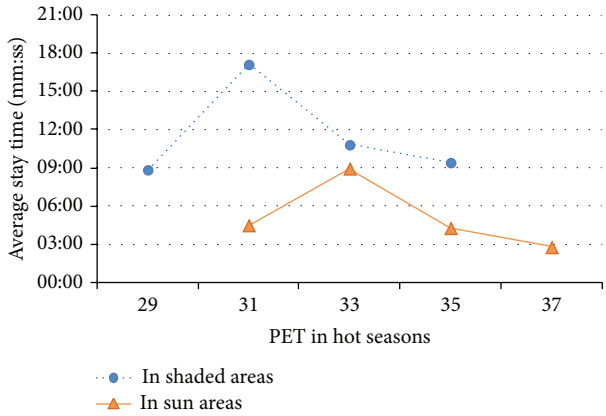

Figure 8: Changes in the mean user time spent in sunny and shaded areas during the hot and cool seasons.

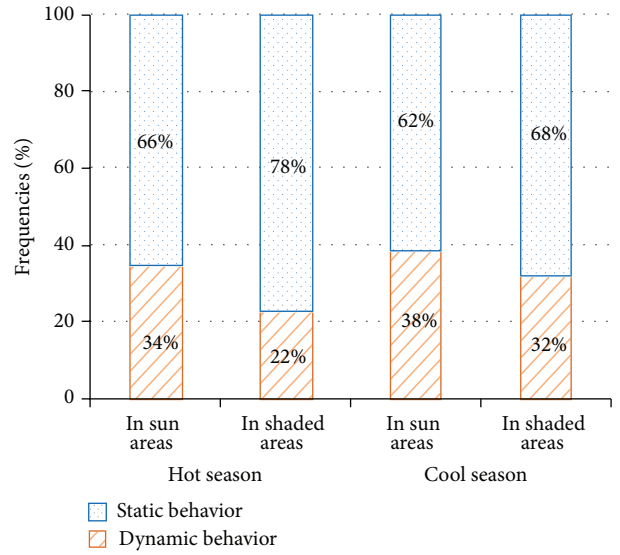

Figure 9: Ratio of dynamic to static behaviors in the sunny and shaded areas during the cool and hot seasons.

decreased as temperatures increased or decreased. Users in sunny areas stayed longest when the PET was 33°C, but it still exhibits lower stay duration in comparison to shaded areas in all PET ranges. Moreover, the association between temperature changes and stay duration in the sunny areas had similar variation trend to that in the shaded areas. The temperature at which people stayed longest in the shaded areas (31°C PET) was lower compared with that of the sunny areas (33°C PET) because people hoped for decreased temperatures based on their expectations of thermal comfort in shaded environments.

3.4. Behavior Patterns. To some extent, behavioral patterns indirectly reflect how users interact with microclimate environments. A previous study of microclimate and the exploratory behaviors of lions and tigers in zoos [26] recorded the activity patterns of animals, dividing animal behaviors into two categories: comfort (e.g., lying down, sitting, and being in water) and movement behaviors (e.g., standing, walking, and running). Similarly, in the current study, we observed the detailed behaviors of users from the images, dividing them into static (e.g., sitting, talking, eating and drinking, and reading) and dynamic behaviors (e.g., standing and walking). The frequencies of static and dynamic behaviors were calculated based on the season (hot and cool) and location (sunny and shaded areas). It is assumed that a high frequency of static activity indicated that people felt stable and comfortable. To some degree, this indicates that the microclimate of the environment is considered comfortable.

Figure 9 indicates that, during both seasons, more users engaged in static behaviors compared with dynamic behaviors in the stepped plaza. During the hot season, more users adopted static behaviors than in the cool season. The primary reason for this is that metabolic rates are decreased when sitting compared with standing or walking [27]. In the attached table from the American Society of Heating, Refrigerating, and Air-Conditioning Engineers [28], metabolic rates were approximately 60 W/m^2 when sitting and reading and approximately 80–100 W/m^2 when standing or slow walking. Therefore, people tend to adopt static activities during the hot season, producing decreased metabolic heat inside the body to increase comfort.

Comparing behavior patterns in spaces that demonstrate varied shade indicates that users in sunny areas were more likely to adopt dynamic behaviors than users in shaded areas were. This can be explained based on the stay durations addressed in the previous section. Figures 7 and 8 indicate that users stayed in sunny areas for less duration than they stayed in shaded areas. In other words, compared with people in shaded areas, those in sunny areas were more likely to adopt dynamic behaviors such as leaving the plaza or moving to locations. By contrast, when people were in shaded areas that provided relatively comfortable thermal environments, their calm moods facilitated adopting static activities, such as sitting, talking, and reading.

4. Discussion: Verification through Thermal Adaptation Theory

To provide an objective discussion of the association between user behaviors and the environment, thermal comfort theory and previous investigations are referenced to describe and verify the close relation between the behavior and the thermal environment.

4.1. Thermal Adaptation Theory. The ASHRAE defined thermal comfort as "a state of mind expressing satisfaction toward the thermal environment (temperature, humidity, wind speed, and radiation) assessed through subjective evaluation" [28]. In the field of thermal comfort, scholars have attempted to combine temperature, humidity, wind speed, radiation, amount of clothing, and metabolic rates to represent thermal comfort as a single index. The ASHRAE guidelines highlight that thermal comfort is a psychological condition; thus, subjective perceptions cannot be interpreted

using a physiological index based on body heat balances. Because psychological factors influence perceptions, the subjective perceptions of people within environments that exhibit identical thermal comfort indices can differ substantially based on their experiences, expectations, exposure durations, cultural characteristics, perceived control, and other factors. This refers to "thermal adaptability," which numerous studies have discussed and validated [29–35].

Seasonal changes are the most obvious experience factor. For example, people distinctly perceive summer and winter temperatures. Spatial types (e.g., shaded or open) are also relevant to expectations (e.g., people anticipate disparate feelings when they are exposed to the shade or hot sun). Accordingly, the obtained behavioral observations were explored in detail based on the above two factors (seasonal and spatial behavioral differences) as follows. The results were also validated with previous studies conducted in Taiwan.

4.2. Verification of Seasonal Behavioral Differences. Lin [7] used subjective questionnaires and objective physical environmental measurements in Taiwan to analyze neutral temperature (T_n) and preferred temperature (T_p). T_n is a temperature that is perceived as neither cold nor hot; thus, it can be considered a comfortable temperature. T_p is a temperature that people prefer; at this temperature they do not seek to become cooler or warmer. Thus, the T_p can be considered the expected temperature. In this study, the T_n was 23.7°C and 25.6°C during the cool and hot seasons, respectively. The T_p was 23°C and 24.5°C during the cool and hot seasons, respectively.

In this study, our observations regarding the numbers of participants in the PET groups (Section 3.1) indicate that the thermal index ranges in which the most people appeared during the cool and hot seasons were 20°C PET–22°C PET and 34°C PET–36°C PET, respectively. Comparing these values with the on-site measurements, the 20°C PET–22°C PET range, in which the most people appeared during the cool season, was close to the T_n and T_p values of the cool season. However, the 34°C PET–36°C PET range, in which the most people appeared during the hot season, was nearly 10°C PET higher compared with the T_p (25.6°C) of the hot season.

We can view the difference between these temperatures as the gap between psychological feelings (T_n or T_p) and actual behaviors (the temperatures at which people attend an area). This difference was not clear during the cool season, but it was obvious during the hot season, indicating that although people psychologically preferred low temperatures during the hot season, they continued to move to the observed site when temperatures were high. People demonstrated a high tolerance to increased summer temperatures, indicating their adaptability to the local climate.

4.3. Verification of Spatial Behavioral Differences. The constructed environment strongly influences the thermal conditions to which people are exposed in outdoor spaces [36–41]. Among several environmental attributes of the outdoors, shading can block solar radiation and has been proven to influence outdoor thermal environments significantly. Certain studies have examined street orientation and height-to-width ratios for representing the shading factors [42–48]. Other studies have used SVF to represent the degree of shading [49–52]. Previous on-site measurements in Taiwan [15, 16] proved that areas exhibiting high levels of shading would provide superior long-term comfort. Lin [7] used questionnaires to determine that people prefer taking shade under trees or other shelters when exhibiting adaptive behaviors to relieve increases in outdoor temperatures. This explains why more than 75% of users in this study preferred shaded areas and remained in these areas longer in comparison with those who chose sunny areas.

It could be logically assumed that users prefer direct insolation to ameliorate coldness during the cool season; however, Figure 6 indicates that users were more likely to go to and stayed in shaded areas during the cool season than they were during the hot season. The phenomenon that people tended to stay in shaded areas during the cool season can be elucidated based on a study performed in Taiwan. Lin et al. [53] examined four factors in the physical environment that influenced outdoor thermal comfort in Taiwan: the air temperature, air humidity, solar radiation level, and wind speed. The analysis indicated that air temperature was the critical factor (64.3%) during the hot season, followed by radiation (34.3%). During the cool season, solar radiation contributed considerably more (58.3%) to the thermal comfort level than the air temperature did (38.7%) because air temperatures are moderate during the cool season in Taiwan. When the subjects were exposed to comfortable environments, the intensity of the sun insolation flexibly represented perceptions of heat or cold (radiation could improve comfort). Therefore, the solar radiation influenced thermal perceptions more than the air temperatures did and, as a result, people continued to prefer conducting their activities in shaded areas during the cool season.

5. Conclusion

In this study, physical microclimate measurements, image recordings, and dynamic behavior observations of users in a stepped plaza at the outdoor garden of the NMNS in Taichung City, Taiwan, were performed. We discussed whether and how the resting location choices, stay durations, and dynamic or static activities were associated with the thermal environment in seasonal and spatial type perspectives of a recreational field that coexist with both shaded and unshaded areas.

The dynamic image recordings and user behavior observations were novel for use in this field. This method enabled recording all user behaviors within the observational range and comparing the images with physical measurements of the thermal environment to determine how microclimates affect occupant's adaptive behaviors. The disadvantage of this method was that we could not interfere with the users (e.g., conducting interviews or providing questionnaires) to precisely determine their microclimate feelings and preferences. In addition to recording videos, subsequent studies

can design questionnaires to investigate user feelings toward the thermal environment; however, care must be taken not to interfere with the subjects. The primary findings of this study are as follows.

(1) More people rested on the stepped plaza during the cool season compared with the hot season. The number of people present during the hot season decreased as temperatures increased. The temperature ranges at which most people were present were 34°C PET–36°C PET during the hot season and 20°C PET–22°C PET during the cool season.

(2) More than 75% of users preferred shaded areas. Users also stayed longer in shaded areas than they did in sunny areas.

(3) In highly shaded environments, people preferred static activities. The shaded areas were ideal for static activities, particularly during the hot season.

We also referenced thermal comfort theory and previous local on-site investigations to describe and verify the relation between behavior and the thermal environment. It is proved that the observed subjects demonstrated an extremely high tolerance to increased summer temperatures despite their psychological preferences for lower temperatures. This was reflected in the attendance and behavior during the hot season, demonstrating human adaptability toward the local climate. We confirmed that people psychologically disliked high levels of outdoor insolation; this was evidenced by their spatial use behaviors. People substantially preferred to conduct activities in shaded areas even during the cool season.

This study elucidates the association between the thermal environment and adaptive behaviors of users. It differs from past studies, which investigated only participant numbers, and extends to assess user stay locations, stay durations, and behavior patterns. The findings prove that the people of Taiwan, which are living in a hot and humid region, avoid sunlight and desire shaded spaces based on their previous microclimate experiences and expectations. This is distinct from the trends observed in countries in the temperate zone. In addition, the findings proved that people often use their past experiences to determine whether to move to a space after observing the sun and shade conditions to ensure their thermal comfort. Because people rarely make second move after choosing a location, designing spaces that include sufficient trees or shading shelters could facilitate users' recognition of thermal comfort. Furthermore, by integrating user climate experiences and awareness to outdoor environmental planning and design, a successful outdoor space that is attractive to the public could be achieved.

Conflict of Interests

The authors declare that there is no conflict of interests regarding the publication of this paper.

References

[1] M. Carmona, T. Heath, T. Oc, and S. Tiesdell, *Public Places-Urban Spaces: The Dimensions of Urban Design*, Architectural Press, Elsevier, Burlington, NJ, USA, 2003.

[2] J. Zacharias, T. Stathopoulos, and H. Wu, "Microclimate and downtown open space activity," *Environment and Behavior*, vol. 33, no. 2, pp. 296–315, 2001.

[3] M. Nikolopoulou, N. Baker, and K. Steemers, "Thermal comfort in outdoor urban spaces: understanding the human parameter," *Solar Energy*, vol. 70, no. 3, pp. 227–235, 2001.

[4] S. Thorsson, M. Lindqvist, and S. Lindqvist, "Thermal bioclimatic conditions and patterns of behaviour in an urban park in Göteborg, Sweden," *International Journal of Biometeorology*, vol. 48, no. 3, pp. 149–156, 2004.

[5] I. Eliasson, I. Knez, U. Westerberg, S. Thorsson, and F. Lindberg, "Climate and behaviour in a Nordic city," *Landscape and Urban Planning*, vol. 82, no. 1-2, pp. 72–84, 2007.

[6] S. Thorsson, T. Honjo, F. Lindberg, I. Eliasson, and E.-M. Lim, "Thermal comfort and outdoor activity in Japanese urban public places," *Environment and Behavior*, vol. 39, no. 5, pp. 660–684, 2007.

[7] T.-P. Lin, "Thermal perception, adaptation and attendance in a public square in hot and humid regions," *Building and Environment*, vol. 44, no. 10, pp. 2017–2026, 2009.

[8] C. H. Lin, T. P. Lin, and R. L. Hwang, "Thermal comfort for urban parks in subtropics: understanding visitor's perceptions, behavior and attendance," *Advances in Meteorology*, vol. 2013, Article ID 640473, 8 pages, 2013.

[9] M. Nikolopoulou and S. Lykoudis, "Use of outdoor spaces and microclimate in a Mediterranean urban area," *Building and Environment*, vol. 42, no. 10, pp. 3691–3707, 2007.

[10] N. Kántor and J. Unger, "Benefits and opportunities of adopting GIS in thermal comfort studies in resting places: an urban park as an example," *Landscape and Urban Planning*, vol. 98, no. 1, pp. 36–46, 2010.

[11] S. Lenzholzer and J. Koh, "Immersed in microclimatic space: microclimate experience and perception of spatial configurations in Dutch squares," *Landscape and Urban Planning*, vol. 95, no. 1-2, pp. 1–15, 2010.

[12] T. P. Lin, K. T. Tsai, R. L. Hwang, and A. Matzarakis, "Quantification of the effect of thermal indices and sky view factor on park attendance," *Landscape and Urban Planning*, vol. 107, no. 2, pp. 137–146, 2012.

[13] T.-P. Lin, K.-T. Tsai, C.-C. Liao, and Y.-C. Huang, "Effects of thermal comfort and adaptation on park attendance regarding different shading levels and activity types," *Building and Environment*, vol. 59, pp. 599–611, 2013.

[14] M. B. Gómez-Martín and E. Martínez-Ibarra, "Tourism demand and atmospheric parameters: non-intrusive observation techniques," *Climate Research*, vol. 51, no. 2, pp. 135–145, 2012.

[15] R.-L. Hwang, T.-P. Lin, and A. Matzarakis, "Seasonal effects of urban street shading on long-term outdoor thermal comfort," *Building and Environment*, vol. 46, no. 4, pp. 863–870, 2011.

[16] T.-P. Lin, A. Matzarakis, and R.-L. Hwang, "Shading effect on long-term outdoor thermal comfort," *Building and Environment*, vol. 45, no. 1, pp. 213–221, 2010.

[17] T. R. Oke, "Canyon geometry and the nocturnal urban heat island: comparison of scale model and field observations," *Journal of Climatology*, vol. 1, no. 3, pp. 237–254, 1981.

[18] T. R. Oke, *Boundary Layer Climates*, Metheun, London, UK, 1987.

[19] VDI, *Methods for the Human Biometeorological Evaluation of Climate and Air Quality for the Urban and Regional Planning. Part I: Climate. VDI Guideline 3787. Part 2*, Beuth, Berlin, Germany, 1998.

[20] H. Mayer and P. Höppe, "Thermal comfort of man in different urban environments," *Theoretical and Applied Climatology*, vol. 38, no. 1, pp. 43–49, 1987.

[21] P. Höppe, "The physiological equivalent temperature—a universal index for the biometeorological assessment of the thermal environment," *International Journal of Biometeorology*, vol. 43, no. 2, pp. 71–75, 1999.

[22] A. Matzarakis, F. Rutz, and H. Mayer, "Modelling radiation fluxes in simple and complex environments—application of the RayMan model," *International Journal of Biometeorology*, vol. 51, no. 4, pp. 323–334, 2007.

[23] A. Matzarakis, F. Rutz, and H. Mayer, "Modelling radiation fluxes in simple and complex environments: basics of the RayMan model," *International Journal of Biometeorology*, vol. 54, no. 2, pp. 131–139, 2010.

[24] ISO, "Thermal environment-instruments and method for measuring physical quantities," International Standard 7726, International Standard Organization, Geneva, Switzerland, 1998.

[25] T. P. Lin and A. Matzarakis, "Estimation of outdoor mean radiant temperature by filed experiment and modelling for human-biometeorology use," in *Proceedings of the 11th Annual Meeting of the European Meteorological Society*, EMS2011-89, Berlin, Germany, 2011.

[26] T. Young, E. Finegan, and R. D. Brown, "Effects of summer microclimates on behavior of lions and tigers in zoos," *International Journal of Biometeorology*, vol. 57, no. 3, pp. 381–390, 2013.

[27] P. O. Fanger, *Thermal Comfort*, McGraw Hill, New York, NY, USA, 1972.

[28] ASHRAE, *ASHRAE Standard 55-2010, Thermal Environmental Conditions for Human Occupancy*, American Society of Heating, Refrigerating and Air-Conditioning Engineers, Atlanta, Ga, USA, 2010.

[29] Y. Fan, S. Lang, and W. Xu, "Field study on acceptable thermal conditions for residential buildings in transition zone of China," in *Proceedings of the 6th International Conference on Indoor Air Quality and limate (Indoor Air '93)*, J. J. K. Jaakkola, R. Ilmarinen, and O. Seppänen, Eds., Helsinki, Finland, July 1993.

[30] R.-L. Hwang and T.-P. Lin, "Thermal comfort requirements for occupants of semi-outdoor and outdoor environments in hot-humid regions," *Architectural Science Review*, vol. 50, no. 4, pp. 357–364, 2007.

[31] D. A. McIntyre, *Indoor Climate*, Applied Science Publishers, London, UK, 1980.

[32] M. Paciuk, "The role of personal control of the environment in thermal comfort and satisfaction at the workplace," in *Coming of Age*, R. Selby, K. Anthony, J. Choi, and B. Orland, Eds., Environment Design Research Association, Edmond, Okla, USA, 1990.

[33] G. S. Brager, G. Paliaga, R. de Dear et al., "Operable windows, personal control, and occupant comfort," *ASHRAE Transactions*, vol. 110, pp. 17–35, 2004.

[34] B. Givoni, *Climate Considerations in Building and Urban Design*, Van Nostrand Reinhold, New York, NY, USA, 1997.

[35] A. Malama, S. Sharples, A. C. Pitts, and K. Jitkhajornwanich, "Investigation of the thermal comfort adaptive model in a tropical upland climate," in *Proceedings of the 1998 ASHRAE Winter Meeting*, pp. 1194–1206, January 1998.

[36] T. P. Lin, Y. F. Ho, and Y. S. Huang, "Seasonal effect of pavement on outdoor thermal environments in subtropical Taiwan," *Building and Environment*, vol. 42, no. 12, pp. 4124–4131, 2007.

[37] S.-A. Tan and T.-F. Fwa, "Influence of pavement materials on the thermal environment of outdoor spaces," *Building and Environment*, vol. 27, no. 3, pp. 289–295, 1992.

[38] H. Taha, "Urban climates and heat islands: albedo, evapotranspiration, and anthropogenic heat," *Energy and Buildings*, vol. 25, no. 2, pp. 99–103, 1997.

[39] T. Asaeda and V. T. Ca, "Characteristics of permeable pavement during hot summer weather and impact on the thermal environment," *Building and Environment*, vol. 35, no. 4, pp. 363–375, 2000.

[40] N. H. Wong, S. K. Jusuf, A. A. la Win, H. K. Thu, T. S. Negara, and X. C. Wu, "Environmental study of the impact of greenery in an institutional campus in the tropics," *Building and Environment*, vol. 42, no. 8, pp. 2949–2970, 2007.

[41] T. Ichinose, K. Shimodozono, and K. Hanaki, "Impact of anthropogenic heat on urban climate in Tokyo," *Atmospheric Environment*, vol. 33, no. 24-25, pp. 3897–3909, 1999.

[42] E. Johansson, "Influence of urban geometry on outdoor thermal comfort in a hot dry climate: a study in Fez, Morocco," *Building and Environment*, vol. 41, no. 10, pp. 1326–1338, 2006.

[43] E. Johansson and R. Emmanuel, "The influence of urban design on outdoor thermal comfort in the hot, humid city of Colombo, Sri Lanka," *International Journal of Biometeorology*, vol. 51, no. 2, pp. 119–133, 2006.

[44] R. Emmanuel and E. Johansson, "Influence of urban morphology and sea breeze on hot humid microclimate: the case of Colombo, Sri Lanka," *Climate Research*, vol. 30, no. 3, pp. 189–200, 2006.

[45] F. Ali-Toudert and H. Mayer, "Thermal comfort in an east-west oriented street canyon in Freiburg (Germany) under hot summer conditions," *Theoretical and Applied Climatology*, vol. 87, no. 1–4, pp. 223–237, 2007.

[46] F. Ali-Toudert and H. Mayer, "Numerical study on the effects of aspect ratio and orientation of an urban street canyon on outdoor thermal comfort in hot and dry climate," *Building and Environment*, vol. 41, no. 2, pp. 94–108, 2006.

[47] F. Ali-Toudert and H. Mayer, "Effects of asymmetry, galleries, overhanging façades and vegetation on thermal comfort in urban street canyons," *Solar Energy*, vol. 81, no. 6, pp. 742–754, 2007.

[48] R. Emmanuel, H. Rosenlund, and E. Johansson, "Urban shading—a design option for the tropics? A study in Colombo, Sri Lanka," *International Journal of Climatology*, vol. 27, no. 14, pp. 1995–2004, 2007.

[49] R. Giridharan, S. S. Y. Lau, and S. Ganesan, "Nocturnal heat island effect in urban residential developments of Hong Kong," *Energy and Buildings*, vol. 37, no. 9, pp. 964–971, 2005.

[50] Z. Bottyán and J. Unger, "A multiple linear statistical model for estimating the mean maximum urban heat island," *Theoretical and Applied Climatology*, vol. 75, no. 3-4, pp. 233–243, 2003.

[51] R. Hamdi and G. Schayes, "Sensitivity study of the urban heat island intensity to urban characteristics," *International Journal of Climatology*, vol. 28, no. 7, pp. 973–982, 2008.

[52] R. Giridharan, S. S. Y. Lau, S. Ganesan, and B. Givoni, "Urban design factors influencing heat island intensity in high-rise high-density environments of Hong Kong," *Building and Environment*, vol. 42, no. 10, pp. 3669–3684, 2007.

[53] T.-P. Lin, R. de Dear, and R.-L. Hwang, "Effect of thermal adaptation on seasonal outdoor thermal comfort," *International Journal of Climatology*, vol. 31, no. 2, pp. 302–312, 2011.